SINGLE STAGE EXPERIMENTAL EVALUATION

OF

SLOTTED ROTOR AND STATOR BLADING

Part IX - Final Report

by

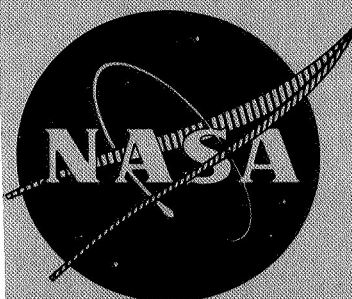R. W. Rockenbach

Prepared For

National Aeronautics and Space Administration

Contract NAS3-7603

Pratt & Whitney Aircraft DIVISION OF UNITED AIRCRAFT CORPORATION

FLORIDA RESEARCH AND DEVELOPMENT CENTER

BOX 2691, WEST PALM BEACH, FLORIDA 33402

UA®

35

Requests for copies of this report should be referred to

National Aeronautics and Space Administration
Office of Scientific and Technical Information
Attention: AFSS-A
Washington, D.C. 20546

SINGLE STAGE EXPERIMENTAL EVALUATION

OF

SLOTTED ROTOR AND STATOR BLADING

Part IX - Final Report

by

R. W. Rockenbach

Prepared For

National Aeronautics and Space Administration

Contract NAS3-7603

26 SEPTEMBER 1968

Technical Management
NASA Lewis Research Center
Cleveland, Ohio

NASA Project Manager: John E. McAulay
Air Breathing Engines Division

NASA Research Advisor: L. Joseph Herrig
Fluid Systems Components Division

ABSTRACT

Three slotted rotors and three slotted stators with design diffusion
factors in the range 0.5 to 0.7 were tested to determine the effect of
the slots on performance. The slots reduced blade element losses in
the midspan region without affecting deviation angle, and a small
increase in unstalled operating range was noted. All blade rows tested
showed strong wall stall, and no beneficial effect was noted from the
slots in this region. It is hypothesized that slots must be located
nearer to the leading edge in this region to be effective.

CONTENTS

SUMMARY

Three slotted axial flow compressor rotors and three slotted stators were designed and tested to determine the effectiveness of the slots in improving the performance of highly loaded blading. The configuration of the slots and their chordal location were established from the results of (1) a series of 11 annular cascade tests and (2) theoretical calculations of the boundary layer separation point conducted as a part of this program. The slot configuration selected reduced the loss coefficient of the annular cascade blading from 0.071 to 0.012 at an angle of incidence of approximately one degree.

The performance of the slotted blading, when tested in the single-stage compressor, was controlled to a large extent by three-dimensional flow effects, and, consequently, performance gains of the order of magnitude of that experienced during the cascade portion of the test program were not attained. The large secondary flows at the walls resulted in losses several times greater than the values used for design purposes, even though boundary layer bleed was used at the rotor tip and stator hub and tip. The high losses in the wall region increased the discharge axial velocity in the midspan region, and thus prevented the attainment of the high diffusion factors intended for these blades.

The effectiveness of the slots was evaluated on the basis of the blade element performance at five equally spaced radial locations between 10 and 90% of span. It was concluded that the deviation angle was not affected by the slot in either the rotor or stator. At midspan, the minimum loss coefficients were found to be on the lower side of the region describing the state-of-the-art in a loss parameter - diffusion factor plot. At hub and tip, the minimum loss performance of the slotted blades was not noticeably different from that with unslotted blading. The slotted blades were found to have an average unstalled incidence angle operating range approximately one-half to one degree larger than the unslotted blading tested in this program.

A direct comparison of the slotted and unslotted performance of Stator 1 (lowest camber stator) was made. At midspan, it was shown that the slot reduced the loss coefficient to approximately 40% of its unslotted value. This performance improvement did not exist near the

1

walls, where the slotted blading produced approximately the same loss as the unslotted blade. This direct comparison of the performance of this stator is considered to be the best indication of the effect of the slots, not only because of geometric similarity but also because the levels of inlet Mach number, incidence, and diffusion factor, as well as the spanwise distributions of these quantities, were nearly identical when tested with and without slots.

The relative effectiveness of the slots at midspan and their in-effectiveness near the wall are attributed to the chordal placement of the slots, the lack of effectiveness of the wall boundary layer bleed, and insufficient blade camber in the wall region. The blade camber distributions were based on the assumption that the slots and boundary layer bleed would result in the low loss in the wall region, an assumption which later proved optimistic. The combination of insufficient boundary layer bleed and blade camber at the walls led to large secondary flow and blade stall in the suction surface-wall region. The chordal location of the slot was based on theoretical calculations of the separation point and on midspan annular cascade data that indi-cated flow separation at 85% of chord, and thus did not allow for separation near the leading edge as was probably experienced in the region of the wall. As a consequence, the slot may have been located downstream of the separation point and may have been ineffective for that reason.

INTRODUCTION

The advancement of the state-of-the-art of compressor design by continued research on conventional blading concepts must be expected to provide continually diminishing returns. As a consequence, the NASA-Lewis Research Center is supporting experimental evaluations of unconventional blading concepts that may yield large improvements relative to those possible with conventional methods. These new con-cepts generally are based on methods that have found effective appli-cation in external aerodynamics. They include (1) new blade section profiles, (2) variable geometry blading, (3) blowing and suction control of boundary layers, and (4) slotted blading. The specific task herein reported concerns the evaluation of slotted blade sections in single-stage, axial flow compressors.

2

The employment of slotted (flapped) wing sections for maximum lift generation during aircraft approach and takeoff conditions is common practice. This application is not completely analogous with compressor aerodynamics because, during these flight conditions, the low lift-drag ratio attendant with the high lift slotted (flapped) wing is not a factor of primary importance. In the compressor application, the achievement of high lift at a low lift-drag ratio tends toward poor fuel consumption. This could be unattractive for installations other than those in which weight is the primary consideration, if other compensating influences did not exist. Another difference between these two applications is the greater importance of secondary flows in the compressor because of the large influence of the flowpath annulus walls. A third difference is that compressor applications require a much higher operational Mach number than exists during applications involving external aerodynamics. For these reasons, the effect of blade slots cannot be directly estimated from the available literature on isolated airfoil applications, and an evaluation in the environment of a highly loaded compressor is required.

The objective of this program was to explore the extent to which slotted airfoil sections could be used to extend compressor blade operating range and reduce compressor blade operating losses. This exploratory evaluation must include the interactions of slotted blades with other inflences peculiar to compressor aerodynamics to be meaningful. This consideration precludes obtaining final results from two-dimensional cascade testing, and, to a lesser degree, from annular cascade testing because of the lack of simulation of three-dimensional effects and rotor-stator interactions. A single-stage test program was therefore selected to simulate the largest portion of the three-dimensional flow effects without incurring the higher costs of complete, or multistage, duplication.

The scope of the single-stage testing was planned to determine the effectiveness of slots in extending the low-loss loading range of rotor and stator blades that are, in respects other than the slots and design loading, representative of current design practice. Thus, the size, clearances, aspect ratio, hub-tip ratio, solidity, tip speed, etc., were established within the region describing the state-of-the-art

of high pressure compressor design. The design loading, defined in terms of the diffusion factor, was arbitrarily selected to cover the region from 0.5 to 0.70 at the rotor tips and 0.60 to 0.75 at stator roots. The lower limit of this region is approximately the upper limit of current design practice. Within this framework, the three slotted rotors and three slotted stators were designed using annular cascade tests and theoretical calculations to provide the basis for establishing the slot conformation and location.

The testing of these stages was planned to provide blade element data for both rotors and stators at five radial positions, in addition to the overall or average stage and blade row performance. In evaluating the effectiveness of the blade slots on compressor performance, the more important data were expected to be those concerned with the blade element performance. This is because the average performance is largely limited by matching considerations, both radially within a blade row and also between the component rows. Experience with unslotted blading has shown that these matching problems are amplified as blade loading is increased and usually lead to a highly developed three-dimensional (rather than a nearly two-dimensional) flow.

The analysis and design, cascade testing, and the data and performance reports for the slotted blading tested are listed as References 1 through 8. The information presented in the above eight references is collated and discussed herein as required to evaluate the effectiveness of these slotted blade sections.

PRESENTATION OF PROGRAM RESULTS

The information generated during this program has been presented in eight reports and is concluded in this Final Report. The content and intent of the other eight reports are summarized in the following paragraphs:

Part I - Analysis and Design

The concepts employed in the aerodynamic and mechanical design of the three slotted rotors and three slotted stators are summarized in Reference 1, and tabulations of the geometric and aerodynamic quantities describing the blade rows and their as-designed operation are presented.

4

Part II - Annular Cascade Investigation of Slot Location and Geometry

The results of cascade tests of blades slotted at two chordal locations with a variety of slot configurations are presented and discussed in Reference 2. The selection of the best slot configuration is described, and the criterion for chordal location is established.

Parts III through VIII - Data and Performance

Each of these reports (References 3 through 8) contains a description of the testing of one of the six stages containing slotted blade rows. Overall and blade element performance data, both plotted and tabulated, are presented.

DESIGN SELECTION

General Approach

The selection of the rotor and stator blade rows was largely based on three considerations. The most significant of these was the loading (diffusion factor) range that was arbitrarily selected to place the blade rows at, or beyond, the current practice. This consideration is related directly to the program objectives of extending compressor operating limits. Secondly, the stator inlet and rotor exit conditions were to be nearly the same for all blade rows. This commonality was required to provide the option of testing any rotor with any stator. The final requirement is the broad one of designing these stages to be, in all remaining respects, typical of a middle stage in a multistage compressor.

The determination of the design velocity diagrams was initiated with an analysis of the requirements of the three stators. Within the desired hub diffusion factor range of 0.6 to 0.75 and the state-of-the-art stator exit air angle range of 0 to 30 degrees, it is possible, as shown in figure 1, to set the stator inlet air angle between 50 and 53 degrees, and all three stators can have the same inlet air angle, as required. Similarly, the region of possible rotor designs (figure 2) is fixed as a function of inlet guide vane exit air angle at an arbitrary tip speed within the requirement of a tip diffusion factor of 0.5 to 0.7 and the already established stator inlet air angle range. Because tip speed and inlet guide vane exit angle are related,

5

several values of tip speed were evaluated prior to making the selection of the best combination of inlet guide vane turning and tip speed. Other considerations, such as rotor and stator inlet Mach number, rotor turning angle, and inlet guide vane turning, were used to make the selection of tip speed.

Rotor and stator blading was selected from the NACA 65-Series airfoil sections because the performance of these sections is well documented, they have a good Mach number range, and their thickness distribution is sufficient to permit slots to be incorporated without grossly affecting the blade strength. NACA four-digit sections were used for the inlet guide vanes because of the lower inlet Mach number. These sections had their maximum camber at 40% of chord. The blade camber, incidence, and loss at the design point were selected using P&WA cascade data and were not compensated for blade-wall interactions. The deviation angle was determined from the correlation presented in equation 287 of Reference 9 for the unslotted blading, and the deviation was assumed to be halved for the blades with slots.

The configuration of the blade slots for slotted Rotor 1 is presented in figure 3. The cross section of the slot is typical of all three rotors and stators with the exception that slotted Stator 1 had increased radii at all points except that denoted r_2. Slots were located at 50% of chord in the rotors and 55% of chord in the stators, reflecting a small difference in their respective calculated separation points. The stator slots were located between 5% and 95% of span, and the slots in Rotors 1 and 2 between 5% and 45%, and 50% and 90%, of span from the tip. The slots in Rotor 3 extended from 5% to 45% and from 50% to 100% of span. Details of the slot configurations in each of the blade sets are presented in their respective "Data and Performance" reports (References 3 through 8). The suction and pressure surfaces of a typical slotted blade (Rotor 1) are shown in figure 4.

The slot geometry was selected from a series of 11 configurations of annular cascade blades that were tested for this purpose (Reference 2). Selection was based on achievement of the lowest wake pressure loss and the highest relative lift coefficient. During these tests, it was also noted that a slot in the midchord of the blade section was considerably more effective than one located closer (75% of chord) to the trailing edge.

6

Analytical estimates of the probable separation points on the program
blading were made and showed that flow separation was not expected ahead
of 72% of chord for any rotor, or 80% for any stator, at the midspan
location. Details of this analysis are presented in Reference 1. The
location of the slots was therefore selected as 50% of chord for the
rotors and 55% of chord for the stators. These locations were generally
consistent with the annular cascade tests and placed the slots approxi-
mately half of the distance between the theoretically determined minimum
pressure point and the predicted separation point. The latter criterion
was a compromise between locating the slot at the minimum pressure point,
where the pressure differential and thus the slot flow velocity would be
greatest, and just ahead of the expected separation point, where the
greatest effectiveness was anticipated, but where the small pressure
differential would produce only a low velocity slot flow.

Design Details

The three rotor and three stator blade rows were designed in accord-
ance with the procedures outlined in the preceding section. The selected
rotor tip and stator hub Mach numbers, turning angles, and loading levels
for these designs are listed in table I. Rotors 1, 2, and 3 were designed
for progressively higher loading, as were Stators 1, 2, and 3.

Table I. Selected Values of Slotted Blade Row
Aerodynamic Design Variables

	Inlet Mach No., M	Turning, $\Delta\beta$	Diffusion Factor, D
Rotor 1 (tip)	0.813	15.07	0.532
Rotor 2 (tip)	0.833	17.16	0.590
Rotor 3 (tip)	0.784	21.99	0.697
Stator 1 (hub)	0.644	23.53	0.596
Stator 2 (hub)	0.644	29.82	0.668
Stator 3 (hub)	0.644	42.14	0.763

A detailed presentation of the geometry and the design vector diagram
data for the six slotted blade rows is contained in Appendix A. These
latter data are listed for the unslotted blading and for the slotted
configuration. The differences arise solely from the assumption that
the slots will reduce the deviation angle by one-half. The values of
deviation angles listed in Appendix A are the full NASA deviation.

7

Information relating to the design of the various inlet guide vanes and the Flow Generation Rotor (FGR) has not been included herein because it is not of direct concern to the fulfillment of the program objectives. This information is contained in Reference 1.

RIG AND INSTRUMENTATION DESCRIPTION

Test Facility

The compressor test facility utilized during this program is powered by a single-stage turbine driven by the exhaust of a P&WA JT4 (J75) aircraft gas turbine engine. This exhaust gas is also used as the primary gas stream of a two-stage ejector that provides the suction required for the compressor rig wall boundary layer removal and induces the flow through the annular cascade rig.

The compressor airflow is induced from atmosphere through a long inlet duct containing an ASME orifice for primary flow measurement. A plenum chamber is located directly upstream of the compressor rig to ensure uniform inlet conditions. A schematic drawing of the facility is presented in figure 5. The annular cascade rig and the compressor test rig were installed in this facility.

Annular Cascade Rig

The annular cascade rig consisted of a bellmouth inlet, support struts, inlet guide vanes, test stators, and an exhaust diffuser section, as shown schematically in figure 6. Inner and outer wall diameters at axial stations of interest are tabulated in the figure. The desired gas path was formed by fabricated wooden filler sections. A split test case provided convenient accessibility for blading changes without removal of the entire rig from the test stand.

The test section had a hub/tip ratio of approximately 0.8, and was comprised of a row of 50 inlet guide vanes that set the stator inlet conditions and a row of 20 test stators that turned the flow back to the near-axial direction. The inlet guide vane and stator blade row assemblies were each divided into two 180-deg sections. The guide vanes were fabricated from stainless steel and tack-welded to the shrouds. The stator and stator shrouds were fabricated from aluminum, and the stators were positioned with dowel pins and held in place with machine

8

screws. For the slotted stator tests, only the vanes in the upper
180-deg section were slotted.

Compressor Test Rig

The compressor rig consisted of the bellmouth inlet, test section,
and exhaust section. A section view of the rig is shown in figure 7.
The test section has a hub/tip ratio of 0.8 and a rotor tip diameter
of 40.48 in. The rotor assembly and shaft are supported on two bearings
that transmit loads to the outer case through struts located in the
inlet and exhaust case assemblies. The test section has a split outer
case that permits guide vane, rotor, and stator assembly changes without
removing the rig from the test stand. A set of motor-driven throttle
vanes is located in the exhaust section to vary flowrate. Flow is
accelerated through the inlet strut station and guide vanes in a con-
vergent passage to the rotor inlet. Thereafter, the inner wall diameter
remains constant at 32.85 in., while the outer wall converges further
through the rotor blade and stator vane rows to a diameter of 40 in.
In general, the flowpath simulates that of a middle stage of a state-of-
the-art multistage compressor.

Provisions were made for flow to be bled at the rotor tip and stator
hub and tip, as shown in figure 7. Bleed air flowed through perforated
plate shrouds, shroud manifolds, and 24 approximately equally spaced
tubes to individual main collector manifolds for the rotor and stator.
The collector manifolds were exhausted through the facilities ejector
system. Rotor and stator bleed flowrates were controlled and measured
separately.

Instrumentation

Variations were made in the instrumentation used for the various
tests, and, therefore, the pertinent data and performance reports should
be reviewed if a detailed description of the instrumentation is required.
The general configuration of the instrumentation is provided herein.
Descriptions of peripheral instrumentation, such as bleed flow measure-
ments, rotor speed, and rig operation instrumentation, have been omitted
for the sake of brevity.

Compressor flowrate was measured with a thin-plate orifice in the inlet duct, and compressor inlet pressure and temperature were recorded from measurements in the inlet plenum chamber. In addition, wall static pressure was measured upstream of the inlet guide vanes to permit calculation of the flowrate at that location as a check on the orifice flow measurement system.

Measurements of data used for calculation of blade element and overall stage performance were made in a quantity sufficient to provide a representative average value or, in the case of blade element data, to permit the determination of performance at 10, 30, 50, 70, and 90% of span. The axial locations of the instrumentation stations are shown in figure 7.

Inlet guide vane and stator performance was determined by (1) measurements of discharge total pressure using pitot-type wake probes (figure 8) of sufficient size to encompass the vane wake and (2) traversing yaw probes radially across the passage to determine flow direction. Static pressure was measured at all instrumentation stations at both inner and outer walls and, where radial gradients were substantial, 8-deg wedge static pressure probes (figure 8) were traversed across the passage.

Downstream of the rotor, Kiel-type probes were provided to measure total pressure and both 20- and 8-deg wedge traverse probes were used for measurement of total pressure and temperature, flow direction, and radial static pressure distribution. Probes containing high frequency response pressure transducers and hot film anemometers were located at this station for those tests requiring determination of the size and relative motion of rotating stall cells and the size and shape of rotor wakes.

The primary measurement of stage discharge temperature was made with an array of Kiel-type instruments downstream of the measuring station used for stator blade element performance instrumentation. The primary measurement of stage discharge pressure was made with the stator wake rakes.

RESULTS AND DISCUSSION

The complete aerodynamic design of an axial flow compressor is usually the result of the assembling of detailed designs for the numerous

10

blade elements that comprise each blade row. The design analysis is accomplished by calculating performance at sufficient radial locations so that the envelope of these blade elements is a good description of the three-dimensional blade. The two factors of greatest interest in analyzing the relative merits of the different blade elements that could be used to accomplish any given aerodynamic goal are minimum loss and unstalled incidence angle range. A low level of minimum loss is highly desirable from an efficiency standpoint; however, the blade row must operate over a range of inlet angles in nearly all applications. The useful operating range is the more important consideration because it is a measure of the ability of a blade section to tolerate deviations from the design velocity vector without causing large increases in loss or contributing to compressor instability. These deviations from design conditions become increasingly acute as the number of stages is increased. Consequently, a multistage compressor of six or more stages will often be designed with front stages operating near negative stall (or choked) and the rear stages near to stall in an effort to provide compensation for off-design operation. Even when the matching is compromised in this fashion, the front stages will tend to operate near stall, and the rear stages near choke, during part speed operation and engine starting, the reverse of design point operation. Thus, useful operating range becomes the primary blade element criterion for the evaluation of the performance of slotted blading, although the minimum loss level will also be considered.

Overall Performance

Rotors

The three slotted rotors were tested as part of the following stages:

Slotted Rotor Stages

IGV	Rotor	Stator
1	1	1 (Unslotted)
2	2	1 (Unslotted)
3	3	2 (Slotted)

The performance of the three rotors and their respective inlet guide vanes is presented in figure 9, along with the design goals. For this presentation, the design rotor speed data have been normalized into

11

ϕ - ψ plots to account for the different tip speeds of these stages. (Symbols are defined in Appendix D.) The design goals shown are based on full NASA deviation because the original design assumption that the deviation would be halved by the addition of slots was found to be invalid, as will be noted from the following discussion of blade element data. The three slotted rotors and their respective inlet guide vanes exhibit a common characteristic in that all fell short of achieving their design pressure coefficients at design flow coefficient. This is primarily due to the highly three-dimensional character of the flow field when compared with compressor stages designed to state-of-the-art loading. Typically high loss regions are observed in the flow at one or both walls, resulting in a decrease in exit axial velocity in the high-loss region and an increase in exit axial velocity throughout the remainder of the blade span. The overall rotor pressure ratio is lowered both because of high losses in the wall region and because of the low midspan work input induced by the axial velocity ratio, V_{z2}/V_{z1}, being significantly greater than design. The lowered work capacity is implied in the data presented in figure 9 because both slotted Rotors 1 and 2 achieved their design efficiency even through the design pressure ratio was not met. (The power required for pumping the wall bleed flow was not considered in any of the efficiency calculations.) A loss of efficiency with increased design rotor loading may be noted, and the most highly loaded rotor was approximately 6 points lower than its design goal. Unusually high efficiency is indicated for slotted Rotor 3 at low pressure coefficients. This high efficiency is unexplained and must be viewed as questionable. Because the slots were expected to materially reduce separation and because boundary layer suction was employed at rotor tip and stator hub and tip, it was assumed in the design that loss coefficients close to their rectilinear cascade values would be attained throughout the blade span. These data indicate the possibility that this assumption was optimistic. Further discussion of this characteristic is presented in the paragraphs dealing with the blade element performance.

Slotted Rotor 2 has a substantially lower stall margin (referenced to the design point) at design equivalent rotor speed than do slotted Rotors 1 and 3 as shown on the next page.

12

Rotor	*Stall Margin,%
1	15
2	1/2
3	7

Further, as shown in figure 9, the performance of slotted Rotor 2 exhibits a significantly lower ϕ - ψ slope in the region of design flow coefficient. Taken collectively, the performance of this rotor does not comprise an orderly progression with that of the other two slotted rotors but rather has a lower pressure rise characteristic and a low stability limit. Because the efficiency of slotted Rotor 2 is reasonable in comparison to the other rotors, it is expected that the nonconforming characteristic of slotted Rotor 2 is attributable to its ability to work on the fluid.

For an axial flow, this work may be expressed:

$$\Delta h \propto (U_2 V_{\theta 2} - U_1 V_{\theta 1}) \text{ or when } U_2 = U_1$$

Equations 1

$$\frac{\Delta h}{U^2} \propto \frac{(V_{\theta 2} - V_{\theta 1})}{U}$$

The tangential velocities may be expressed in terms of the flow direction and the axial velocity component as follows:

$$V_{\theta 2} = U - V_{z2} \tan \beta_2'$$

Equations 2

$$V_{\theta 1} = V_{z1} \tan \beta_1$$

The airflow direction may in turn be expressed in terms of the appropriate deviation angle and meanline direction, thus:

$$V_{\theta 2} = U - V_{z2} \tan (K_2' + \delta_2^\circ) \quad \text{rotor}$$

Equations 3

$$V_{\theta 1} = V_{z1} \tan (K_2 - \delta_2^\circ) \quad \text{IGV}$$

---

*Stall margin $\equiv \dfrac{(P_2/P_0)_{stall}}{(P_2/P_0)_{design}} \times \dfrac{W\sqrt{\theta}/\delta_{design}}{W\sqrt{\theta}/\delta_{stall}} - 1.0$

13

Combining Equations 1 and 3 and substituting the flow coefficient $\phi_1 \equiv V_{z1}/U$ leaves:

$$\frac{\Delta h}{U^2} \propto 1 - \phi_1 \left[\frac{V_{z2}}{V_{z1}} \tan(\kappa_2' + \delta_2^\circ)_{rotor} + \tan(\kappa_2 - \delta_2^\circ)_{IGV} \right]$$

Thus at design flow coefficient, the normalized work input may be expressed in terms of the rotor axial velocity ratio, the inlet guide vane and rotor deviation angles, and the guide vane and rotor metal angles.

Inspection of the inlet guide vane deviation angle data indicates that the deviation does not vary greatly with flow and may be assumed constant. The remaining variables, V_{z2}/V_{z1} and $\delta_2^\circ{}_{rotor}$, are presented in figure 10 as functions of the flow coefficient for the midspan location of each rotor. Comparison of the axial velocity ratio curves for the three rotors reveals that the slope becomes negative, indicating a work reducing trend as stall is approached for each of the rotors. The inflection point is reached at a more negative incidence for the rotors with increased design diffusion factors; however, the data do form a consistent family and no large anomalies are noted. This consistency is not true of the rotor deviation data presented in figure 10. The slotted Rotor 2 deviation increases sharply with decreasing flow as stage stall is approached and is unique in this respect. This unexplained increase in deviation was the primary cause of the drooping characteristic of slotted Rotor 2.

Stators

The three slotted stators were tested using the same FGR and inlet guide vane to supply airflow. The overall performance of the three stages, each comprised of inlet guide vane, FGR, and slotted stator, is presented in figure 11 using the same format as the overall rotor data. Although achievement of a stage pressure ratio higher than the design point is indicated for slotted Stators 1 and 2 and the stage pressure ratio of slotted Stator 3 closely approaches its design goal, the performance is due to the unusually high pressure ratio produced by the FGR. As noted in Reference 6, this pressure rise is attributable to

14

a high inlet guide vane deviation angle, low rotor deviation angle, and low rotor losses. Stage efficiencies are lower than design and form a progression, indicating reduced efficiency with increased stator diffusion factor. The absolute level of efficiency for these stages is of little importance in evaluating the performance of the slotted stators because the loading level of the FGR is not commensurate with that of the stators. Therefore, the stator losses have a disproportionately large effect on stage efficiency.

Blade Element Performance

General

Blade element performance data are available at 10, 30, 50, 70, and 90% of blade span (measured from the tip) for all rotor and stator configurations tested. These data are presented in tabular and plotted forms in the appropriate data and performance reports (References 3 through 8), and, therefore, no general presentation of these data is required herein. The objective of this section of the report is to segregate and discuss those blade element data considered most pertinent to the performance of slotted blade elements.

The variable that is primarily used to correlate or compare blade losses is Lieblein's diffusion factor (Reference 10). Because by definition and usage the diffusion factor is associated with blade element flows in which the effects of high relative inlet Mach number of performance are not present or considered, it is first necessary to examine the data in this regard and eliminate those data that are nonconforming. One method of accomplishing this elimination is to review the blade element loss-incidence characteristics taken at the various rotor speeds and corrected airflows and observe if, and at what conditions, a rapid rise in minimum loss coefficient occurs that may be attributed to the attainment of locally supersonic flow within the blading. This method is subjective but useful because it will serve to eliminate those data that appear to be affected by shock losses.

In rendering the judgment, the data for all five spanwise locations were viewed collectively to determine if a loss coefficient increase with increasing rotor speed was general, i.e., across the span, or local.

15

The latter was not considered to be evidence of Mach number effects but
rather is attributed to secondary or three-dimensional flow. These
flows, which are observed to be strong in these relatively highly loaded
blade rows, have a substantial effect on blade element performance. In
addition, it should be noted that the concept of "blade element performance"
is derived from two-dimensional compressor cascade analysis. The application
of the concept to single stage compressor analysis to tenuous because of
the changing three-dimensional nature of the flow. As a result, the
"blade element performance" is not only dependent on incidence and rela-
tive inlet Mach number (as in the case of the two-dimensional cascade),
but is also dependent upon numerous other variables descriptive of the
three-dimensional flow.

A second approach to the elimination of these effects is to compare
the value of relative inlet Mach number, calculated from the data, with
the predicted value of the limiting Mach number for the blade element
being considered. A P&WA correlation of the limiting or critical Mach
number based on cascade data was used for this purpose. To provide maxi-
mum assurance that high relative inlet Mach number effects are excluded,
these methods were used to disqualify data. The highest corrected rotor
speed for which the data are judged to be free of these effects is tab-
ulated in table II. Except as specifically noted, the discussion of
blade element data refers to speeds at or below those listed.

Table II.   Sub-Limiting Mach Number Data

Slotted Rotor 1	100% $N/\sqrt{\theta}$
Slotted Rotor 2	*70% $N/\sqrt{\theta}$
Slotted Rotor 3	90% $N/\sqrt{\theta}$
Slotted Stator 1	100% $N/\sqrt{\theta}$
Slotted Stator 2 (with FGR)	100% $N/\sqrt{\theta}$
(with slotted Rotor 3)	100% $N/\sqrt{\theta}$
Slotted Stator 3	100% $N/\sqrt{\theta}$

*90% $N/\sqrt{\theta}$ data were not taken.

Design Incidence Performance

The performance of the elements of the three slotted rotors and
three slotted stators operating at design incidence is presented in

16

figures 12 through 17. The data for each blade configuration were summarized from the curves presented in the pertinent data and performance report (References 2 through 8) and represent a condition that was not simultaneously achieved at all spanwise locations. Particularly for Rotors 2 and 3, the most conspicuous single characteristic of these data is the high-loss coefficient in the vicinity of the walls, even though the incidence is near the expected minimum loss value.

High losses near the walls were not expected because a boundary layer bleed of approximately 1-1/2% was employed at the rotor tip and at both stator walls, and because the slot was expected to maintain a more nearly two-dimensional flow in the blade row. The boundary layer bleed flow was withdrawn through a porous plate of 5% open area consisting of 0.078-inch diameter holes on 0.35-inch centers. The relatively widely spaced, large holes were not as effective in maintaining a thin boundary layer as would be closely spaced holes of small diameter.

In the midspan region, both rotors and stators have a conventional trend toward increasing loss coefficient with increasing diffusion factor (figure 18); however, the stators are shown to have a higher loss level and a somewhat larger rate of increase with diffusion factor than the rotors. The deviation data show reasonably good correspondence with the design deviation near midspan, but also show substantial departure in the wall region, generally toward increased deviation. This trend toward increased deviation at the walls is not directly indicative of a strong secondary flow because such a flow is expected to result in low deviation near the walls rather than high deviation. The effect of the secondary flow on loss coefficient, however, is not in direct proportion but may be amplified when the wall boundary layer circulates onto the blade suction surface and causes separation. When this occurs, high losses in the wall region will be noted, and an increase in deviation may also be noted due to a reduction in lift caused by the separation.

The flow directions at the design points of the six blade rows (based on full NASA deviation) are presented in figure 19 for both the tip and hub regions. These data are shown in a β_1 vs β_2 (or β_1' vs β_2') plane, and the region bounded by the loci of points at which $\cos\beta_1/\cos\beta_2 = 0.72$ is indicated. This ratio is proposed by DeHaller

17

(Reference 11) as the limit of operation without wall stall. Design values of this ratio for all blade rows fall in or near the region of potential wall stall. Because these blade rows were designed as extensions of the state-of-the-art, it is not unusual that they fall in this region. Of course, the employment of slots and the use of wall boundary layer removal were expected to reduce the onset of wall stall.

The controlling influence of the flow in the wall region may be illustrated by comparing the hub, mean, and tip section loadings and their relative rates of loading increase as the various slotted blade stages were operated at a constant rotor speed. The hub (90% of span) and tip (10% of span) diffusion factors are presented in figures 20 through 26 as functions of the midspan diffusion factor for the six slotted blade rows. The data for slotted Rotor 1 (figure 20) indicate that at low loading (stage throttle valve is wide open) the spanwise loading distribution is fairly uniform, with the hub loading slightly greater than that at midspan and the tip loading slightly greater than that of the hub. As the stage is back-pressured with the throttle valve, the midspan, hub, and tip diffusion factors all increase by approximately the same amounts, as evidenced by the slope of both the hub and tip characteristics being close to 1.0. As loading is further increased, however, the slope of these curves also increases, indicating that a greater portion of the additional loading is being imposed in the wall regions. In the case of slotted Rotor 1, this trend is especially noticeable in the hub region. The existence of the relatively high loss regions near the walls, previously noted, causes a reduction in the blade discharge velocity in these regions and thereby leads directly to increased loading, as indicated by the diffusion factor. Continuity of flow necessitates higher velocities in the midspan section at the rotor discharge, thus tending to lower the blade loading. Because the blade element loss coefficient is, to a first order approximation, dependent upon the diffusion factor, the wall losses are further increased and the midspan losses decreased. This progression, ultimately leading to the stalling of the stage, is defined as wall stall (Reference 12).

In the case of slotted Rotor 2 (figure 21), the hub and tip characteristics are slightly different from those of slotted Rotor 1. As

18

in the former case, the hub section loading rises at a greater rate than that at midspan; however, the tip characteristic displays a tendency toward a lower slope as stall is approached. This tendency is caused by the hub high-loss region becoming so large as to start unloading the tip region in addition to the midspan region. The wall regions at both hub and tip of slotted Rotor 3 (figure 22) progress into stall simultaneously. This trend was augmented by the midspan blade element matching because the midspan was close to reference incidence as the hub and tip stalled. It may be noted that the slope of these curves is becoming almost vertical at stall; thus further increases in overall rotor loading are being borne entirely by the wall regions.

The characteristics of the three slotted stators were strongly influenced by the flow field of the Flow Generation Rotor, as shown in figure 23. The FGR shows a strong tendency to stall at the tip. At the hub, the unloading tendency noted at the tip of slotted Rotor 2 is again evident. The performance of the slotted stators is affected by the flow distribution leaving the FGR because the stator incidence increases downstream of a stalled region of the rotor.

All three slotted stators (figures 24 through 26) have steep tip characteristics at stage stall, reflecting the condition of the tip flow leaving the rotor. The hub section of slotted Stator 2 has a negative slope, largely due to an unexplained reduction in loss as incidence increased.

The fact that these characteristics are related to the spanwise matching of blade elements within a blade row and of the relative matching of blade rows is evident in figure 25. The data for the test of slotted Stator 2 with slotted Rotor 3 indicate a more orderly uniform approach to stage stall than do the data with the FGR. This may be attributed to the relative balance between hub and tip noted for slotted Rotor 3 while the FGR had a markedly stalled tip section.

Viewed collectively, these data indicate a general trend toward high wall loading and low midspan loading that is attributable to the low velocities near the walls as a result of losses considerably higher than the design losses. The design losses were predicated on the achievement of quasi-two-dimensional flow through the use of the slots and the

19

employment of boundary layer bleed. It is evident from these data that improvements in the boundary layer bleed and increased slot effectiveness in the wall region are required to permit attainment of the design loss distribution.

Comparisons of Unslotted and Slotted Blading Performance at Minimum Loss

The minimum loss coefficient or reference incidence angle performance of the slotted blading is presented in figures 27 and 28. The data were derived from curves of loss coefficient, deviation, and diffusion factor representing the data at and below the corrected wheel speeds listed in table II. A complete summary of these minimum loss data is contained in Appendix B for reference if required. The form of this presentation has been made similar to that used in figure 192 of Reference 9, and the NASA data presented in the referenced figure have been included in figures 27 and 28 in the form of a dashed curve representing the NASA 2D cascade correlation and an outlined region representing the envelope of the data for 22 NASA stages. In this way, the NASA compressor stage experience and correlated cascade data may be conveniently compared with the results of this program.

All of the rotor data are within the region of experience with un-slotted rotors except that the midspan of slotted Rotor 3 exceeded the highest loading for which data are presented in Reference 9. The value of the loss parameter (0.023) attained at this loading (D = 0.6) rep-resents some cause for optimism concerning the performance of highly cambered and loaded slotted blading because it indicates performance on the low-loss side of an extrapolation of the data band of Reference 9. It is also evident that the low loss parameter associated with slotted Rotors 1 and 2 in the midspan region, when compared with the data of Reference 9, further strengthens the conclusion that the slots may be producing a beneficial effect on loss in the absence of large secondary (wall) flow effects.

The data representing stator hub performance (figure 28) indicate losses substantially above the reference level with the exception of that for the slotted Rotor 3/slotted Stator 2 test. Stator tip losses are large and the data exhibit a high degree of scatter, making com-parison with the extrapolation of the data of Reference 9 difficult.

20

It is certain, however, that no benefit from the slots is evident at the stator tip as well as the stator hub. As in the case of the rotors, the midspan performance is noticeably better than that in the wall region. Of the three slotted stators, Stator 2 produced the best performance. The loss data representing the tests of slotted Stator 2, both with slotted Rotor 3 and with the Flow Generation Rotor, are slightly below the region of Reference 9 data.

Taken collectively, these minimum loss coefficient data indicate the slotted rotor performance to be generally typical of unslotted rotors in the tip and hub regions and slightly better than unslotted in the midspan region. Similarly, the slotted stators show better than average (unslotted) performance at midspan with progressively poorer performance at the tip and hub, respectively. Both rotors and stators display strong spanwise performance gradients with poor performance near the walls and good midspan performance. At midspan, some indications of performance improvement due to the slots are observed, but clear conclusions cannot be drawn until the wall region performance is improved and higher loading achieved.

Comparisons of Slotted and Unslotted Blade Incidence Range

The range of incidence angles over which a blade element is capable of unstalled operation is a highly significant variable because it directly affects the compressor stall line and indirectly, through stage matching compromises, affects compressor efficiency. The slot was expected to permit a blade element to operate unstalled at higher incidence angles than the unslotted blade and thus result in increased range of operation. During operation at negative incidence angles, the slot flow could tend to have a detrimental effect on the flow over what is normally the pressure surface of the airfoil and may promote separation and reduce operating range. This effect was expected to be minor because of the small pressure difference available to produce a slot flow at low incidence angles and because the orientation of the slot is unfavorable to the production of slot flow under this condition. Hence, the net effect of the slots was anticipated to be an increase of range and a displacement of the operating range to higher incidence and thus to higher diffusion factor.

21

The determination of the effect of the slots on operating range is difficult because of the lack of comparative data for unslotted blades operating in compressor stages. For this reason, the comparison presented herein is with the range predicted for unslotted blading by a proprietary P&WA correlation of compressor cascade data. A limited amount of available unslotted blade element data for the contract blading is also included to provide information on differences between cascade and stage data as well as direct comparison between slotted and unslotted blading. Operating range has been defined, for this comparison, as the incidence range in which the loss coefficient is within 0.04 of the minimum value at a constant relative inlet Mach number. The mean value of this Mach number for each speed line was used for the stage blade element data at each spanwise location.

The cascade prediction and the range data for slotted Stator 2 at 50% of span are presented in figure 29, which illustrates this comparison. The ordinate scale is the blade element incidence range as defined in the foregoing paragraph. The trend toward decreasing range as relative inlet Mach number is increased is apparent from these data and is closely that predicted from the cascade data. The scatter in the data is, however, sufficient to make a conclusion as to the effect of the slot on range difficult in this case.

Similar information for all configurations for which a clearly defined incidence range was discernable from the data (without extrapolation) is summarized in figure 30. Although the range itself is strongly dependent upon relative inlet Mach number, it may be noted from this figure that the difference between the observed (data) and predicted (cascade) ranges is not Mach number dependent. Furthermore, no correlation of this difference with spanwise location is apparent from the limited data available. The average difference between the observed and predicted range is +1.3 degrees, indicating a larger range for the slotted blading than predicted from unslotted cascade results. The unslotted blade data from this program, although sparse, average 0.7 degree larger range than the cascade prediction. Thus, both exhibit more range than predicted and the slotted blading shows 1/2 to 1 degree larger range than the unslotted blading. The result cannot be construed as conclusive, how-

ever, because of the data scatter apparent and the paucity of unslotted blade data directly comparable with that of the slotted blades.

Performance of Stator 1 With and Without Slots

Stator 1 was used in three of the six stages tested in this program and is the only blade row which was operated extensively both with and without slots. For this reason, the most direct determination of the effect of the slots is available through analysis of Stator 1 performance. The three stages to be considered are:

IGV and Rotor	Stator
Slotted Rotor 1	Stator 1 (Unslotted)
Slotted Rotor 2	Stator 1 (Unslotted)
Flow Generation Rotor (FGR)	Slotted Stator 1

The two sets of blade element data for Stator 1 without slots differ considerably because of the different inlet flow field generated by slotted Rotors 1 and 2. The selection of the data to be compared with the slotted stator data was based on the similarity of stator incidence and Mach number and in the radial gradients of these two quantities. The stator incidence and Mach number distributions are given in figure 31 for these three stages at their design rotor speed and near zero incidence. It is readily observable that the incidence and incidence gradient of the unslotted stator during the test with slotted Rotor 1 closely corresponds to that of the slotted stator during tests with the Flow Generation Rotor. The maximum difference is only about one degree. During the test with slotted Rotor 2, a substantial gradient of stator incidence is noted, with the hub and tip region about eight degrees of incidence closer to stall than the midspan blade element. This marked difference in incidence distribution is expected to have a strong influence on the radial flow and loading distribution and thus will complicate comparisons with the slotted stator. The inlet Mach number, while of less importance, also indicates that the most direct comparison of slotted stator performance is with the unslotted data of the test with slotted Rotor 1. For these reasons, the comparison is made between these two data sets.

The radial distributions of loss coefficient, deviation angle, and

diffusion factor are presented in figure 32 for Stator 1 both with and without slots. The data points used for this comparison were selected at different inlet corrected airflows to produce a stator incidence angle close to zero in both cases. The loading and deviation distributions are substantially the same; however, the loss coefficient of the slotted configuration is substantially lower (0.05 vs 0.13) than that of the unslotted blade in the midspan region. These data provide a direct measure of the beneficial effect of the slots because of the similarity of the inlet Mach number, incidence,and loading. Near both walls (10 and 90% of span) this improvement in performance due to the slots is not evident and the loss levels are virtually identical.

A second comparison of blade element performance for this stator in these two stages was made near stall and is presented in figures 33 and 34. The incidence angles for the two data sets are not as well matched as those near zero incidence but only diverge near the hub. The loading and loading distribution, an important factor, are nearly the same; higher deviation is noted for the slotted blade near the walls, particularly the hub. This trend toward high deviation for the slotted blade is also evident at the lower incidence angle (figure 32). At midspan, a small improvement in deviation is evident. The midspan loss of the slotted configuration is signficantly lower than that of the same unslotted blade, confirming the midspan improvement shown at the lower incidence of figure 32. At the walls,this improvement was not realized.

In analyzing the data for these tests as presented in the data and performance reports, it was found that the blade element loading tended to be inconsistent with the turning, incidence, and loss coefficient. These inconsistencies are attributable to the measurement of static pressure and are also manifested in differences between the measured and integrated weight flows, as noted in these reports. The diffusion factors used in the foregoing comparisons were determined by scaling the velocities at the stator inlet and discharge as required to match the integrated flows with the measured flows. In scaling the vector diagrams, it was assumed that the density remained constant and that the stator inlet and discharge air angles were unchanged. The axial

24

velocities were then changed in the ratio of the measured flow to the integrated flow.

Comparison of Annular Cascade and Single-Stage Testing

The data from the annular cascade tests of slotted blades (Reference 2) provided clear evidence of the ability of slots to reduce the loss coefficient. The best slot configuration was found (figure 35) to reduce the midspan loss coefficient from a value of 0.071 (unslotted) to a value of 0.012 (slotted). With these data in mind, dramatic changes in performance were expected for the slotted blade compressor stages. In fact, the observed performance of these stages is not primarily controlled by the effect of the slot, but rather, the effect of the slot is quite tenuous. The preceding portions of this discussion of slotted blade element performance have shown that the slots do tend to increase the blade unstalled operating range and reduce the minimum loss coefficient. Further noticeable improvement has been shown for slotted Stator 1 compared with the same stator without the slot. These beneficial effects, however, have been noted in the midspan region but not at the walls. Furthermore, it has been noted that very large losses were incurred in the wall region in spite of the employment of boundary layer bleed on rotor tip and stator hub and tip walls. Thus the favorable performance of the slots in the cascade is similar to the midspan effects noted during the test of the single-stage compressor. A comparison of the slotted and unslotted annular cascade and Stator 1 data at midspan is presented in figure 36 in the format used for figures 27 and 28. Both sets of data show substantial improvement, in the form of reduced losses, due to the slots. The magnitude of the improvement shown for Stator 1 exceeds the improvement of the annular cascade slightly. However, the losses of the unslotted stator were much larger than those of the unslotted annular cascade blading, and thus the percentage change is not so great as for the cascade blade.

The fact that the annular cascade data qualitatively forecast the results of the stage test of slotted blades at midspan may be expected because of the geometric similarity. It is equally obvious that the blade elements in the compressor wall regions were not beneficially affected by the slot and thus that the cascade test was not typical of this region.

25

This may have resulted from the selection of the chordal location of the slots in the subject blade rows on the basis of the annular (midspan) cascade data. The influence of the secondary flow on the performance of compressor blading in the wall region has been widely documented (e.g., References 11 and 12) and leads to separation in the corner between the wall and blade suction surface. This separation is shown in figure 37, which presents a lampblack trace of the boundary layer flow in cascade. In figure 37, the separation is shown to occur on the suction surface at about 30% of chord at the wall and to progress somewhat linearly to the trailing edge at midspan. This results in the possibility that the chordal location of the blade slots for these tests was correct to suppress separation in the midspan locations because the location was so defined by the annular cascade tests. Under the influence of the secondary flow, however, the separation point was forced much closer to the leading edge in the wall region. The slot, at the same chordal position as at midspan, was consequently located well behind the separation and was ineffective.

Stalled Operation of Slotted Rotors

The stall of these stages was characterized as an abrupt development of a single rotating stall cell, as described in References 3 and 4. This cell comprised approximately one-half the flow annulus and rotated at 20% of the rotor speed relative to the compressor case. This relatively low angular velocity implies a relatively high angular velocity of the stall cell relative to the rotor blading (i.e., 80% of wheel speed). Following the onset of rotating stall, the pressures within the compressor become highly nonsteady, indicating that flow reversal (surge) probably occurs. High stresses were developed at this time, thus precluding steady-state stalled operation of the compressor rig. The abrupt stall may be a characteristic that is accentuated by the blade slots because the presence of the slot will tend to surpress separation on the blading until, at high loading, the separation point finally moves upstream of the slot, at which time the slot loses its effectiveness and the blade operates like an unslotted blade in deep stall.

CONCLUDING DISCUSSION

The discussion of the results of this program leads to three major conclusions.

First, it may be concluded that the slots are capable of reducing the loss incurred by highly cambered blades in the midspan region. This conclusion is based on (1) the results of the annular cascade tests, (2) the comparison of data with and without slots for Stator 1, and (3) the comparison of loss parameter, as a function of loading, for the slotted airfoils and the experience level reported in Reference 9 for unslotted blades.

The second conclusion is that a trend toward a larger unstalled operating range for slotted blades than for conventional blades is evident from these data. The uncertainty in establishing the unstalled operating range of a blade element from the data is of the same order of magnitude as the improvement and, thus, a statistical evaluation of this potential benefit is required. Although the unstalled operating range of the slotted blading of this program averaged 0.6 degree more than the unslotted, the number of data points available was not sufficiently large to permit a definite conclusion.

The third conclusion is that the secondary flow and associated wall stall were major factors in the performance of all of the program blade rows. High losses were incurred near the walls, probably as a result of substantial suction surface separation, and the slots had no apparent beneficial effect in this region, nor did the wall boundary layer bleed. This poor performance in the wall region led to radial flow components toward midspan and unloaded the center section of the blading, thus preventing achievement of the program goals with regard to loading level. The classical effect of the secondary flow is to induce separation in the corner formed by the suction surface and the wall. Because the slot location was based on midspan data from the annular cascade tests, it is likely that the slot was behind the separation point near the wall and was not effective for this reason.

The poor performance in the wall region was probably enhanced by the selection of anticipated losses during the design phase. This

27

selection was based on achievement of low (slightly above cascade) losses as a result of the slots and the use of boundary layer bleed to effectively eliminate wall induced losses. As a consequence, insufficient blade camber was present in the wall region to maintain a relatively uniform total pressure profile for the level of end wall losses that actually occurred. The occurrence of a relatively low pressure rise at the walls led to low flow and high incidence and thus had a compounding effect on loss.
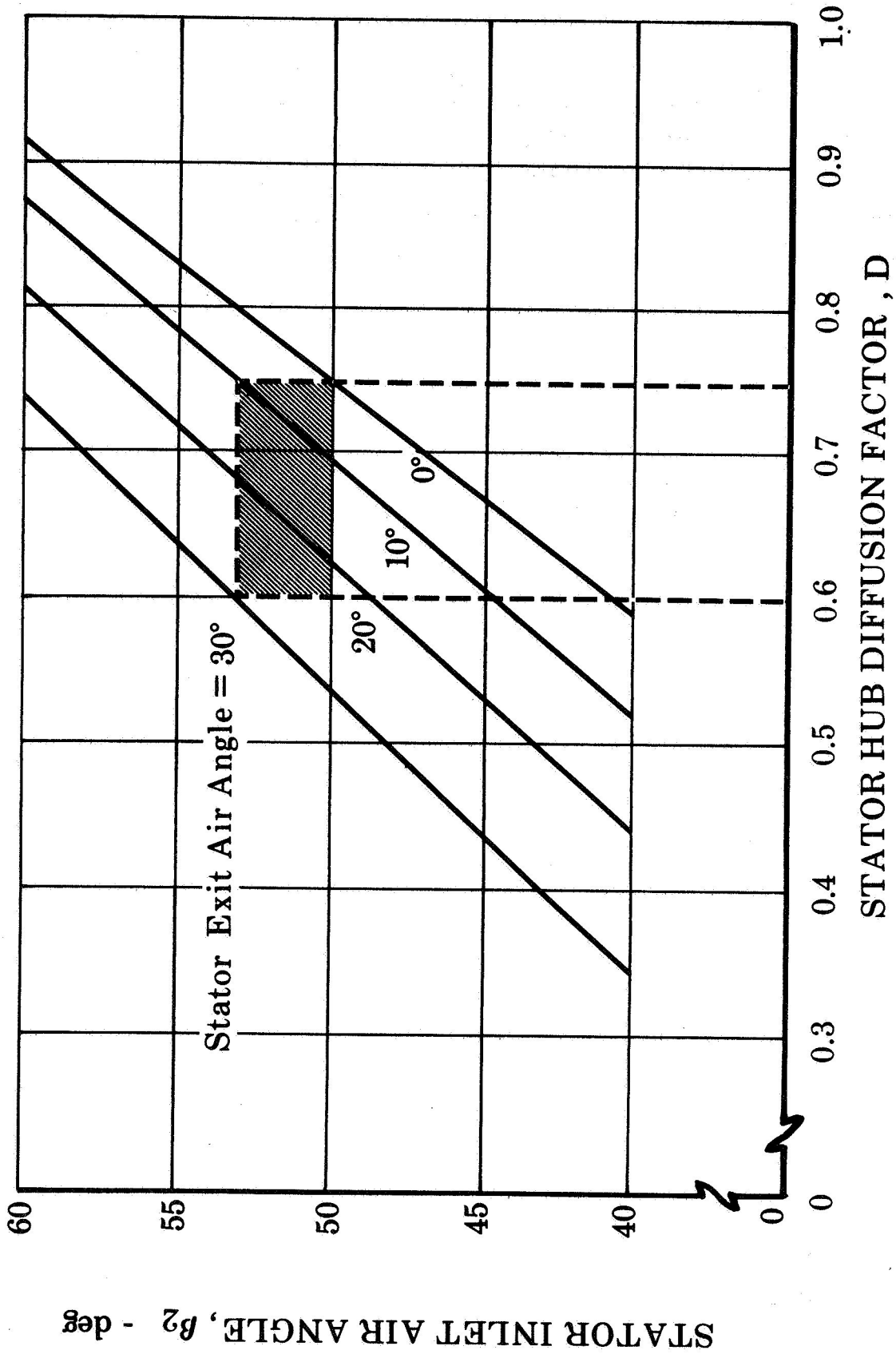
Figure 1. Variation of Stator Hub Loading With Inlet and Exit Air Angle
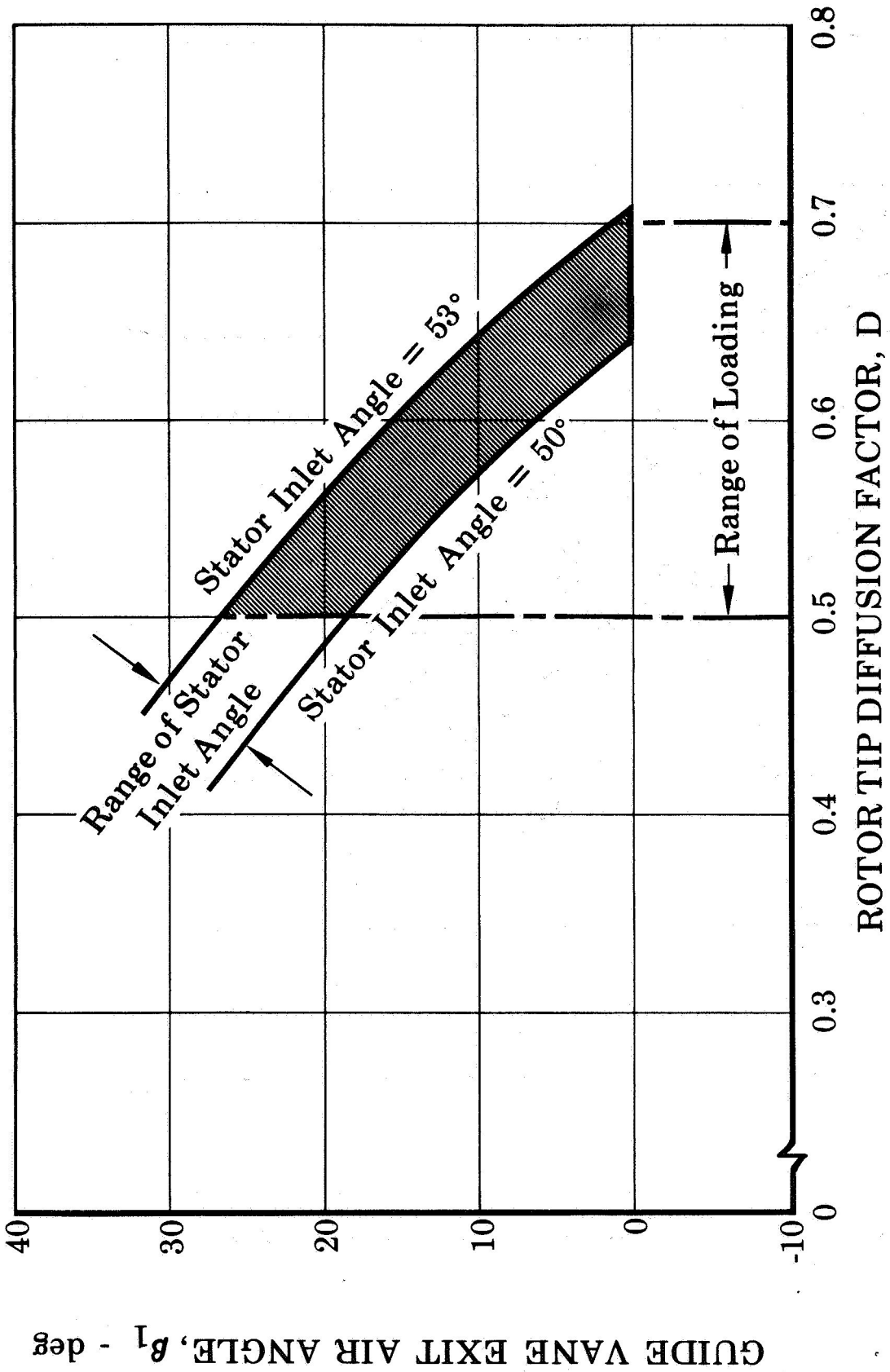
Figure 2. Variation of Slotted Rotor Tip Loading With Inlet Guide Vane Exit Air Angle

	Hub	Mean	Tip
Y_2	0.050	0.050	0.050
t	0.167	0.133	0.098
R	0.105	0.105	0.105
r_1	0.013	0.013	0.013
Y_1	0.092	0.075	0.058
r_2	0.005	0.005	0.005
R_p	0.230	0.230	0.230
ψ	30°	30°	30°

C = 2.21 Inches
s = 3.77 Inches
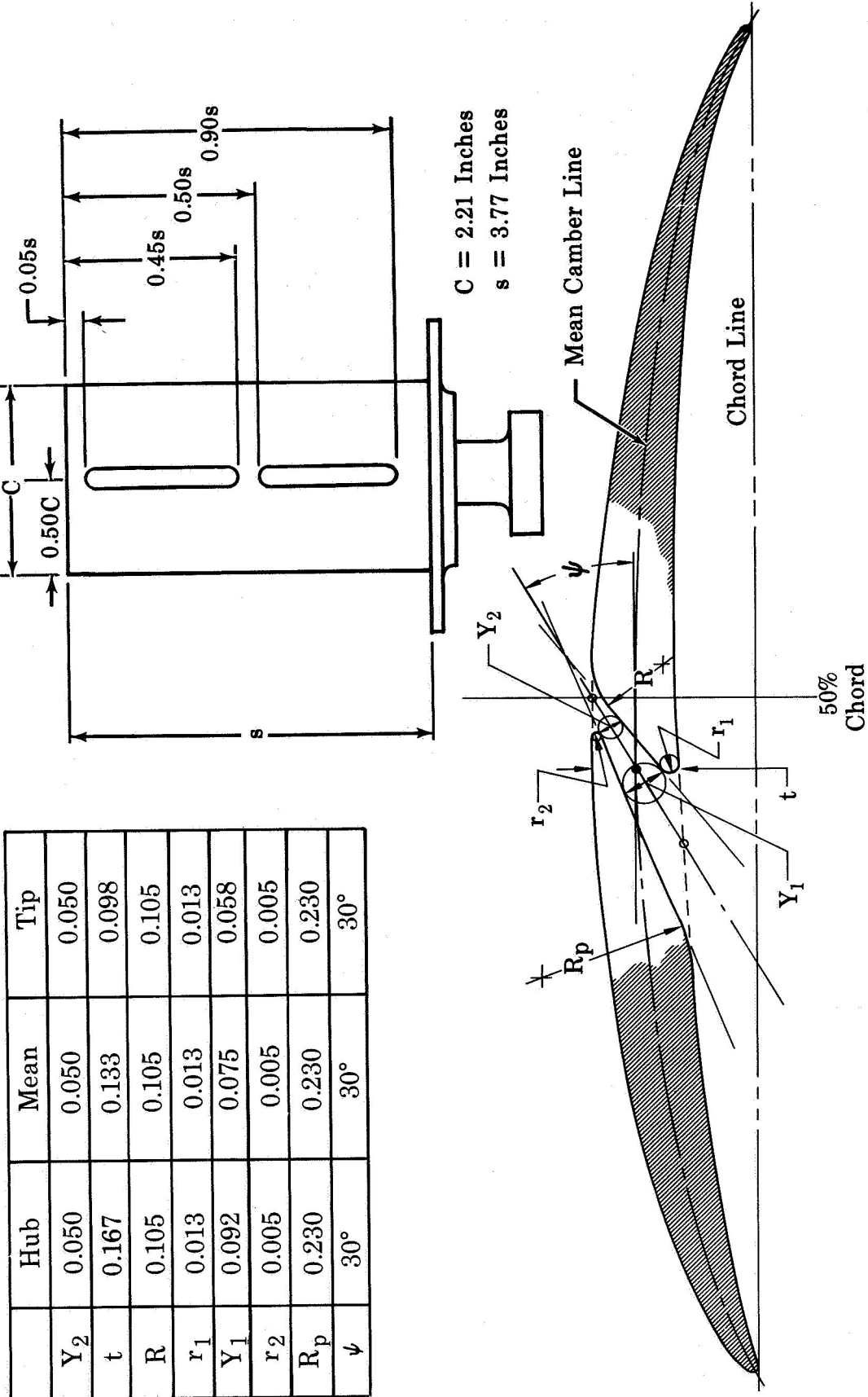
Figure 3. Slot Geometry and Location for Slotted Rotor 1
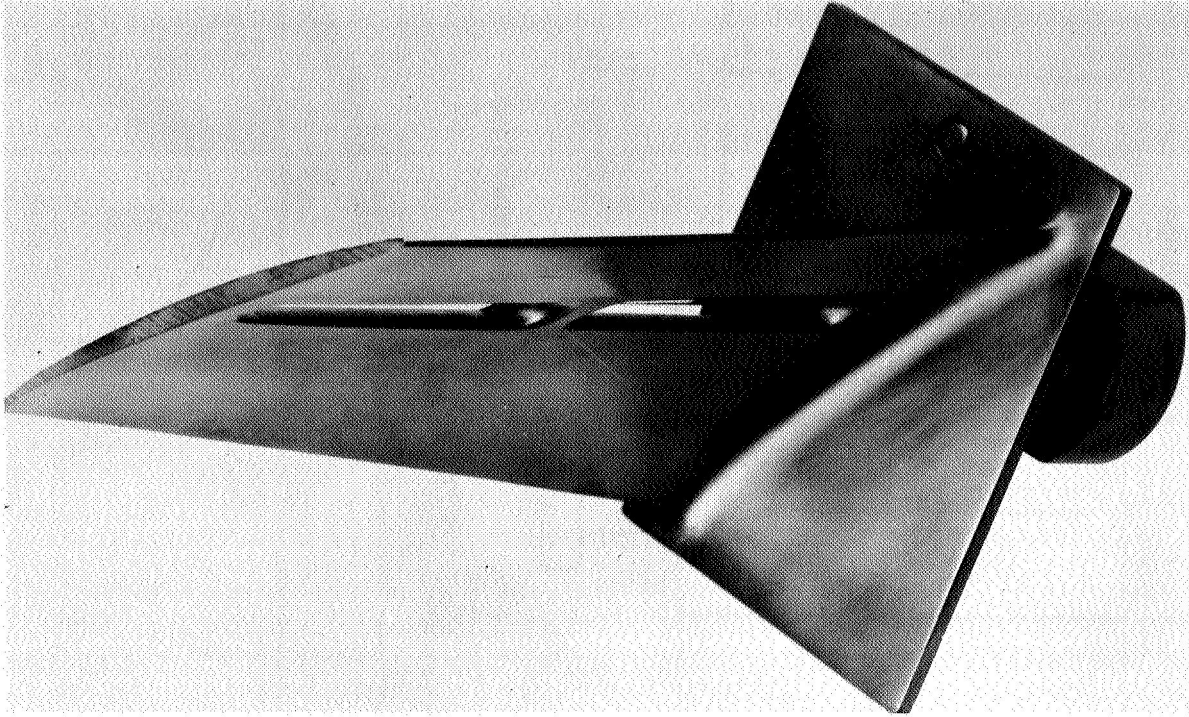
PRESSURE SURFACE
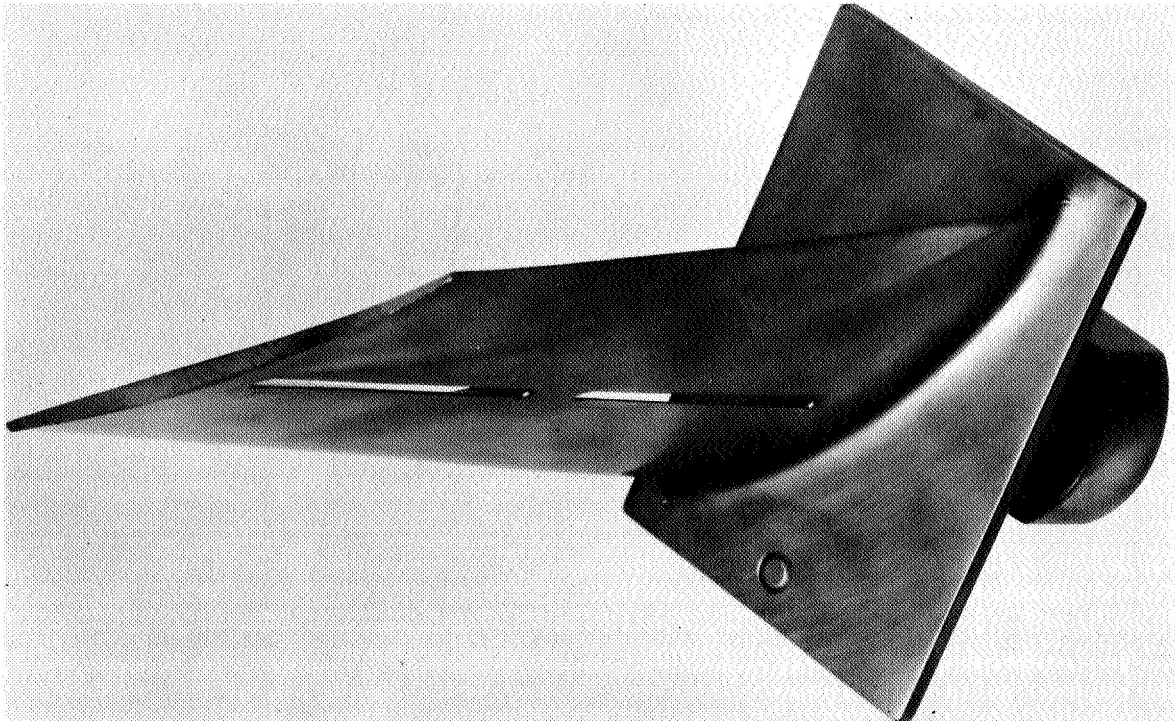
SUCTION SURFACE

Figure 4. Slotted Rotor 1 Blade
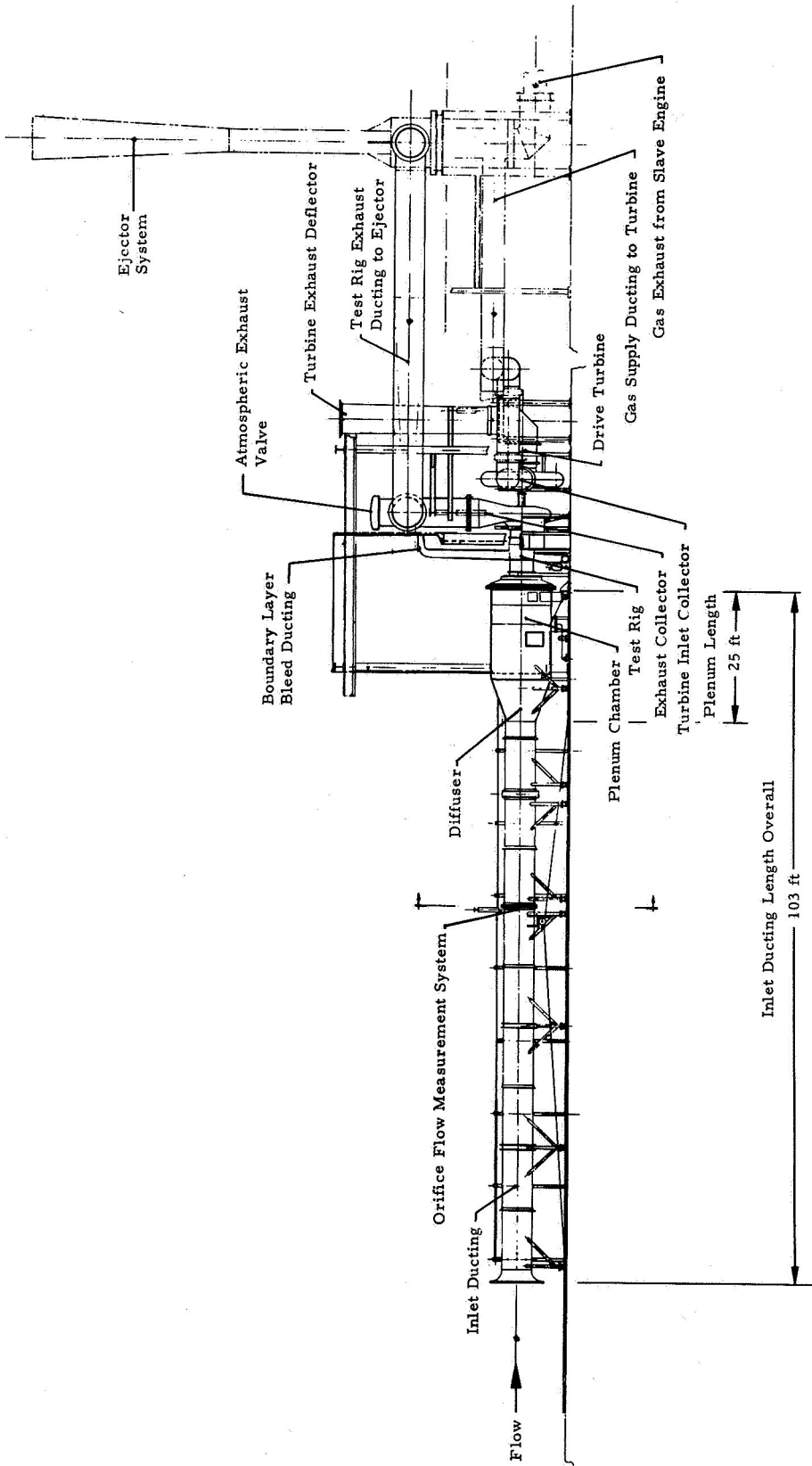
Figure 5. Compressor Research Facility

33

Sta 0 Sta 1 Sta 2 Sta 3A

Airflow

Inlet Guide Vanes

Support Struts

Bellmouth Inlet

Test Stators

Test Section Approx 24 in.

Diffuser Section Approx 24 in.

Measuring Station Diameters - in.

Station	ID	OD
0	32.38	41.12
1	32.85	40.57
2	32.85	40.23
3A	32.85	39.99
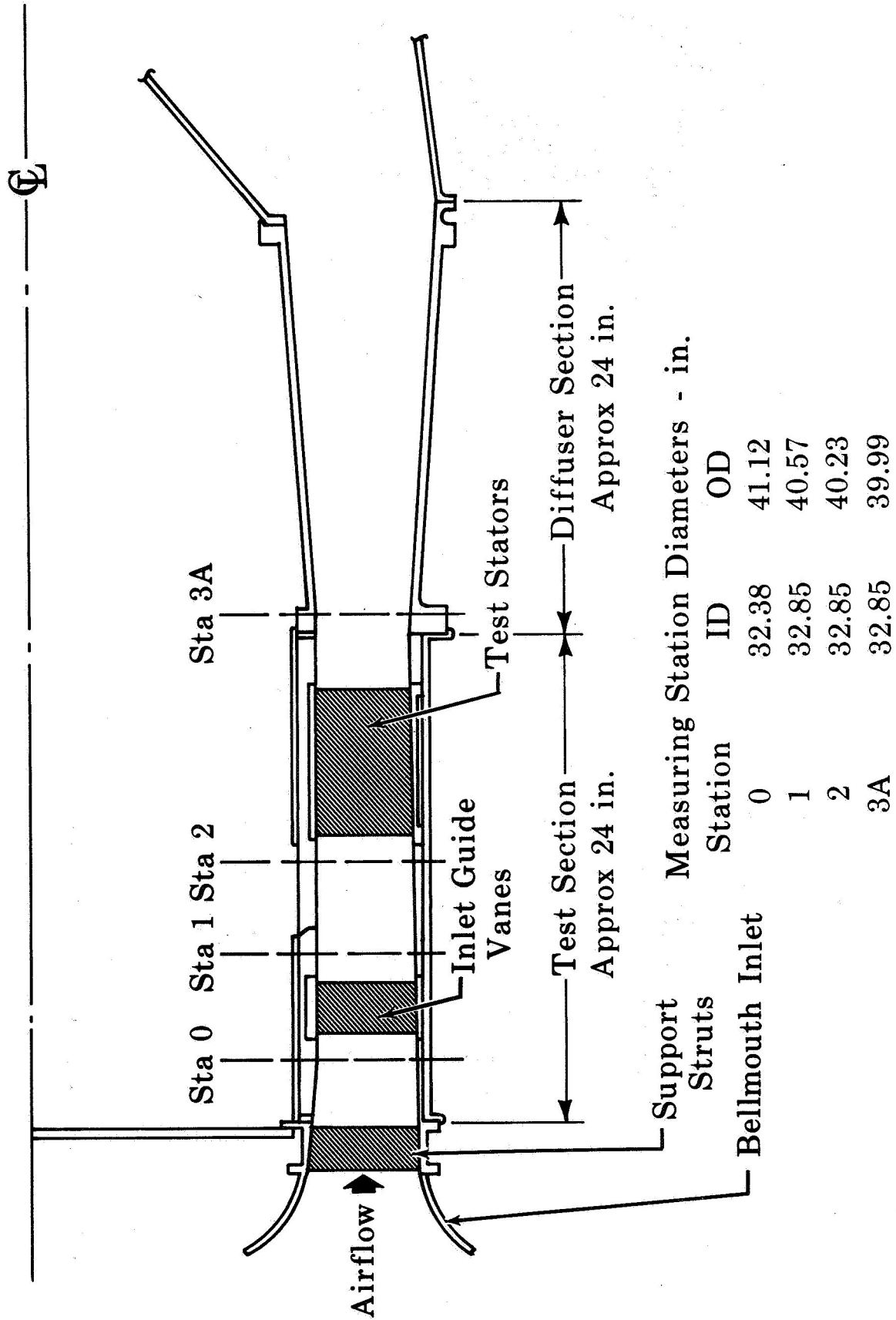
Figure 6. Schematic of Annular Cascade Rig
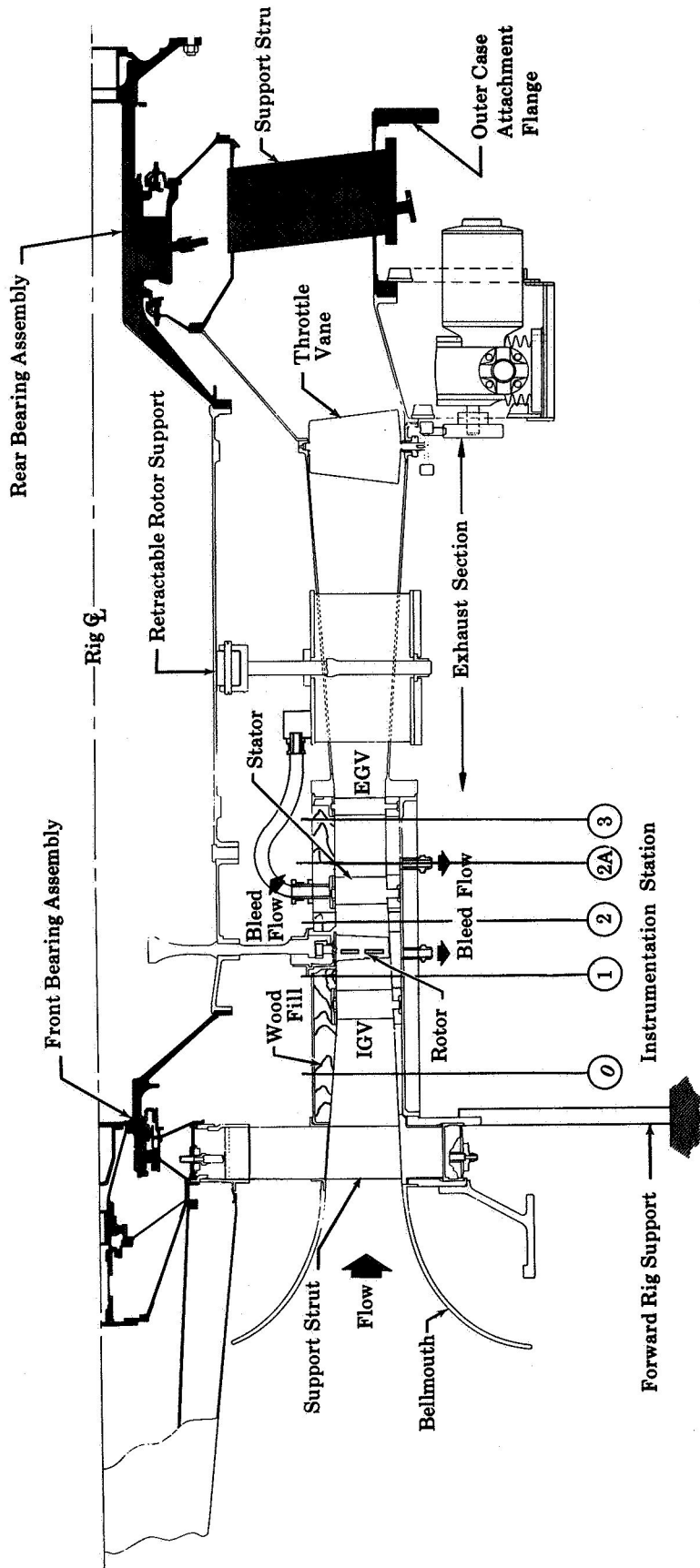
Figure 7. Section View of Compressor Test Rig

Wake Probe (20 Sensors)

0.128
(Typ 19 Places)

2.41

0.218 Dia
0.156

5/32 Dia

14°

0.410

Thermocouple
Junction

0.063 Dia
Aspiration
Hole

Kiel Head
Temperature Probe
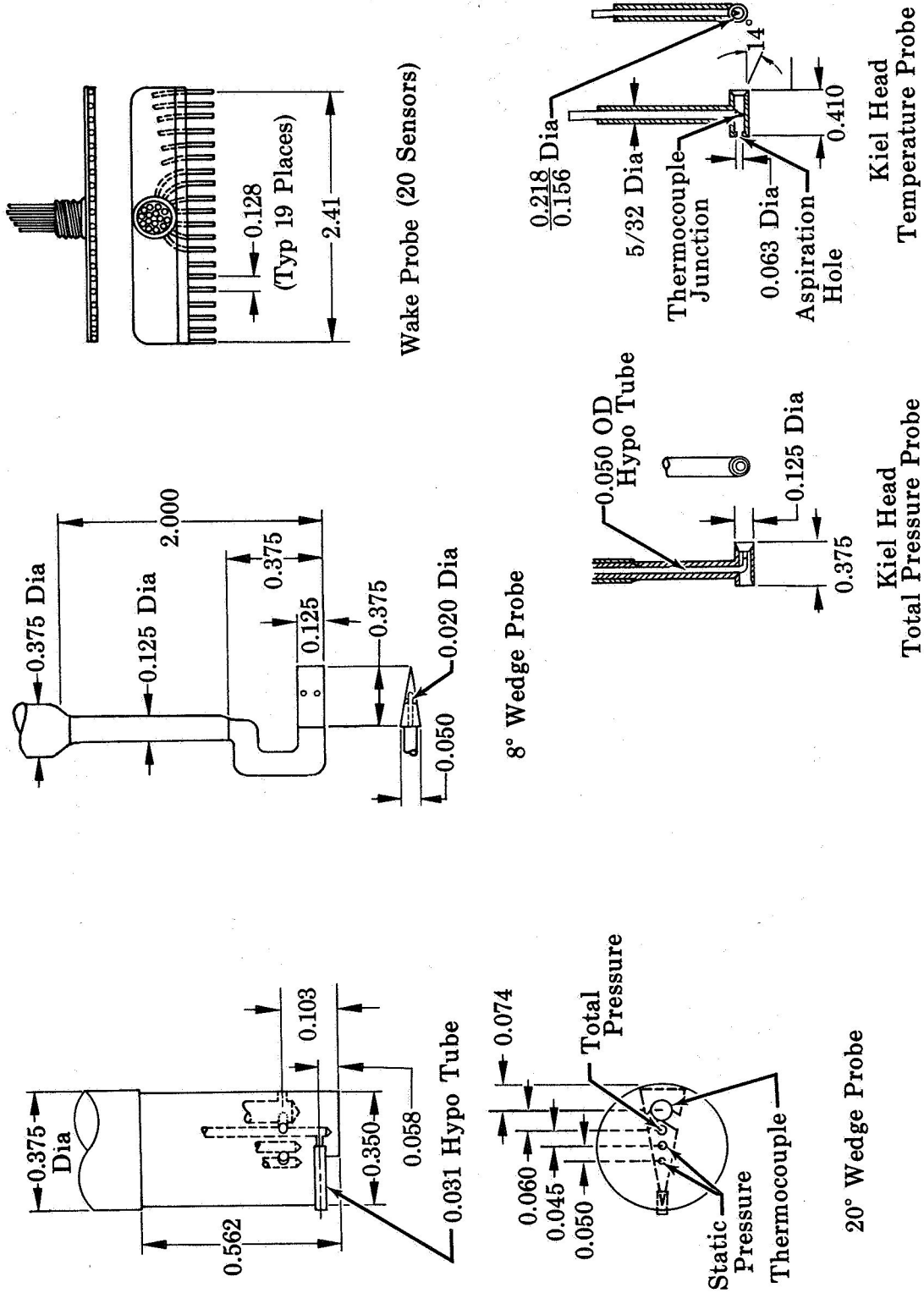
Note: All Dimensions Are in Inches.

2.000

0.375 Dia

0.125 Dia

0.375

0.125

0.375

0.020 Dia

0.050

8° Wedge Probe

0.050 OD
Hypo Tube

0.125 Dia

0.375

Kiel Head
Total Pressure Probe

0.375 Dia

0.103

0.350

0.058

0.031 Hypo Tube

0.074

Total
Pressure

0.060

0.045

0.050

Static
Pressure

Thermocouple

20° Wedge Probe

Figure 8. Probe Configurations
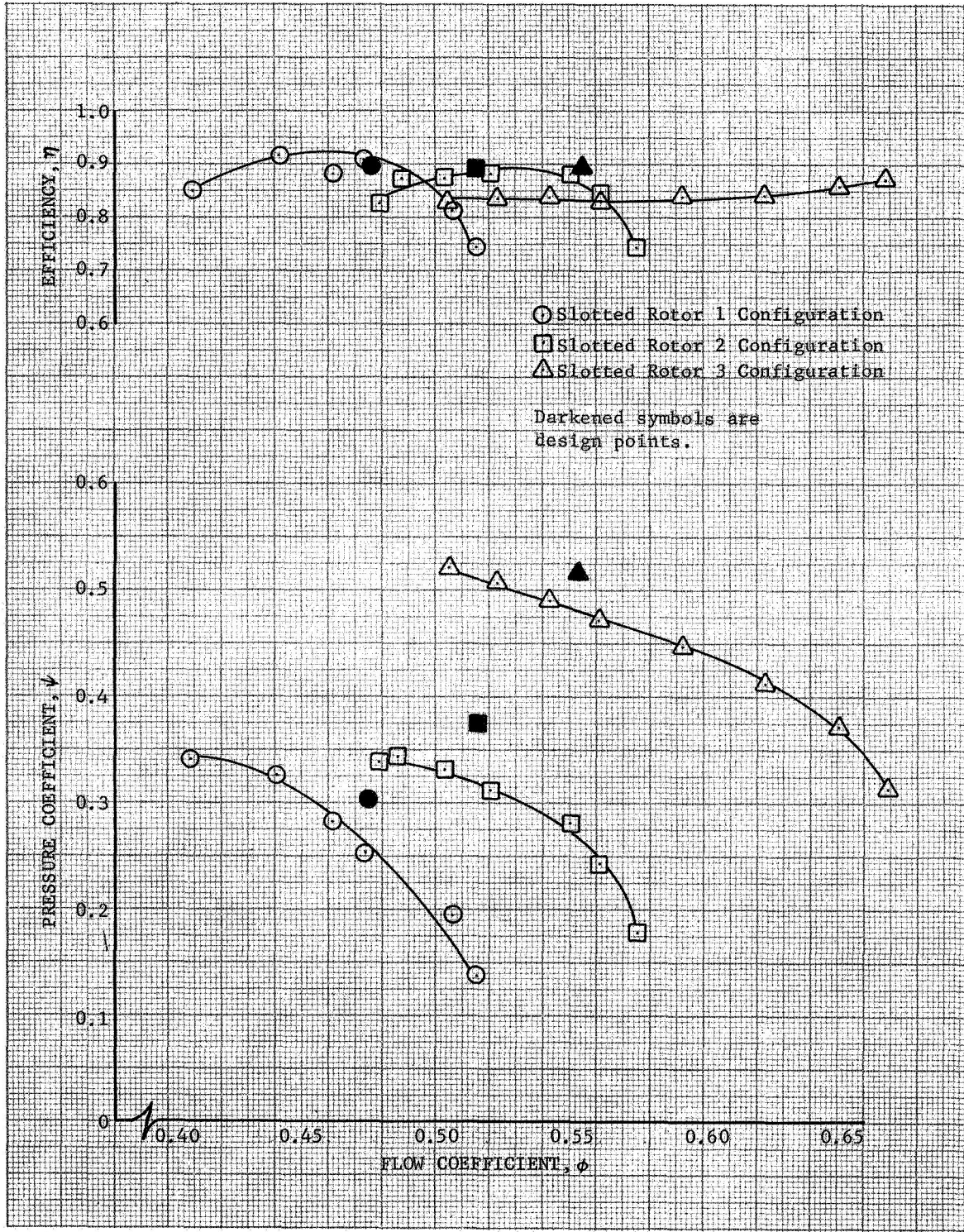
Figure 9. Inlet Guide Vane-Slotted Rotor Overall Performance; 100% Design Equivalent Rotor Speed; Comparison of Ψ and η vs ϕ for All Slotted Rotor Configurations
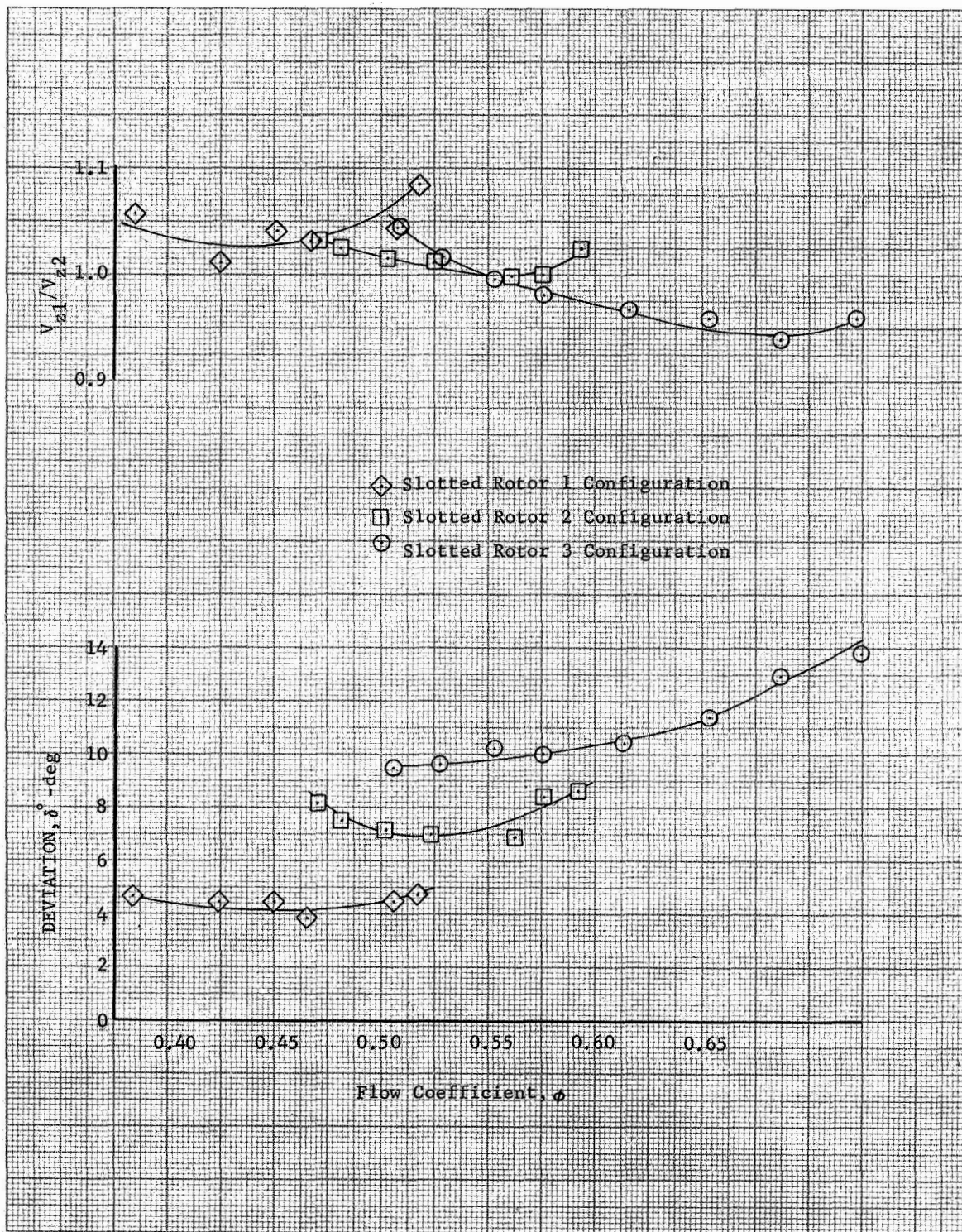
Figure 10. Axial Velocity Ratio and Deviation for Slotted
Rotors; 100% Design Equivalent Rotor Speed
at Midspan
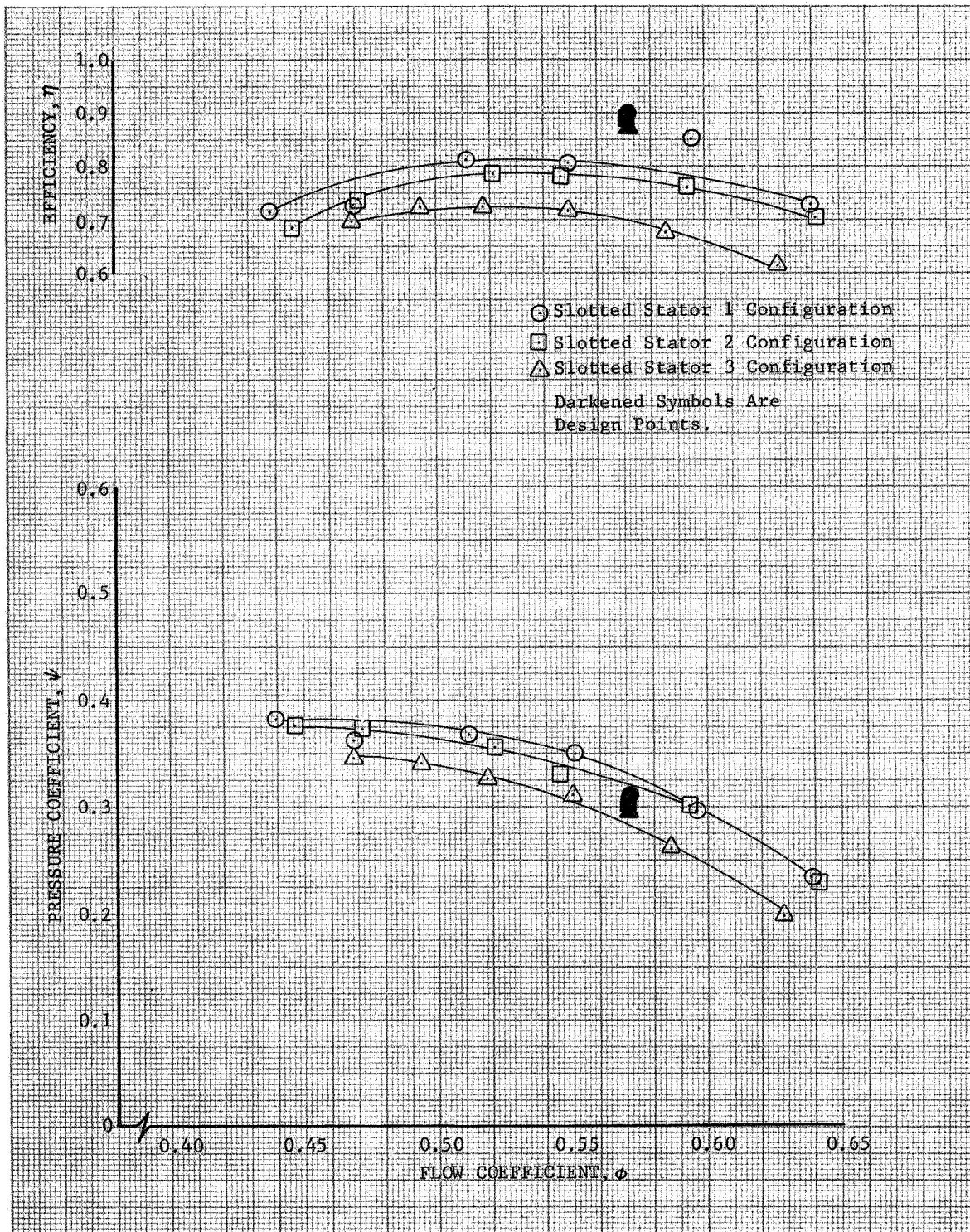
Figure 11. Stage Overall Performance Data, 100% Design
Equivalent Rotor Speed; Comparison of Ψ and
η vs ϕ for All IGV-Flow Generation Rotor-
Slotted Stator Configurations

39
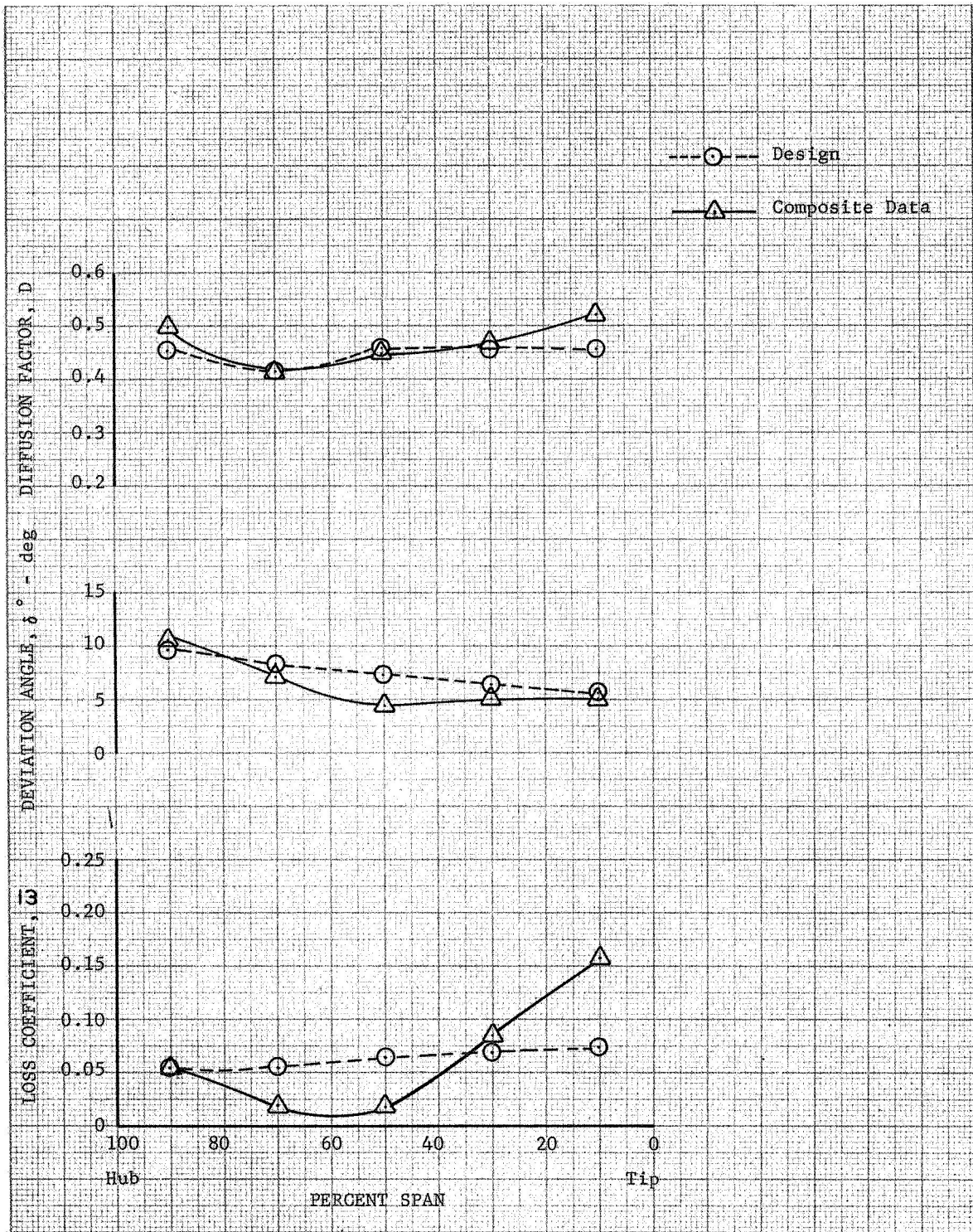
Figure 12.   Blade Element Performance, Slotted Rotor 1
Composite Data for Design Speed at Design
Incidence

40
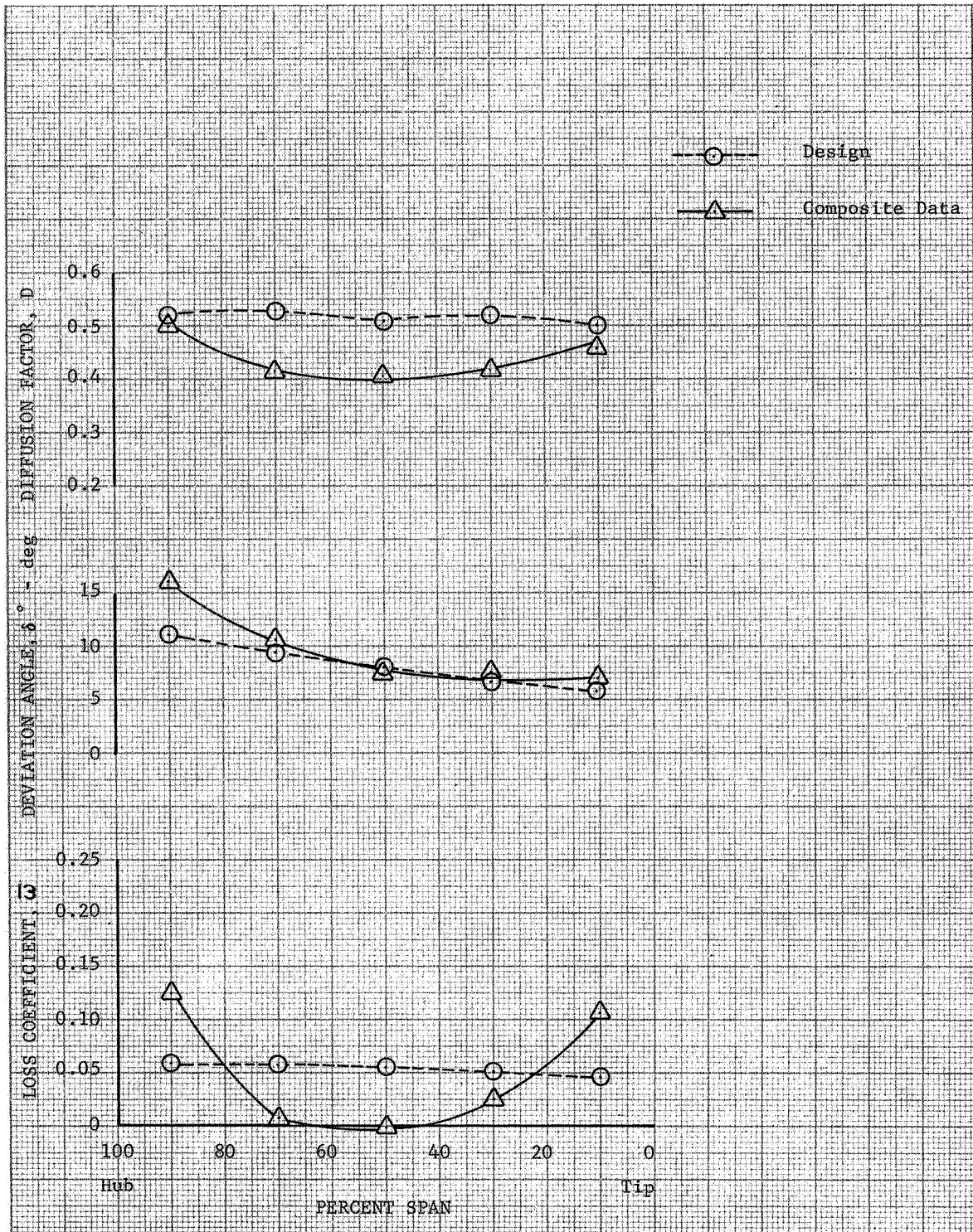
Figure 13.   Blade Element Performance, Slotted Rotor 2
Composite Data for 70% of Design Speed at
Design Incidence

41
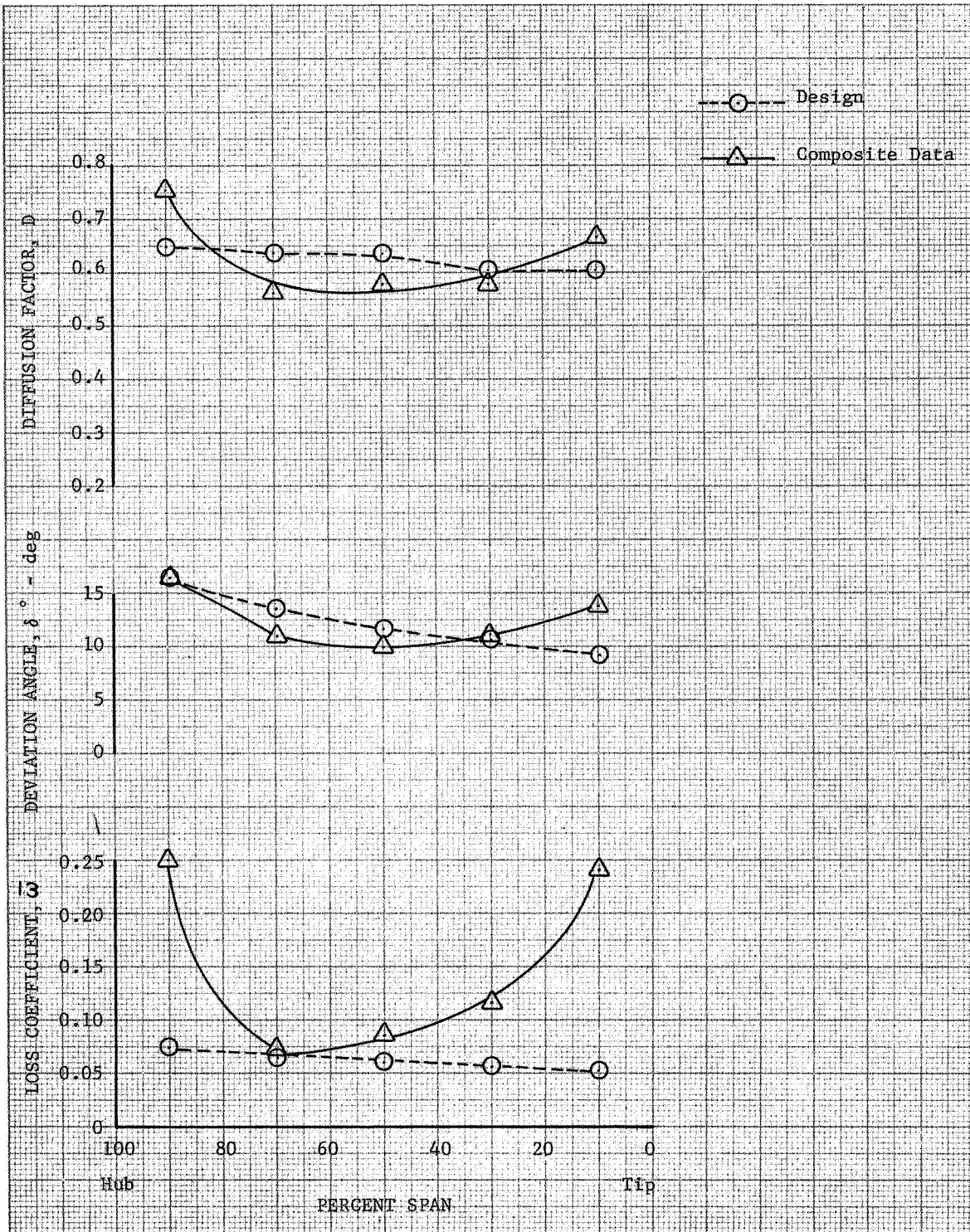
Figure 14. Blade Element Performance, Slotted Rotor 3
Composite Data for 90% of Design Speed at
Design Incidence
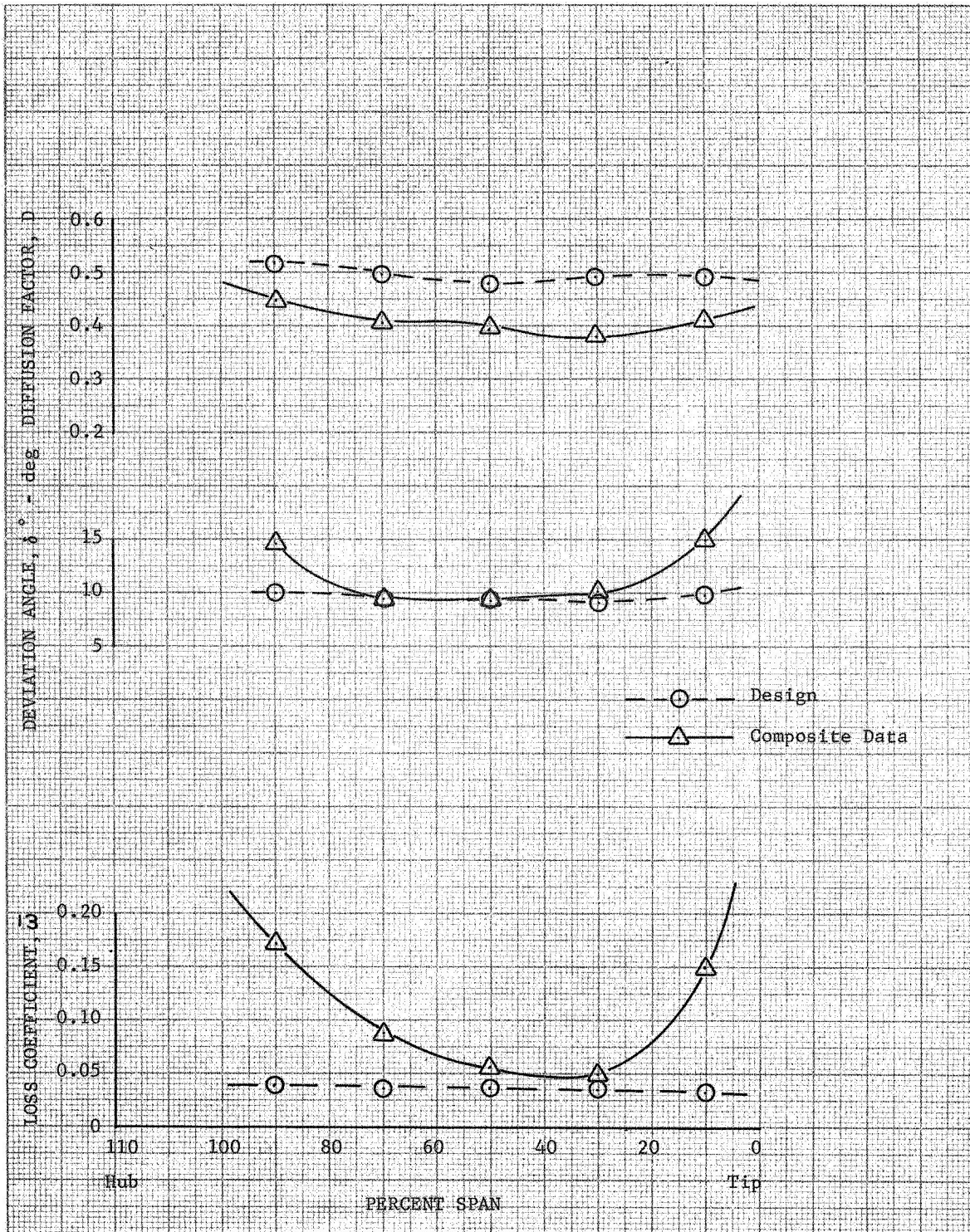
Figure 15. Blade Element Performance, Slotted Stator 1
Composite Data for Design Speed at Design
Incidence

43
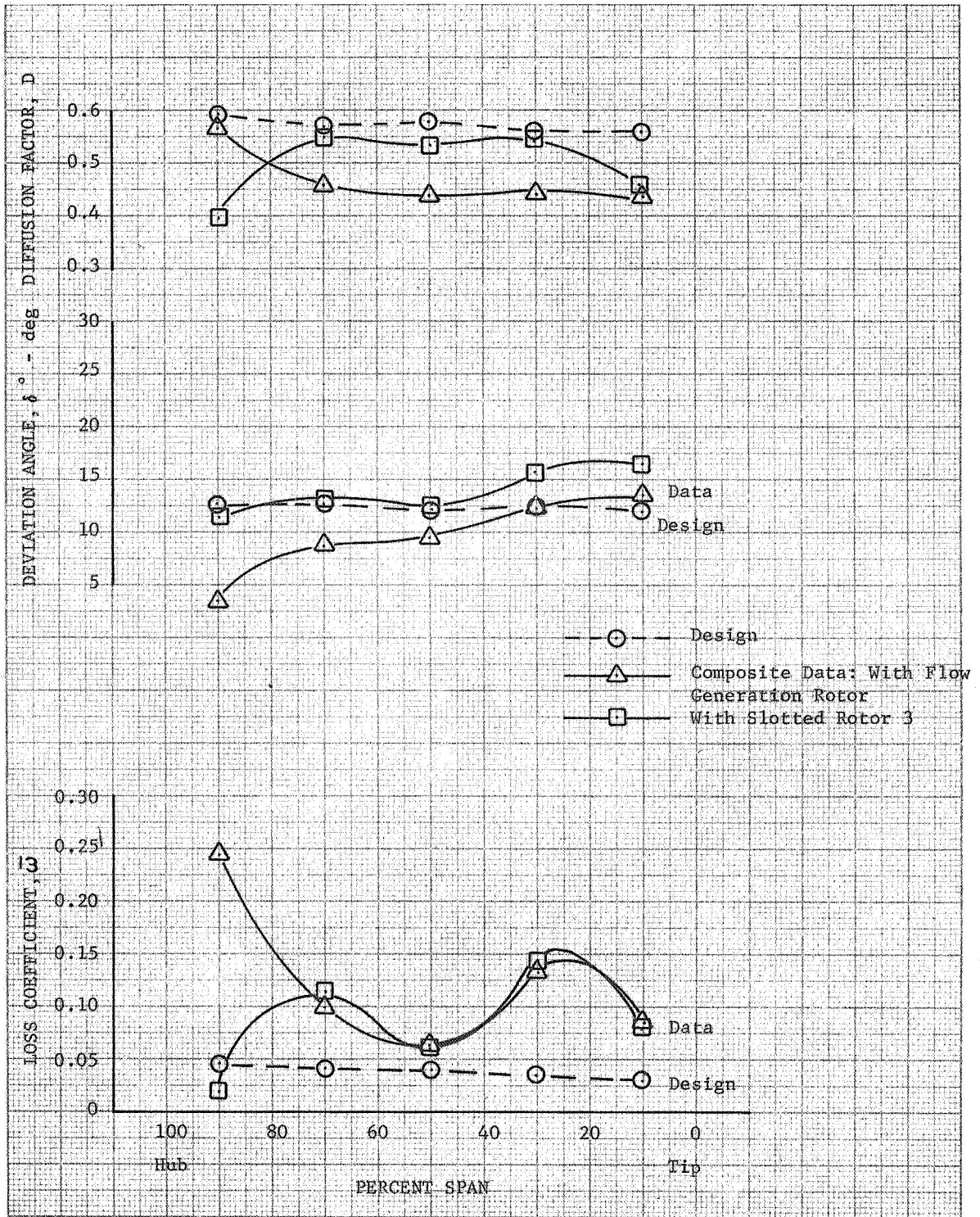
Figure 16. Blade Element Performance, Slotted Stator 2
Composite Data for Design Speed at Design
Incidence
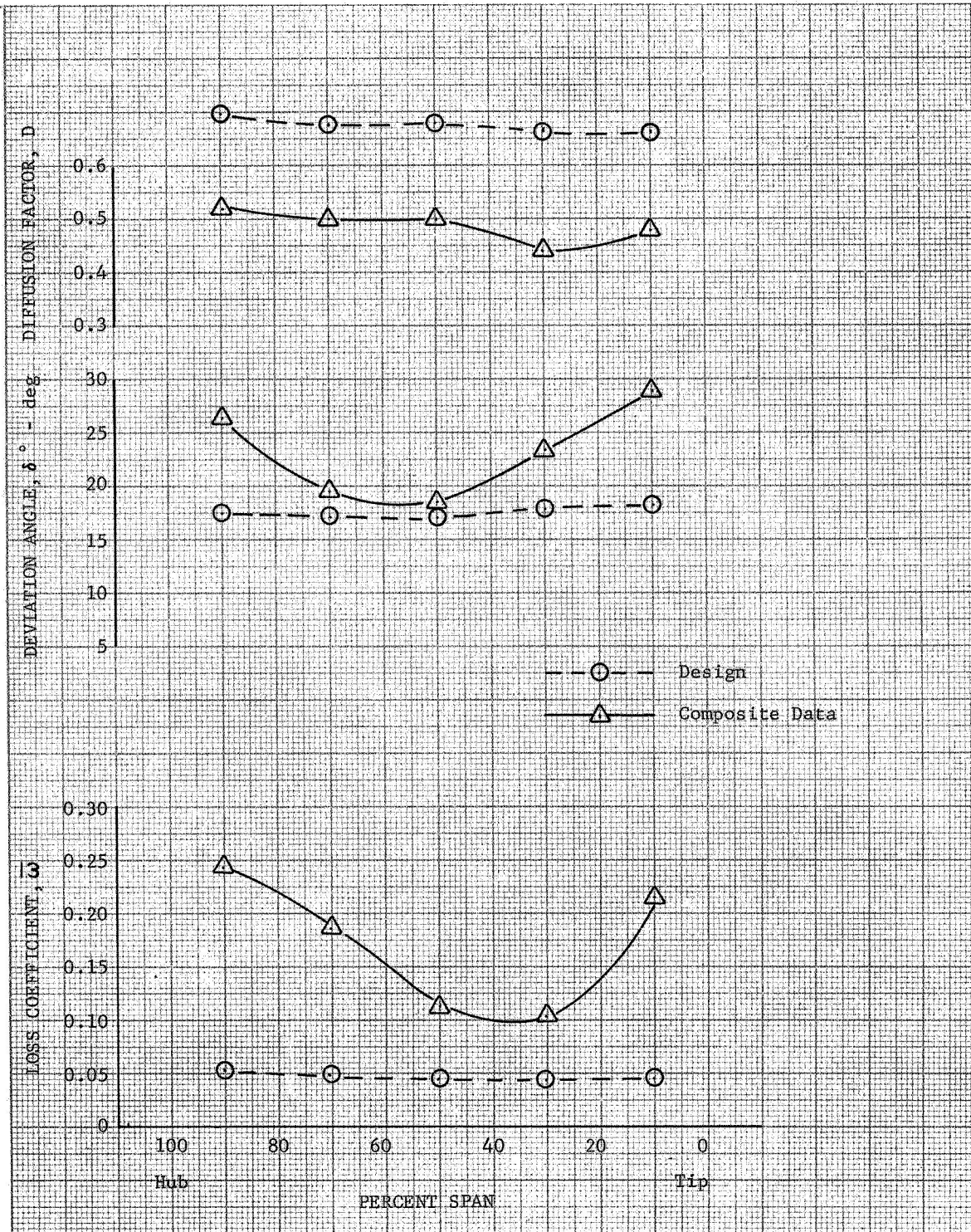
Figure 17.   Blade Element Performance, Slotted Stator 3
            Composite Data for Design Speed at Design
            Incidence

45
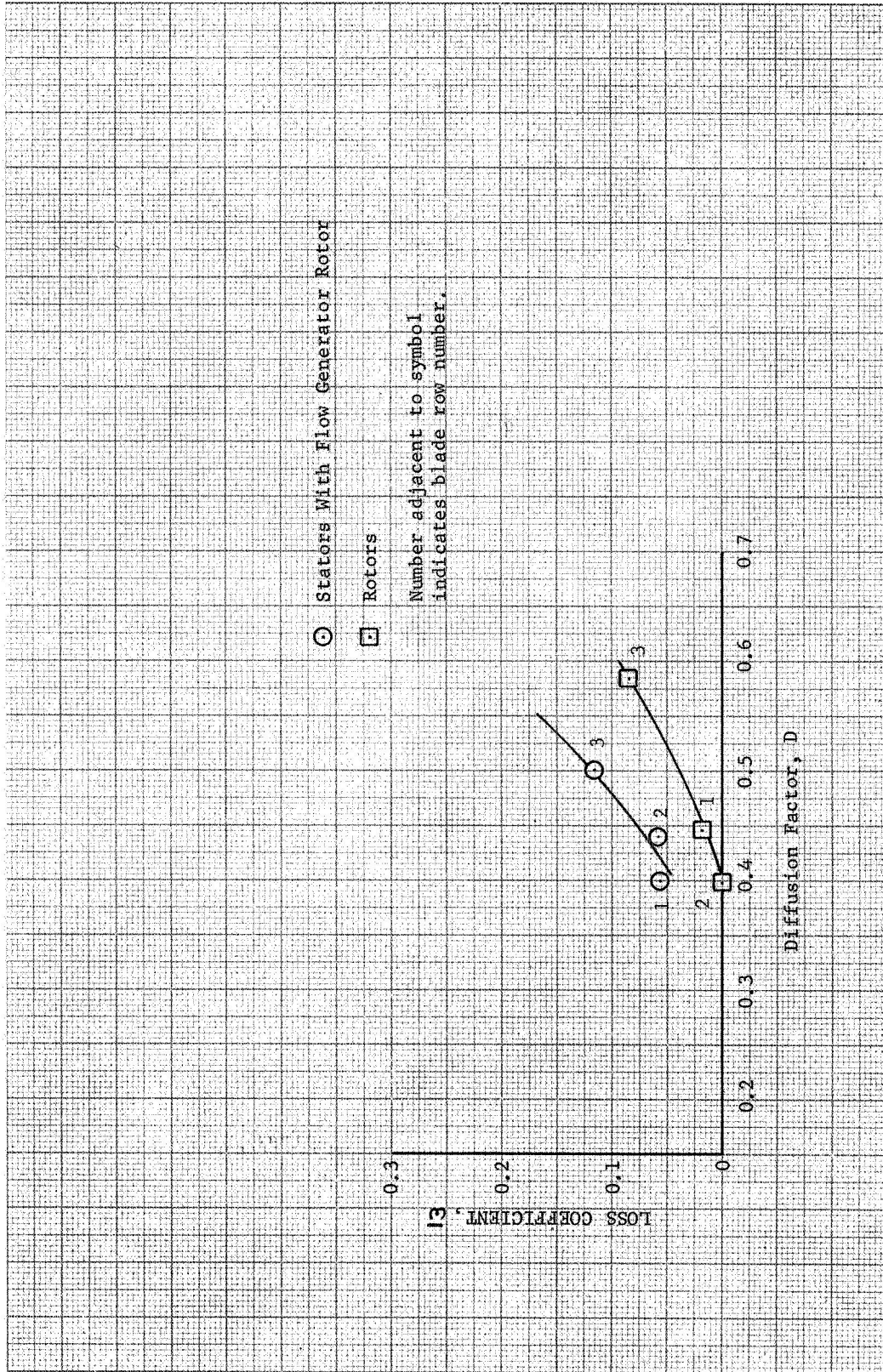
Figure 18. Effect of Loading on Midspan Loss Coefficient at Design Incidence
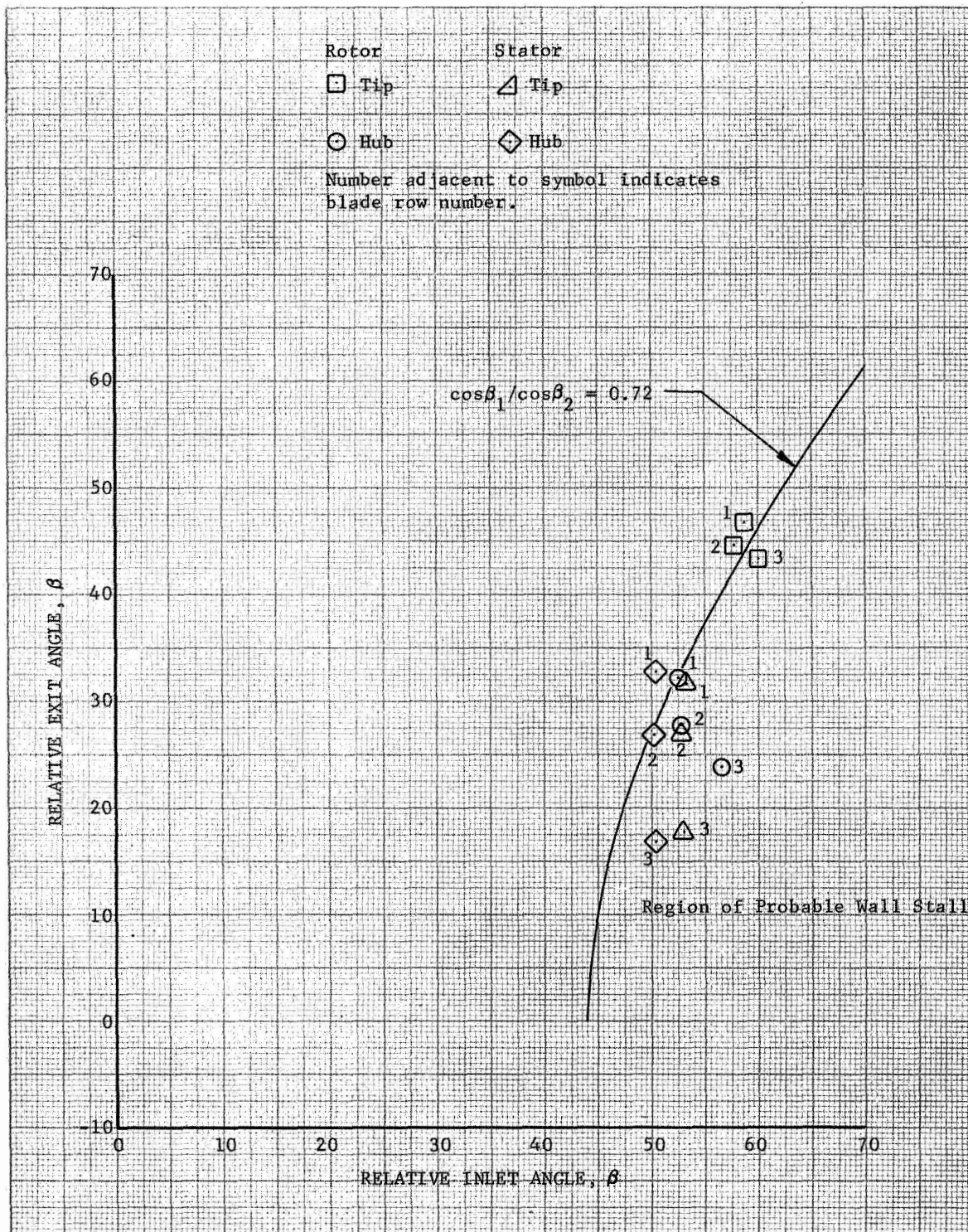
Figure 19. Comparison of Slotted Blade Designs With DeHaller Wall Stall Criterion

47
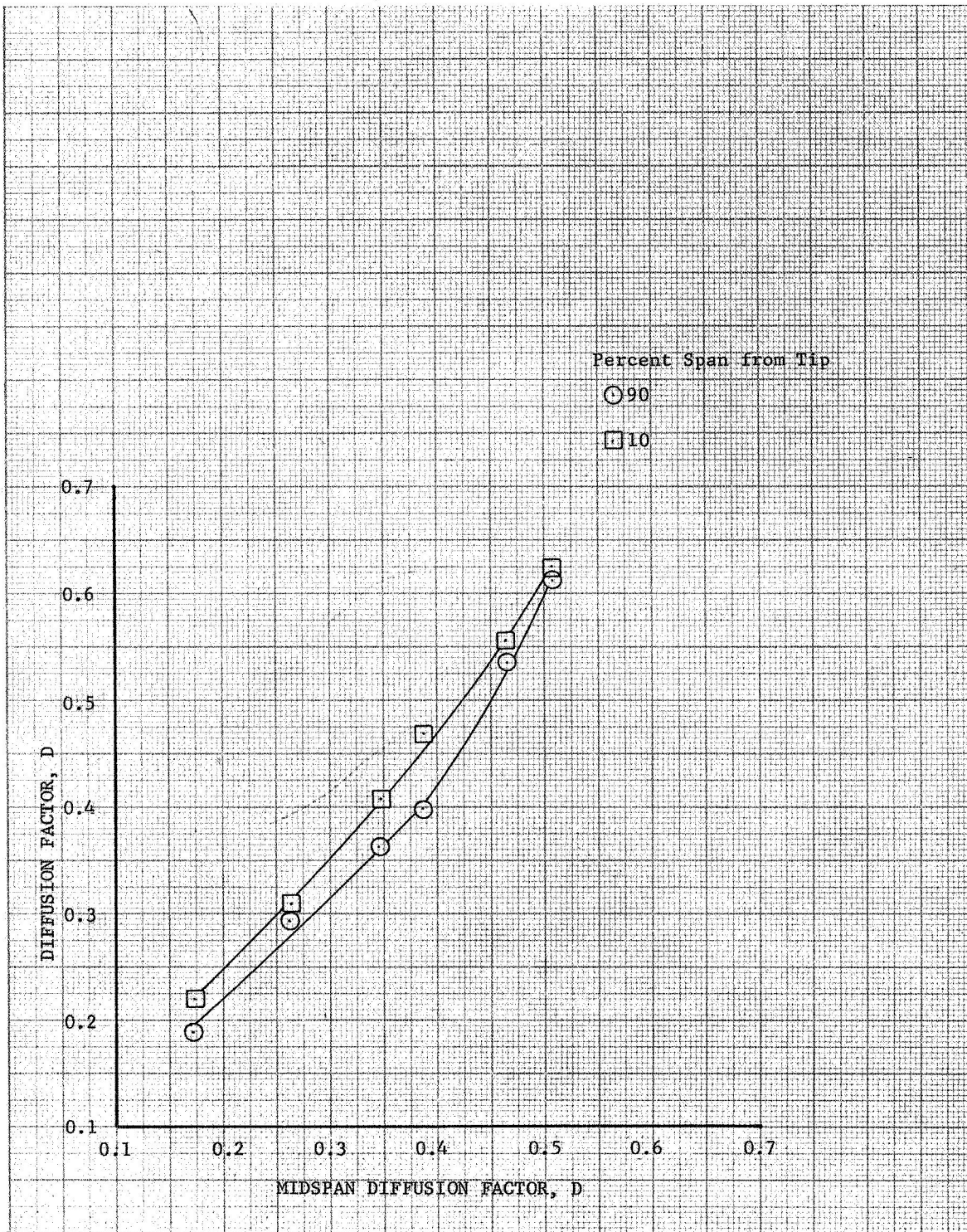
Figure 20. Hub and Tip Diffusion Factor as a Function of
            Midspan Diffusion Factor - Slotted Rotor 1,
            Design Speed
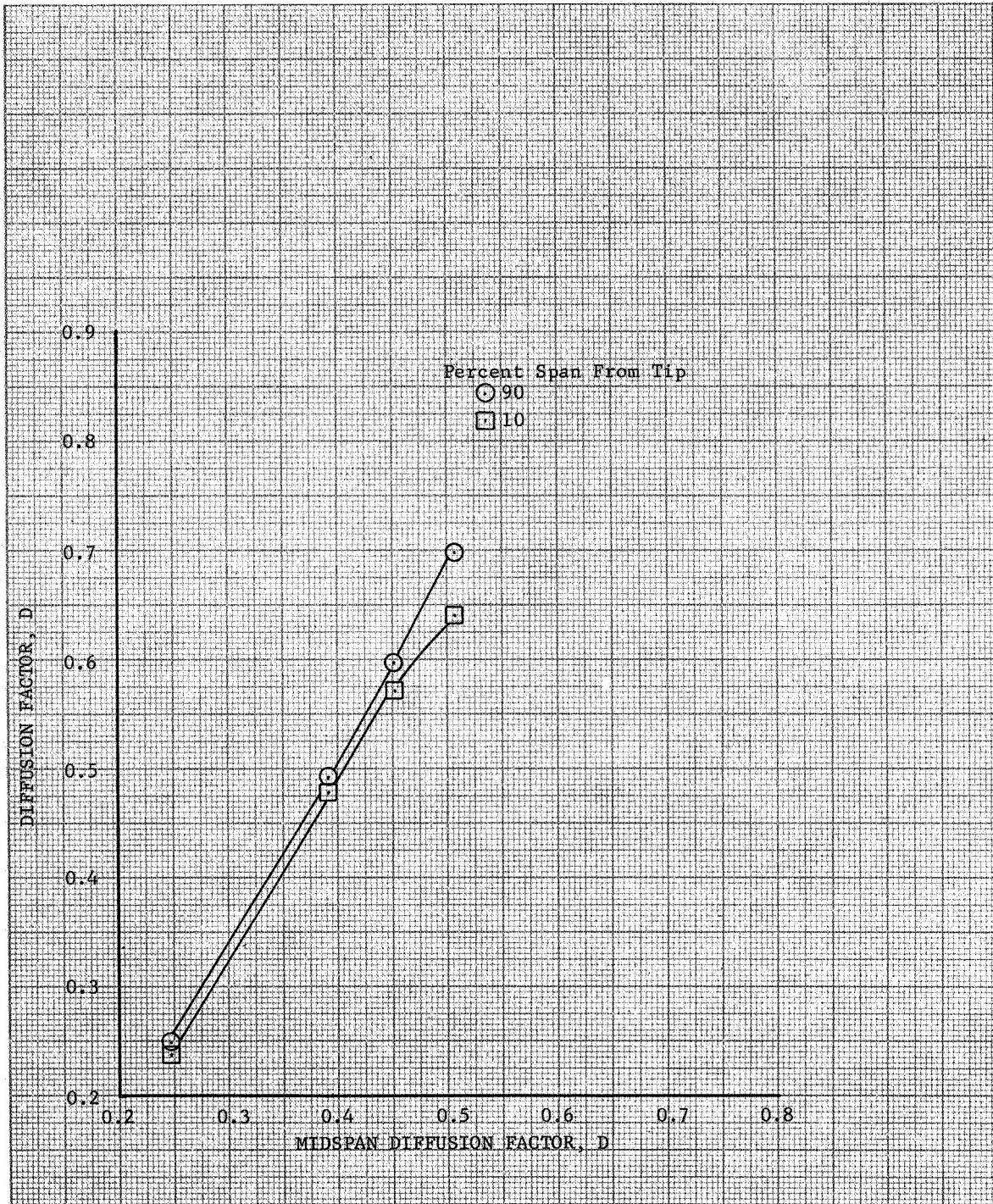
Figure 21. Hub and Tip Diffusion Factor as a Function
of Midspan Diffusion Factor - Slotted Rotor 2,
70% of Design $N/\sqrt{\theta}$
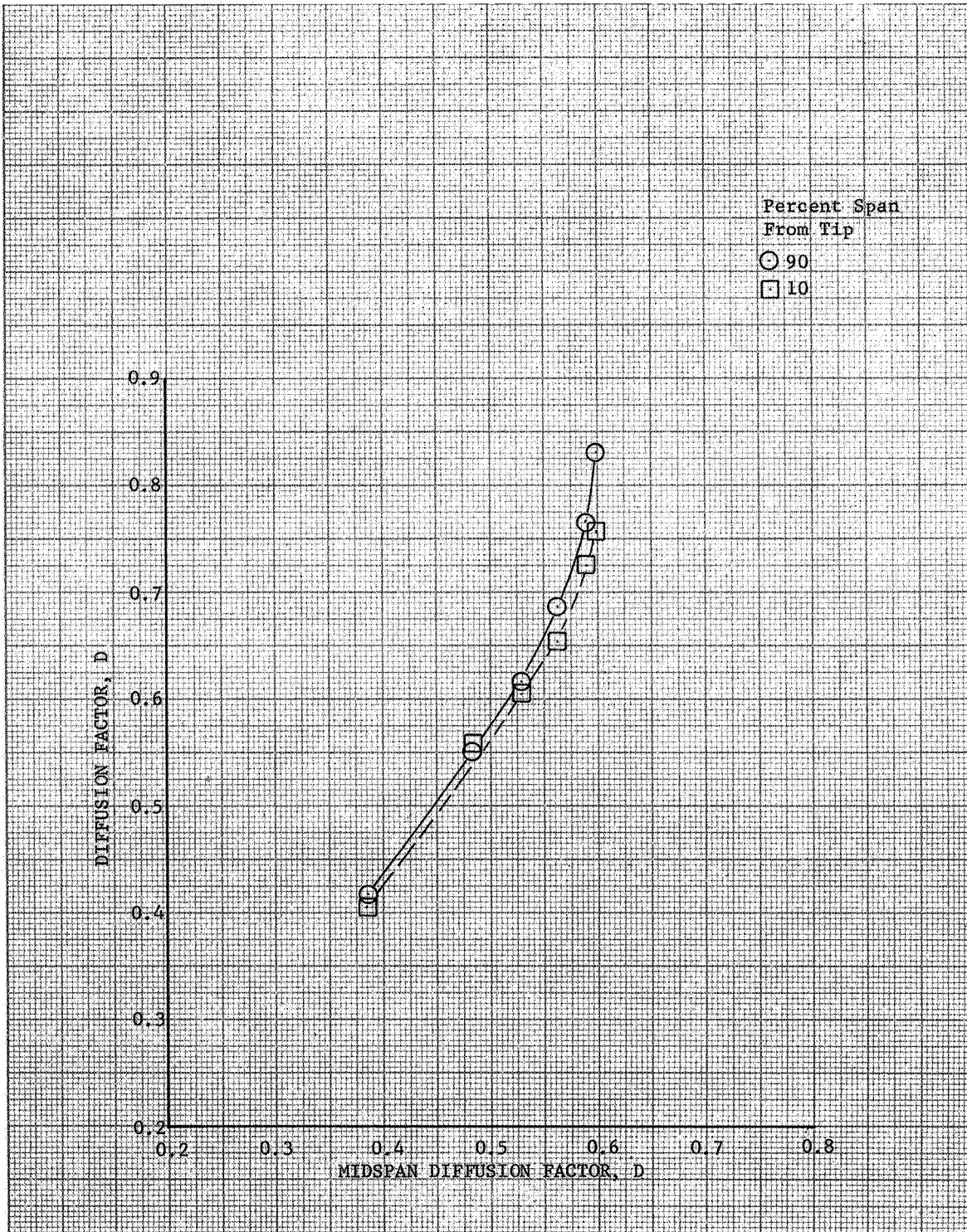
Figure 22. Hub and Tip Diffusion Factor as a Function
of Midspan Diffusion Factor - Slotted Rotor 3,
90% of Design $N/\sqrt{\theta}$

Figure 23. Hub and Tip Diffusion Factor as a Function
of Midspan Diffusion Factor - Flow Generation
Rotor (Slotted Stator 3 Test), Design $N/\sqrt{\theta}$

51
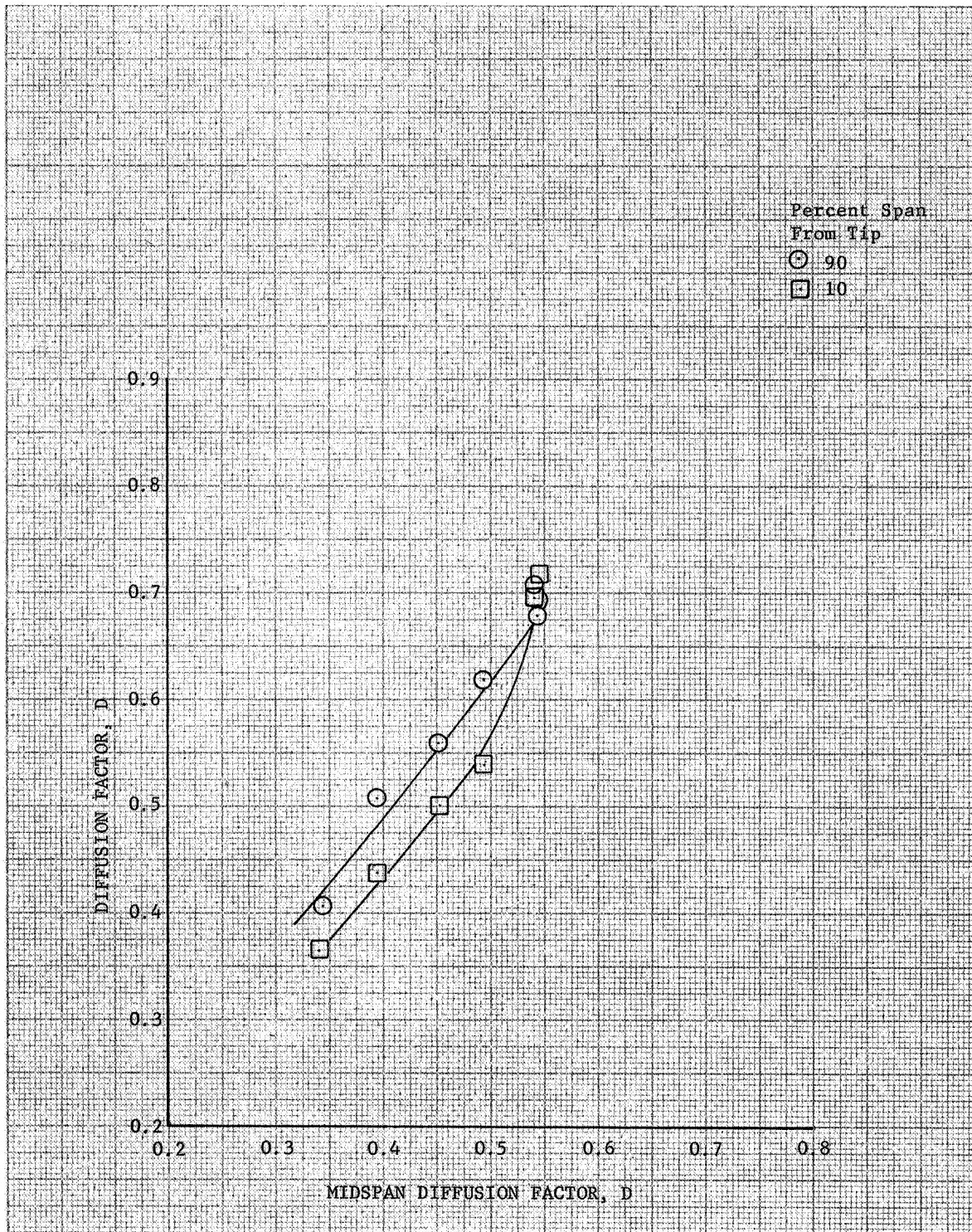
Figure 24.   Hub and Tip Diffusion Factor as a Function of
Midspan Diffusion Factor - Slotted Stator 1,
Design Speed
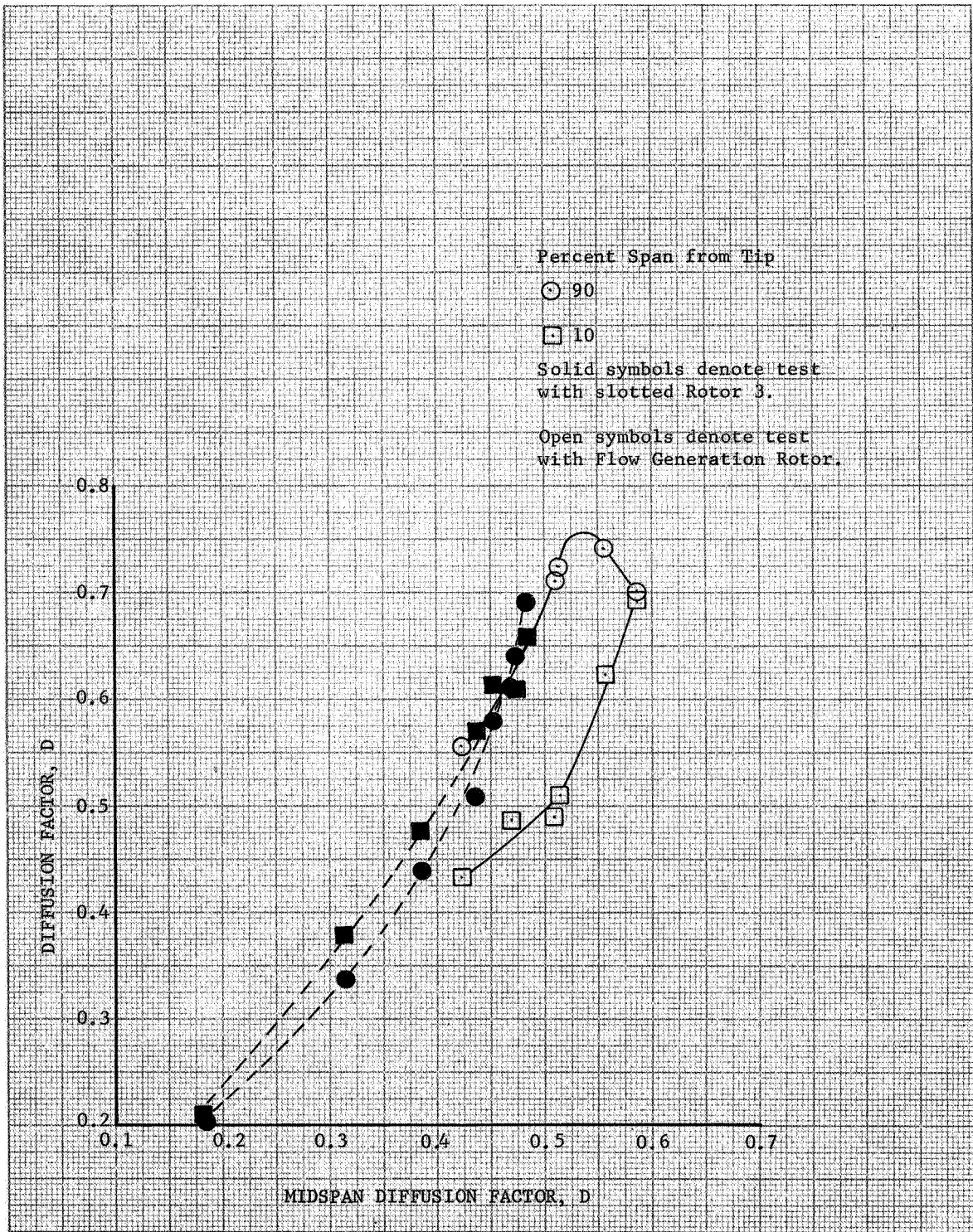
Figure 25. Hub and Tip Diffusion Factor as a Function
of Midspan Diffusion Factor - Slotted
Stator 2, Design Speed
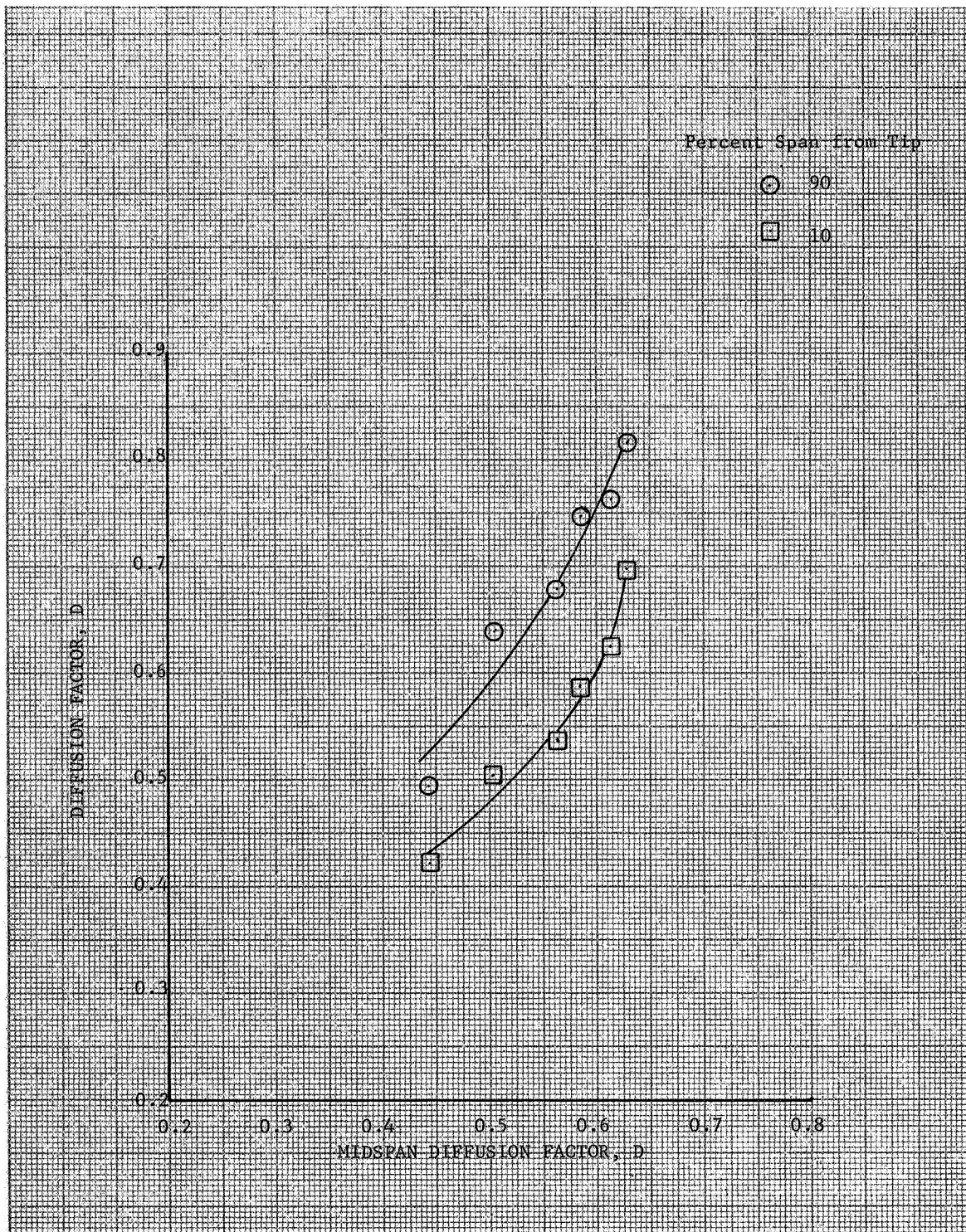
Figure 26. Hub and Tip Diffusion Factor as a Function of
Midspan Diffusion Factor - Slotted Stator 3,
Design Speed

54
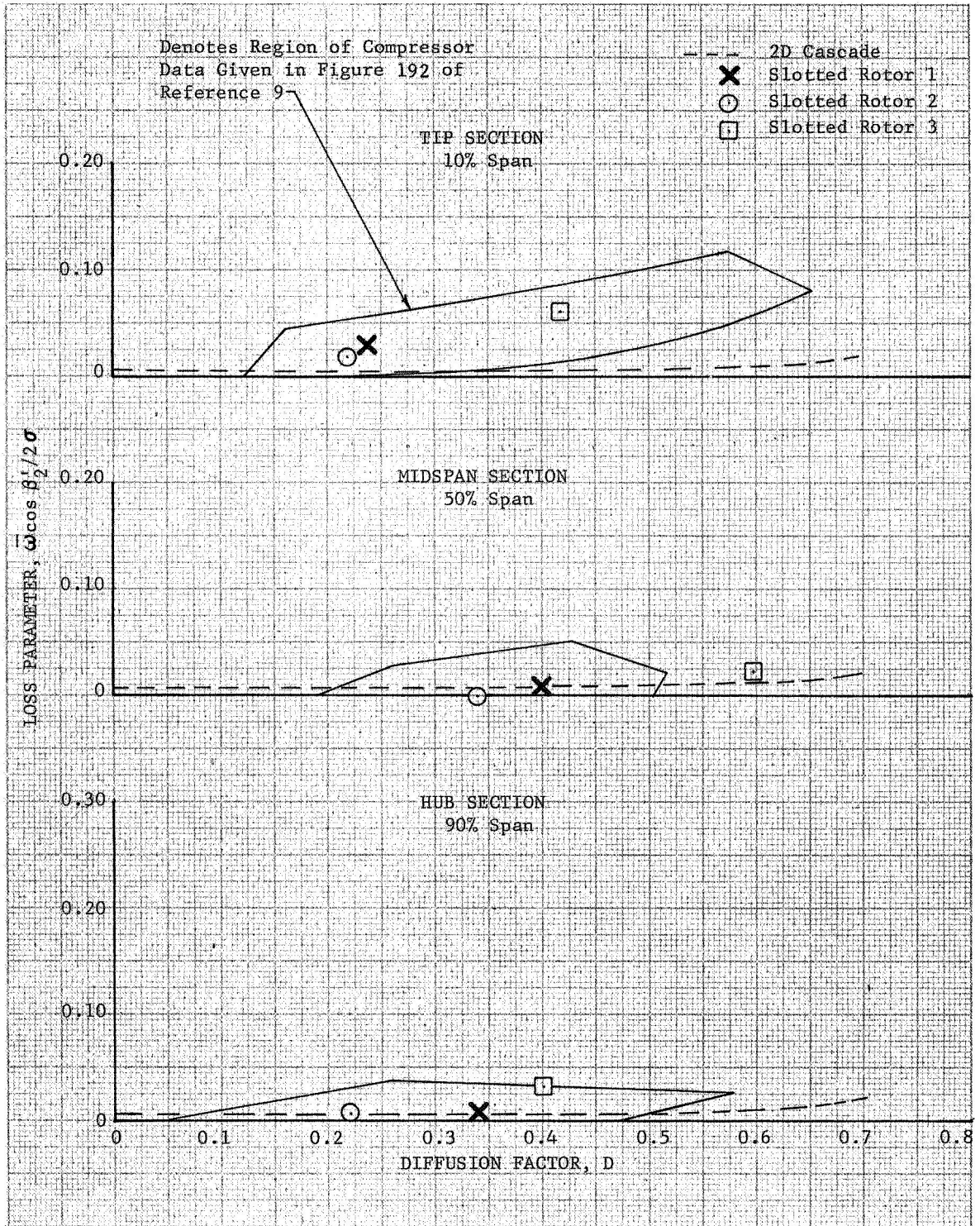
Figure 27.   Rotor Blade Element Performance Comparisons
             at Minimum Loss

55
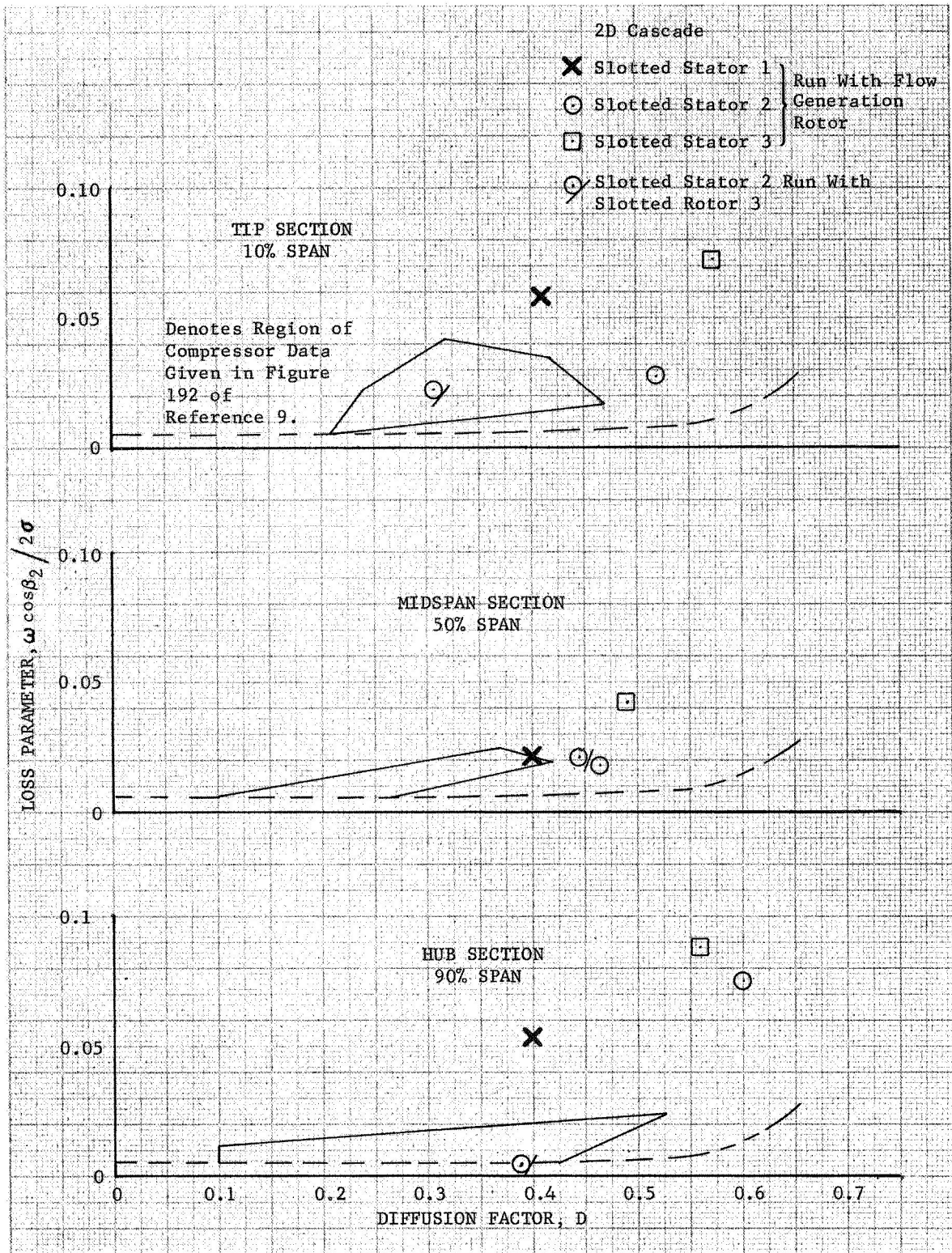
Figure 28.   Stator Blade Element Performance Comparisons
             at Minimum Loss
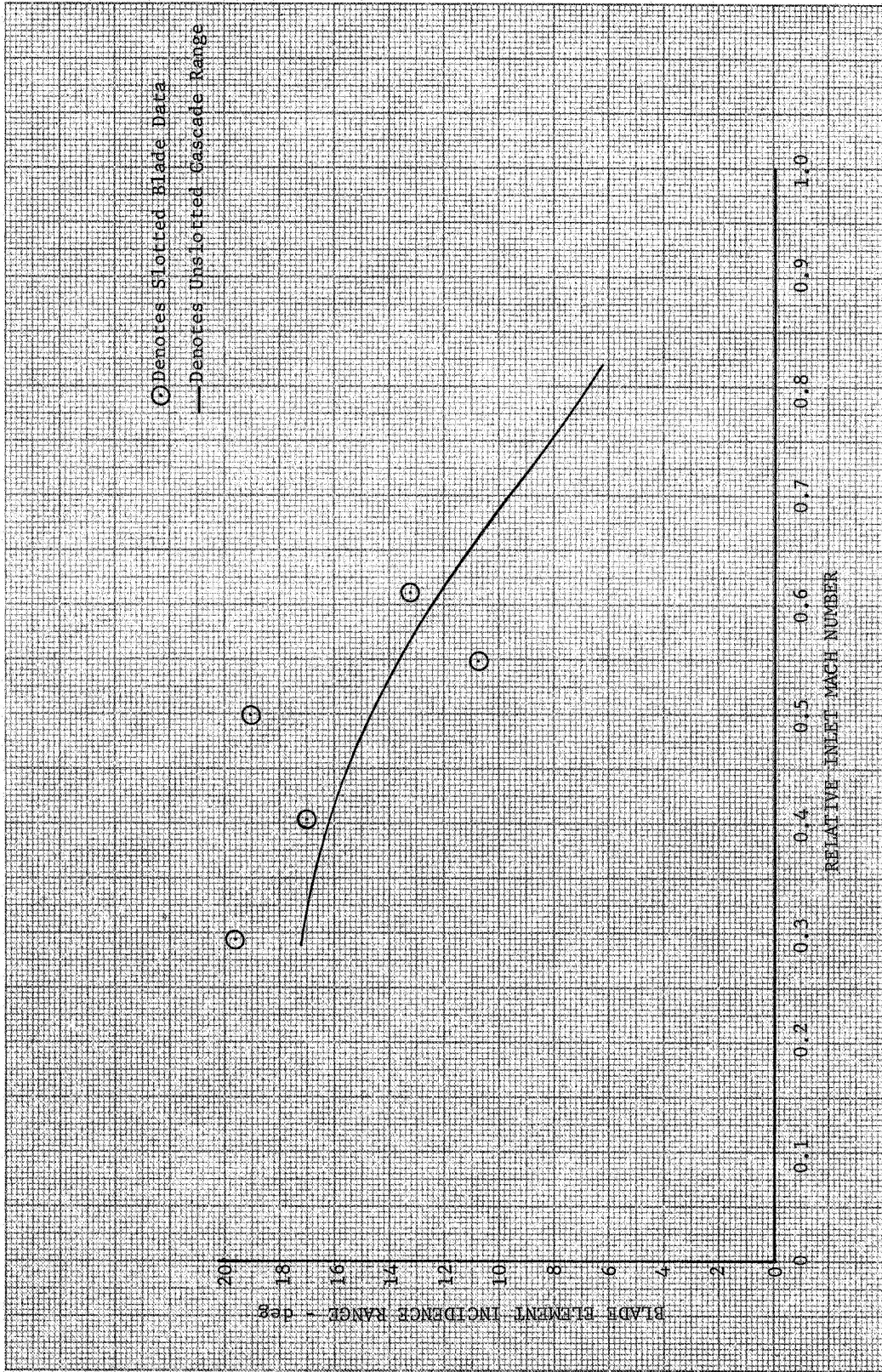
Figure 29. Unstalled Incidence Range - 50% of Span from Tip of Slotted Stator 2

57
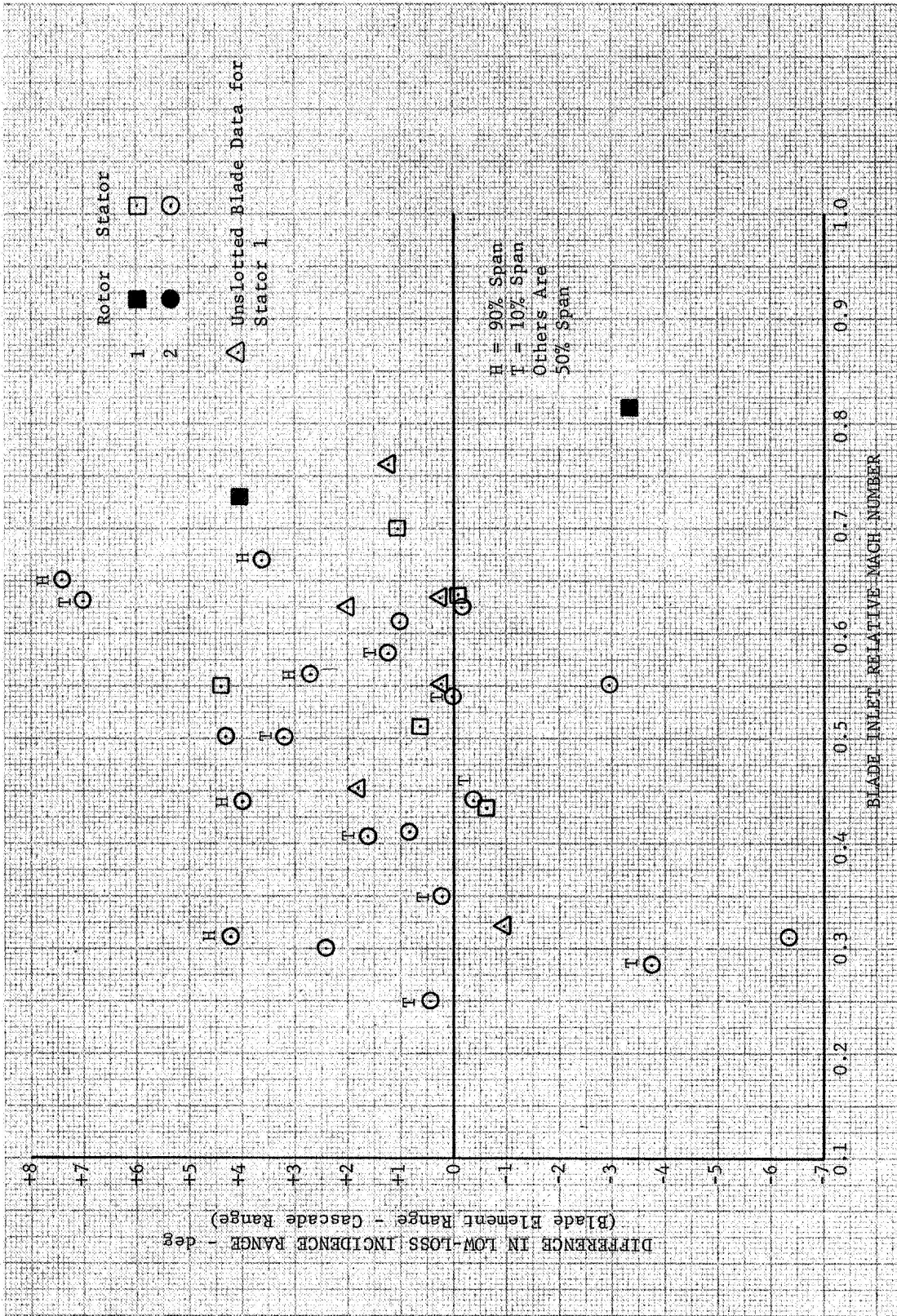
Figure 30. Difference Between Observed and Predicted Low-Loss Incidence Range for Slotted and Unslotted Blades

58
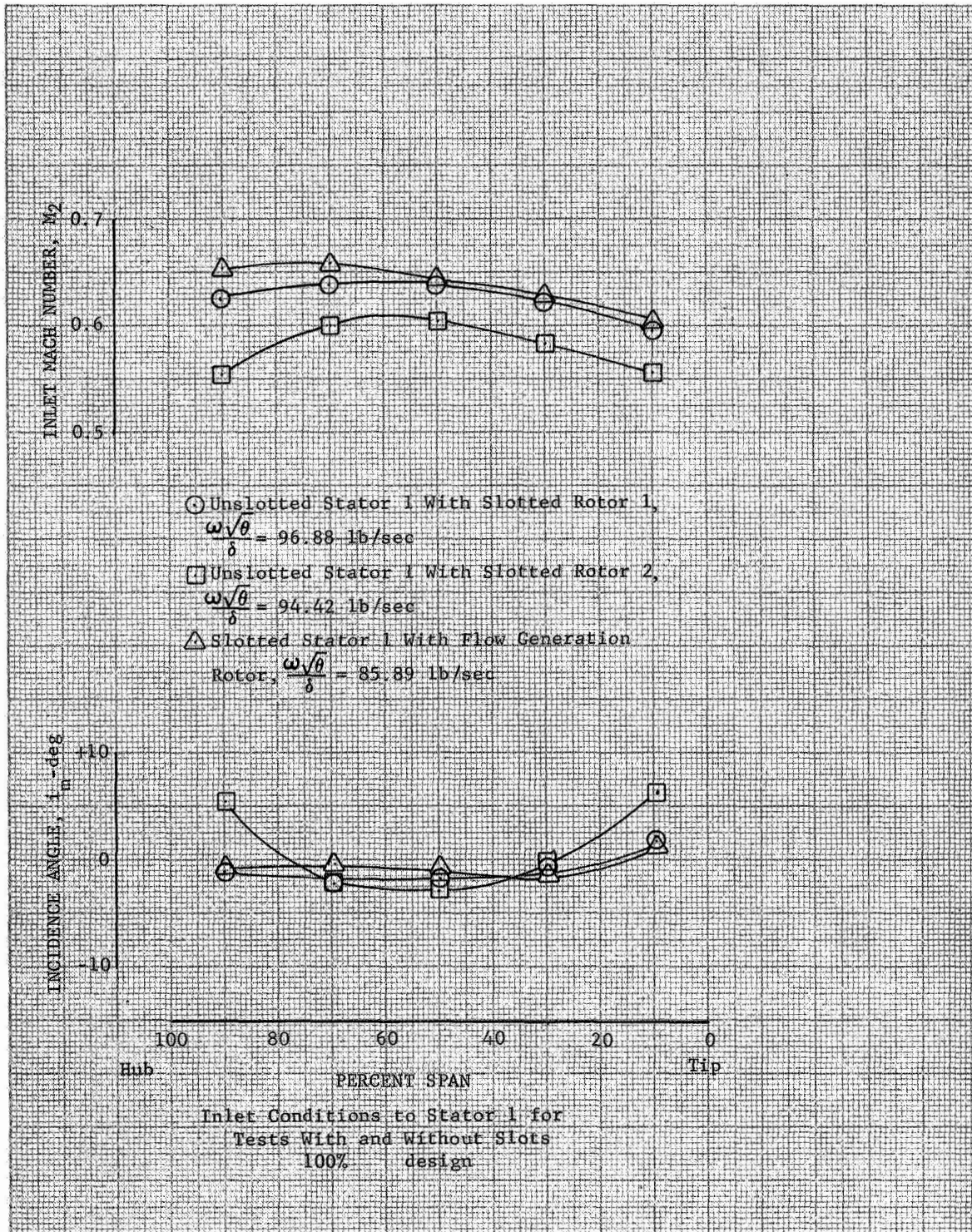
Figure 31. Inlet Conditions to Stator 1 for Tests With
and Without Slots - 100% $N/\sqrt{\theta}$ Design
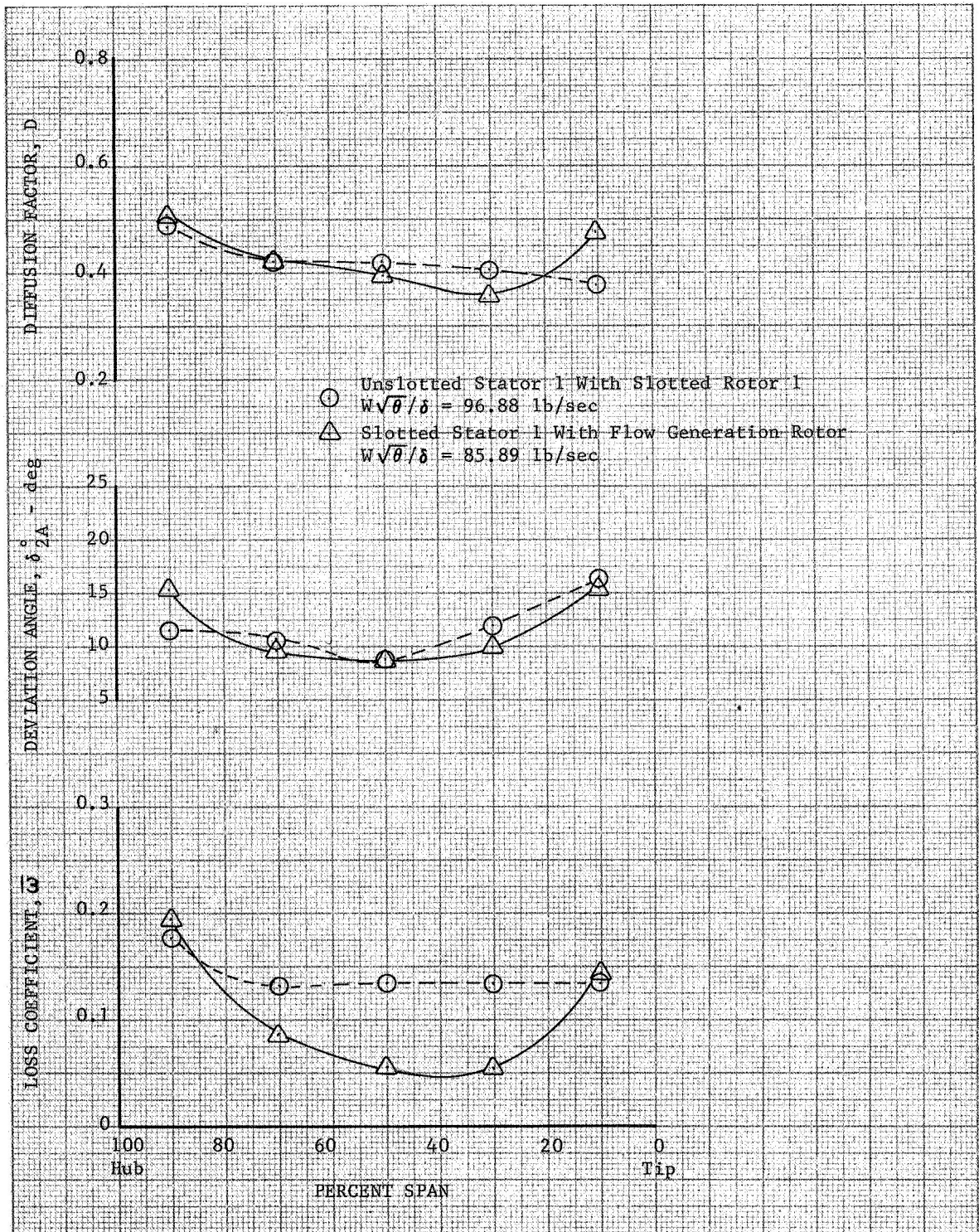
Figure 32. Comparison of Performance of Slotted and
Unslotted Stator 1 - Incidence Angle
Approximately Zero

60
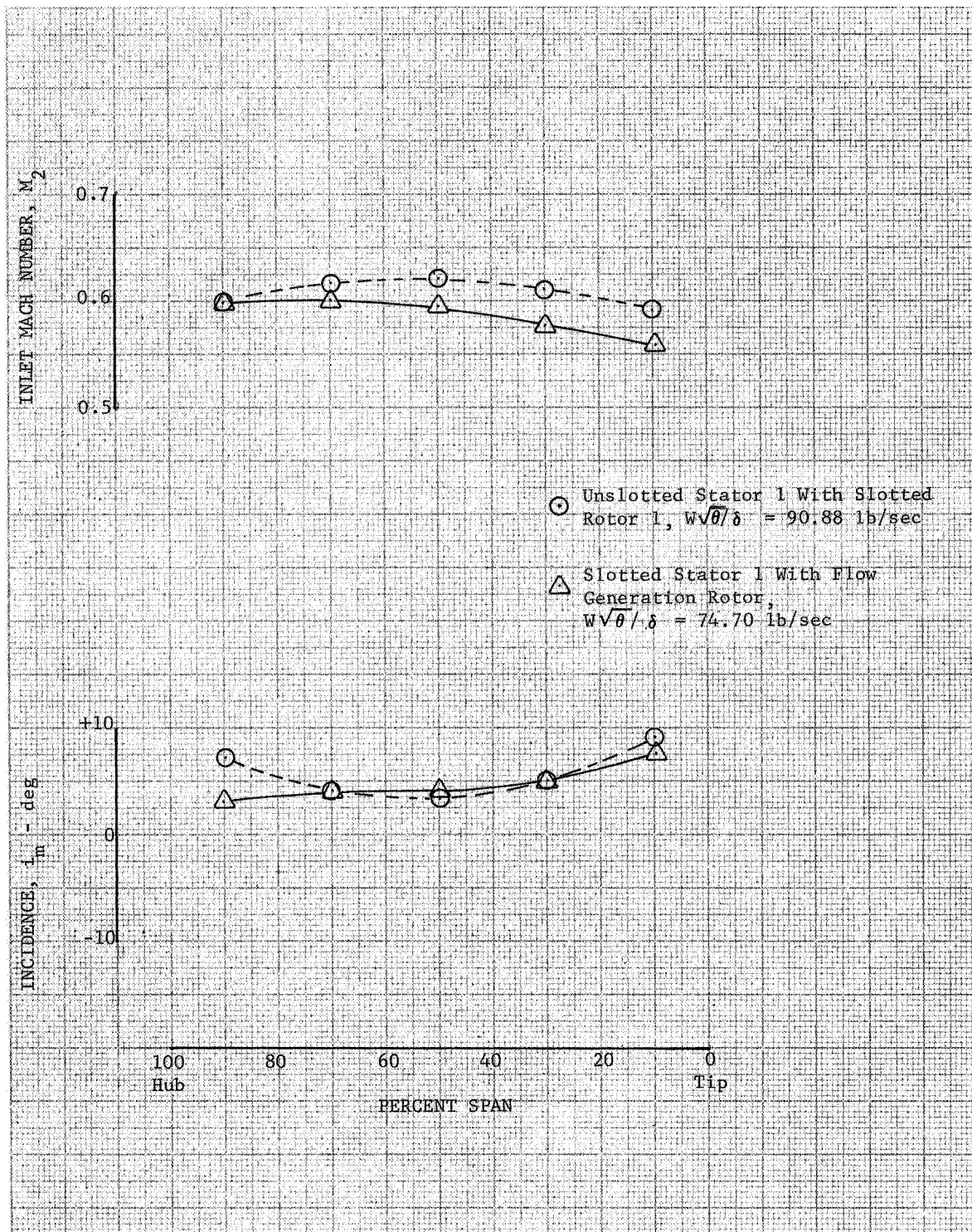
Figure 33. Inlet Conditions to Stator 1 for Tests With
and Without Slots - 100% $N/\sqrt{\theta}$ Design Near
Stall Incidence

61
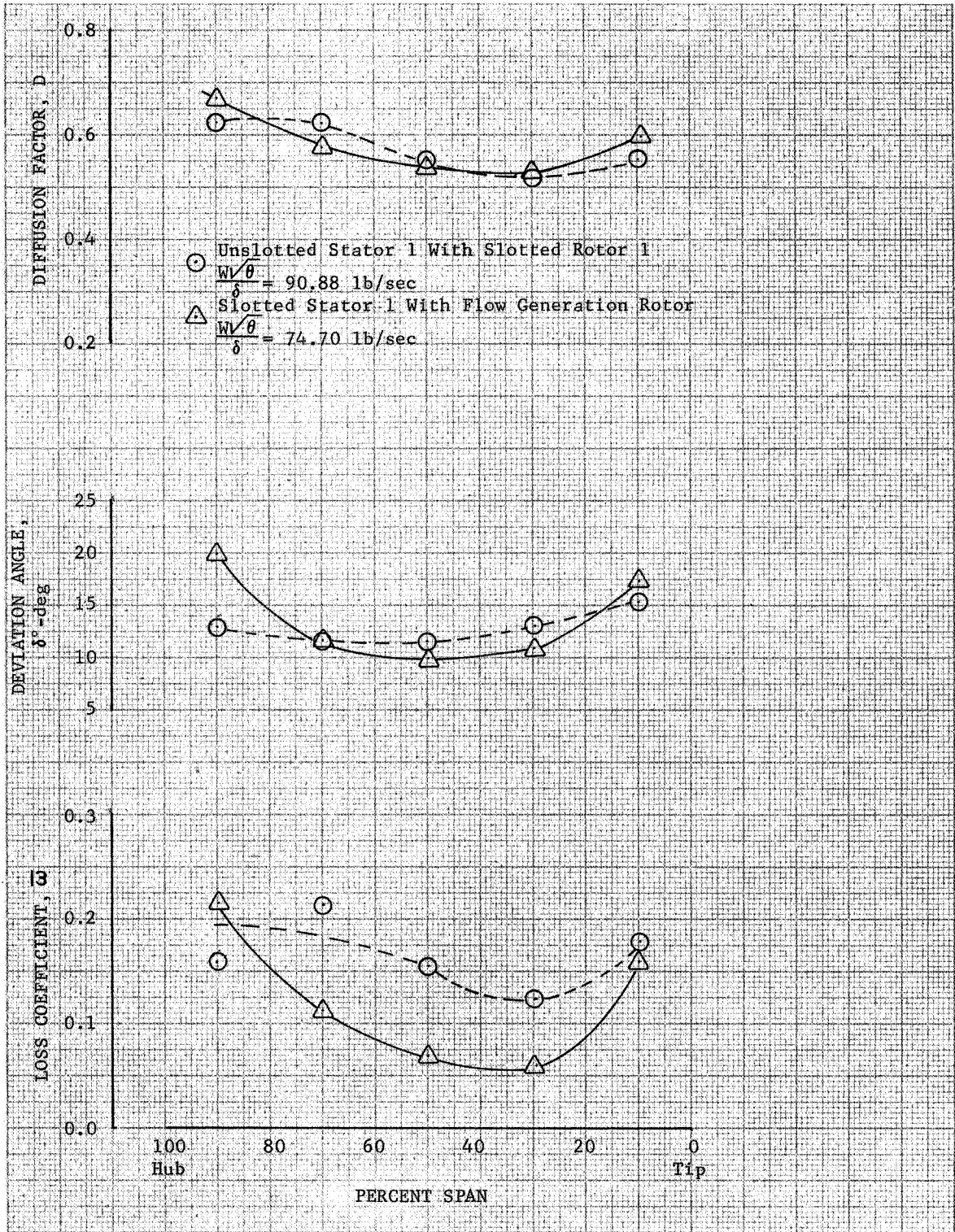
Figure 34. Comparison of Performance of Slotted and
Unslotted Stator 1 Near Stall Incidence
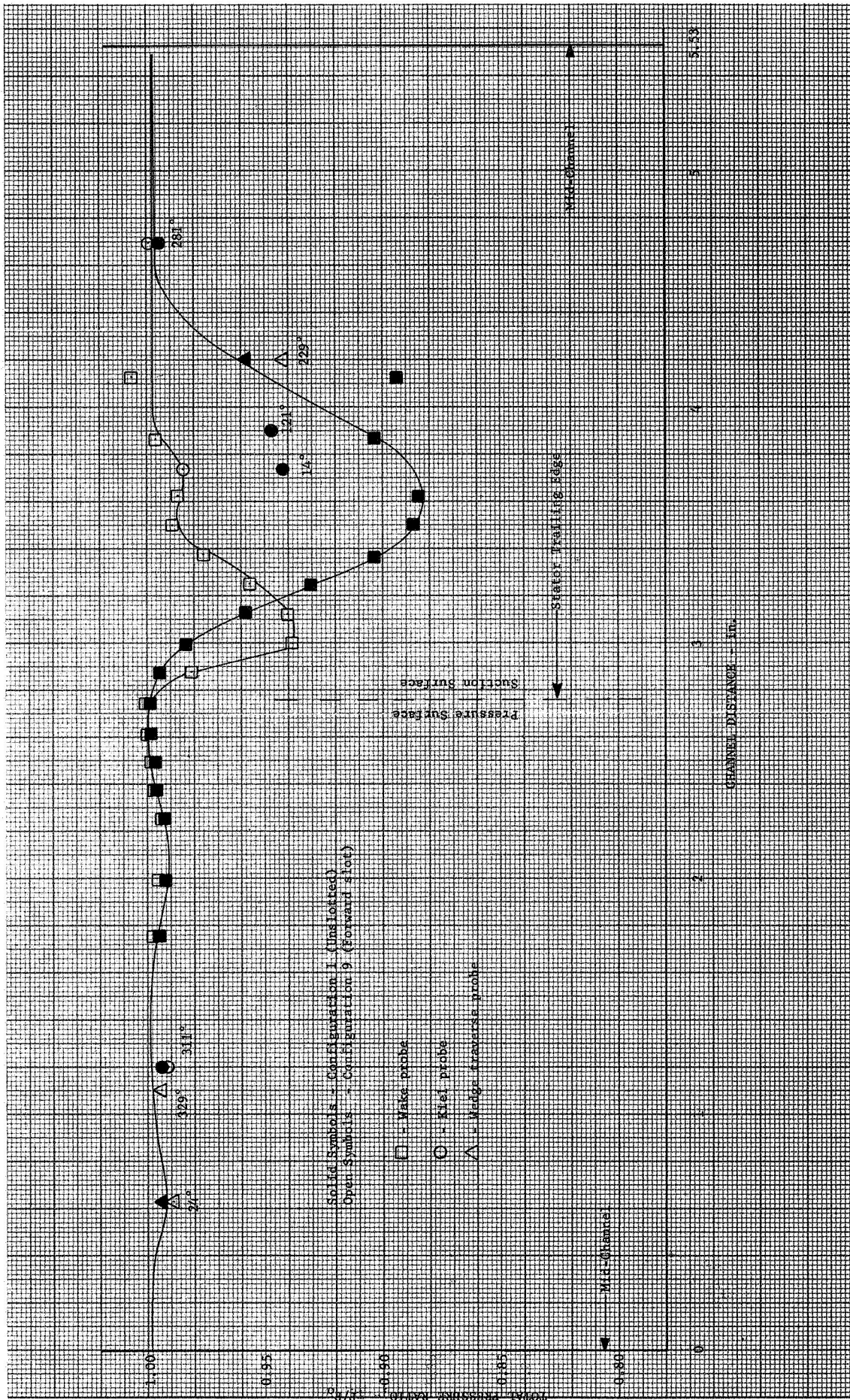
Figure 35. Comparison of Unslotted Annular Cascade Blade Wake With Slotted Blade Wake at Midspan (Loss Coefficients - Unslotted, 0.071; Slotted, 0.012)
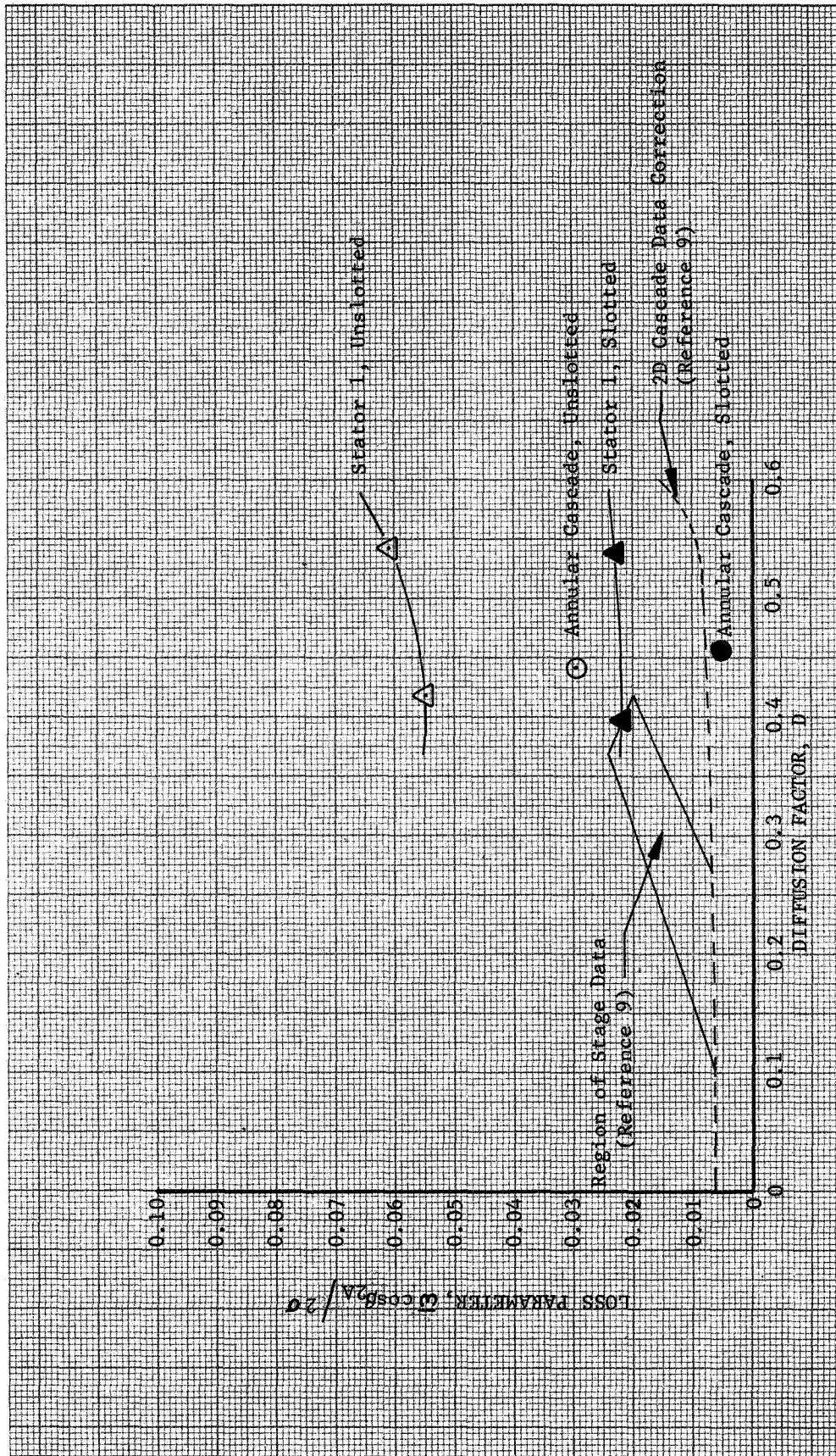
Figure 36. Slotted and Unslotted Stator Performance From Annular Cascade and Compressor Stage Tests at Midspan

64

$\kappa_1 = 65.2°$
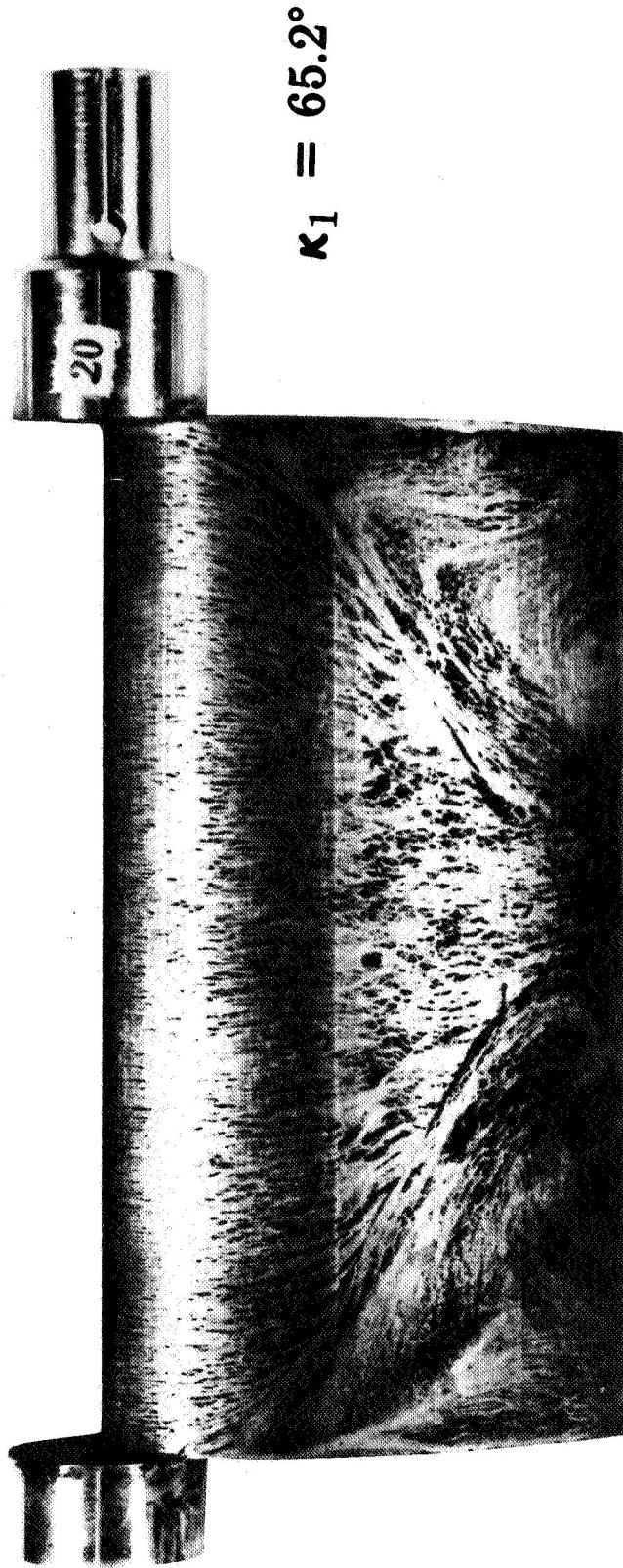
Figure 37. Flow Pattern for NACA 4-Digit Series Airfoil; $\beta_1 = 60°$, $\phi = 45°$, $\sigma = 1.87$, $M_1 = 0.332$

APPENDIX   A

Information relating to the design geometry and design vector
diagrams is tabulated in this appendix. The order of presentation
is:

Rotor 1

Rotor 2

Rotor 3

Stator 1

Stator 2

Stator 3

ROTOR 1 - DESIGN DATA

Airfoil Series: 65   No. of Blades: 60   Aspect Ratio: 1.707

Percent Span (from Tip)	κ_1'	κ_2'	ϕ	$\gamma°$	i_m	$0/0^*$	c	σ	t/c	$\delta°^*$	$\bar\omega$	D
90	51.69	22.44	29.25	37.11	0.69	1.230	2.210	1.250	0.075	9.71	0.058	0.466
70	53.61	28.90	24.71	41.18	0.72	1.227	2.210	1.196	0.067	7.82	0.051	0.458
50	54.98	33.84	21.14	44.35	0.98	1.242	2.210	1.149	0.059	6.73	0.050	0.455
30	55.51	38.14	17.37	46.86	1.88	1.251	2.210	1.109	0.052	5.71	0.049	0.456
10	56.12	41.99	14.13	49.08	2.58	1.259	2.210	1.071	0.044	4.74	0.046	0.455

Vector Diagram Data

Corrected Weight Flow   95.9 lb/sec
Corrected Rotor Speed   5588 rpm

	Pressure Ratio	Efficiency, %
Unslotted	1.31	89
Slotted	1.37	91

	Percent Span (from Tip)	V_1'	V_{z1}	$V_{\theta1}'$	β_1'	V_2'	V_{z2}	$V_{\theta2}'$	β_2'	U_1	M_1'	$\Delta\beta'$	D
Unslotted	90	785.7	479.4	622.5	52.38	550.5	466.1	292.9	32.15	823.8	0.719	20.23	0.466
	70	819.3	477.5	665.8	54.33	577.5	462.9	345.3	36.72	862.6	0.750	17.61	0.458
	50	846.1	473.3	701.3	55.96	596.5	453.1	388.0	40.57	899.7	0.774	15.39	0.455
	30	868.8	467.9	732.0	57.39	611.0	440.6	423.3	43.85	935.3	0.794	13.54	0.456
	10	889.9	462.1	760.5	58.70	626.6	429.4	456.3	46.73	969.7	0.813	11.97	0.455
Slotted	90	785.7	479.4	622.5	52.38	517.5	458.4	240.3	27.66	823.8	0.719	24.72	0.535
	70	819.3	477.5	665.8	54.33	541.6	455.9	292.5	32.69	862.6	0.750	21.64	0.529
	50	846.1	473.3	701.3	55.96	558.0	443.7	338.4	37.34	899.7	0.774	18.62	0.526
	30	868.8	467.9	732.0	57.39	570.1	433.2	370.5	40.54	935.3	0.794	16.85	0.531
	10	889.9	462.1	760.5	58.70	583.4	422.3	402.6	43.63	969.7	0.813	15.07	0.532

*Full NASA Deviation Angles

ROTOR 2 - DESIGN DATA

Airfoil Series: 65   No. of Blades: 60   Aspect Ratio: 1.707

Percent Span (from Tip)	κ_1'	κ_2'	ϕ	$\gamma°$	i_m	$0/0^*$	c	σ	t/c	$\delta°^*$	$\bar{\omega}$
90	52.16	16.15	36.01	34.21	0.42	1.247	2.210	1.250	0.075	11.43	0.062
70	53.61	23.60	30.01	38.63	0.71	1.249	2.210	1.196	0.067	9.30	0.056
50	55.03	29.24	25.79	42.10	0.70	1.253	2.210	1.149	0.059	8.05	0.053
30	56.04	33.91	22.13	44.98	0.90	1.248	2.210	1.109	0.052	7.13	0.052
10	56.79	38.65	18.14	47.75	1.26	1.250	2.210	1.071	0.044	5.97	0.047

Vector Diagram Data

Corrected Weight Flow 99.2 lb/sec
Corrected Rotor Speed 5366 rpm

	Pressure Ratio	Efficiency, %
Unslotted	1.35	90
Slotted	1.42	91

	Percent Span (from Tip)	V_1'	V_{z1}	$V_{\theta 1}'$	β_1'	V_2'	V_{z2}	$V_{\theta 2}'$	β_2'	U_1	M_1'	$\Delta\beta'$	D
Unslotted	90	811.1	492.6	644.4	52.58	533.1	472.5	246.8	27.58	791.1	0.742	25.00	0.538
	70	943.6	491.7	685.5	54.32	559.0	469.3	303.7	32.90	828.3	0.772	21.42	0.526
	50	869.3	489.2	718.6	55.73	577.1	459.1	349.7	37.29	863.9	0.795	18.43	0.520
	30	891.1	485.7	747.0	56.94	590.7	445.4	387.9	41.04	898.2	0.815	15.90	0.518
	10	911.0	481.8	773.2	58.05	606.0	431.3	425.7	44.62	931.1	0.833	13.42	0.512
Slotted	90	811.1	492.6	644.4	52.58	501.8	464.8	189.1	22.14	791.1	0.742	30.43	0.605
	70	843.6	491.7	685.5	54.32	523.9	462.5	246.1	28.02	828.3	0.772	26.30	0.596
	50	869.3	489.2	718.6	55.73	538.8	449.6	297.0	33.45	863.9	0.795	22.27	0.590
	30	891.1	485.7	747.0	56.94	549.5	437.5	332.5	37.24	898.2	0.815	19.71	0.592
	10	911.0	481.8	773.2	58.05	562.3	425.1	368.1	40.89	931.1	0.833	17.16	0.590

*Full NASA Deviation Angles

ROTOR 3 – DESIGN DATA

Airfoil Series: 65 No. of Blades: 60 Aspect Ratio: 1.707

Percent Span (from Tip)	κ_1'	κ_2'	ϕ	$\gamma°$	i_m	$0/0*$	c	σ	t/c	$\delta°*$	$\bar{\beta}$
90	58.80	6.90	51.90	32.87	-2.22	1.280	2.210	1.250	0.075	16.70	0.076
70	59.05	16.05	43.00	37.48	-1.60	1.278	2.210	1.196	0.067	13.58	0.066
50	59.45	22.96	36.49	41.25	-1.20	1.271	2.210	1.149	0.059	11.66	0.061
30	60.15	28.75	31.40	44.54	-1.14	1.261	2.210	1.109	0.052	10.36	0.056
10	61.29	34.01	27.28	47.66	-1.57	1.241	2.210	1.071	0.044	9.20	0.053

Vector Diagram Data

Corrected Weight Flow 91.4 lb/sec
Corrected Rotor Speed 4528 rpm

	Pressure Ratio	Efficiency, %
Unslotted	1.34	90
Slotted	1.41	91

Percent Span (from Tip)	V_1'	V_{z1}	$V_{\theta 1}'$	β_1'	V_2'	V_{z2}	$V_{\theta 2}'$	β_2'	U_1	M_1'	$\Delta\beta'$	D
Unslotted												
90	792.9	436.4	662.0	56.58	467.5	428.4	187.2	23.60	667.5	0.721	32.98	0.649
70	811.2	436.2	684.0	57.45	479.8	417.0	237.2	29.63	698.9	0.738	27.82	0.638
50	828.9	435.8	705.1	58.25	491.7	404.6	279.4	34.62	729.0	0.754	23.63	0.629
30	845.8	435.2	725.3	59.01	504.9	391.7	318.6	39.11	757.9	0.769	19.90	0.619
10	862.2	434.4	744.8	59.72	517.4	377.1	354.3	43.21	785.7	0.784	16.51	0.611
Slotted												
90	792.9	436.4	662.0	56.58	439.3	422.2	121.3	16.03	667.5	0.721	40.54	0.718
70	811.2	436.2	684.0	57.45	446.1	411.4	172.6	22.76	698.9	0.738	34.69	0.713
50	828.9	435.8	705.1	58.25	453.8	396.9	220.0	29.00	729.0	0.754	29.25	0.706
30	845.8	435.2	725.3	59.01	463.6	386.8	255.5	33.44	757.9	0.769	25.57	0.702
10	862.2	434.4	744.8	59.72	473.0	374.1	289.4	37.73	785.7	0.784	21.99	0.697

*Full NASA Deviation Angles

STATOR 1 - DESIGN DATA

Airfoil Series: 65 No. of Blades: 58 Aspect Ratio: 1.663

Percent Span (from Tip)	κ_1	κ_2	ϕ	γ°	i_m	O/O^*	c	σ	t/c	$\delta^{\circ*}$	$\bar{\omega}$
90	52.15	22.14	30.01	37.20	-1.68	1.187	2.182	1.192	0.090	10.14	0.040
70	52.15	22.14	30.01	37.20	-0.77	1.234	2.182	1.143	0.090	9.47	0.037
50	52.15	22.14	30.01	37.20	-0.22	1.273	2.182	1.099	0.090	9.46	0.036
30	52.15	22.14	30.01	37.20	0.22	1.315	2.182	1.060	0.090	9.71	0.035
10	52.15	22.14	30.01	37.20	0.61	1.355	2.182	1.026	0.090	9.93	0.034

Vector Diagram Data

	Percent Span (from Tip)	V_1	V_{z1}	$V_{\theta 1}$	β_1	V_2	V_{z2}	$V_{\theta 2}$	β_2	M_1	$\Delta\beta$	D
Unslotted	90	704.5	448.3	543.4	50.47	462.0	390.6	246.7	32.28	0.644	18.19	0.521
	70	697.3	435.1	544.9	51.38	474.4	403.9	248.7	31.61	0.636	19.77	0.506
	50	683.6	421.4	538.2	51.93	474.8	404.4	248.8	31.60	0.623	20.33	0.498
	30	667.5	407.4	528.8	52.37	470.2	399.4	248.1	31.85	0.607	20.53	0.494
	10	653.8	395.6	520.5	52.76	467.4	396.0	248.2	32.07	0.594	20.69	0.488
Slotted	90	704.5	448.3	543.4	50.47	430.7	384.0	195.1	26.93	0.644	23.53	0.596
	70	697.3	435.1	544.9	51.38	446.0	398.2	200.9	26.78	0.636	24.61	0.576
	50	683.6	421.4	538.2	51.93	448.3	400.8	200.9	26.62	0.623	25.31	0.569
	30	667.5	407.4	528.8	52.37	445.2	397.5	200.4	26.75	0.607	25.62	0.565
	10	653.8	395.6	520.5	52.76	443.7	395.8	200.6	26.88	0.594	25.88	0.560

*Full NASA Deviation Angles

70

STATOR 2 - DESIGN DATA

Airfoil Series: 65 No. of Blades: 58 Aspect Ratio: 1.663

Percent Span (from Tip)	κ_1	κ_2	$\gamma°$	ϕ	i_m	$0/0*$	c	σ	t/c	$\delta°*$	$\bar{\omega}$
90	53.53	14.68	34.11	38.85	-3.06	1.203	2.182	1.192	0.090	12.34	0.044
70	53.53	14.68	34.11	38.85	-2.15	1.248	2.182	1.143	0.090	11.81	0.040
50	53.53	14.68	34.11	38.85	-1.60	1.290	2.182	1.099	0.090	11.88	0.039
30	53.53	14.68	34.11	38.85	-1.16	1.333	2.182	1.060	0.090	12.20	0.037
10	53.53	14.68	34.11	38.85	-0.77	1.374	2.182	1.026	0.090	12.50	0.036

Vector Diagram Data

	Percent Span (from Tip)	V_1	V_{z1}	$V_{\theta 1}$	β_1	V_2	V_{z2}	$V_{\theta 2}$	β_2	M_1	$\Delta\beta$	D
Unslotted	90	704.5	448.3	543.4	50.47	430.3	383.3	195.6	27.02	0.644	23.45	0.596
	70	697.3	435.1	544.9	51.38	446.2	399.4	199.1	26.49	0.636	24.89	0.577
	50	683.6	421.4	538.2	51.93	448.8	401.4	200.7	26.56	0.623	25.37	0.568
	30	667.5	407.4	528.8	52.37	445.8	397.6	201.6	26.88	0.607	25.49	0.563
	10	653.8	395.6	520.5	52.76	444.3	395.3	203.0	27.18	0.594	25.58	0.556
Slotted	90	704.5	448.3	543.4	50.47	402.1	376.2	141.8	20.65	0.644	29.82	0.668
	70	697.3	435.1	544.9	51.38	420.9	394.2	147.7	20.54	0.636	30.85	0.645
	50	683.6	421.4	538.2	51.93	425.2	398.5	148.4	20.43	0.623	31.50	0.637
	30	667.5	407.4	528.8	52.37	423.6	396.5	149.0	20.60	0.607	31.77	0.633
	10	653.8	395.6	520.5	52.76	423.6	396.0	150.2	20.77	0.594	31.99	0.627

*Full NASA Deviation Angles

STATOR 3 - DESIGN DATA

Airfoil Series: 65 No. of Blades: 58 Aspect Ratio: 1.663

Percent Span (from Tip)	κ_1	κ_2	ϕ	$\gamma°$	i_m	$0/0*$	c	σ	t/c	$\delta°*$	$\bar{\omega}$
90	57.70	-0.64	58.34	28.52	-7.23	1.209	2.182	1.192	0.090	17.29	0.053
70	57.70	-0.64	58.34	28.52	-6.32	1.256	2.182	1.143	0.090	17.04	0.049
50	57.70	-0.64	58.34	28.52	-5.77	1.299	2.182	1.099	0.090	17.26	0.047
30	57.70	-0.64	58.34	28.52	-5.33	1.344	2.182	1.060	0.090	17.74	0.045
10	57.70	-0.64	58.34	28.52	-4.94	1.385	2.182	1.026	0.090	18.18	0.044

Vector Diagram Data

	Percent Span (from Tip)	V_1	V_{z1}	$V_{\theta 1}$	β_1	V_2	V_{z2}	$V_{\theta 2}$	β_2	M_1	$\Delta\beta$	D
Unslotted	90	704.5	448.3	543.4	50.47	389.8	373.5	111.8	16.65	0.644	33.81	0.704
	70	697.3	435.1	544.9	51.38	410.1	393.4	115.8	16.40	0.636	34.99	0.681
	50	683.6	421.4	538.2	51.93	415.7	398.3	119.0	16.62	0.623	35.30	0.670
	30	667.5	407.4	528.8	52.37	415.2	396.8	122.1	17.10	0.607	35.27	0.665
	10	653.8	395.6	520.5	52.76	416.1	396.7	125.4	17.54	0.594	35.22	0.657
Slotted	90	704.5	448.3	543.4	50.47	371.9	368.0	53.9	8.33	0.644	42.14	0.763
	70	697.3	435.1	544.9	51.38	394.1	390.0	56.9	8.30	0.636	43.08	0.741
	50	683.6	421.4	538.2	51.93	400.9	396.7	57.7	8.25	0.623	43.65	0.733
	30	667.5	407.4	528.8	52.37	401.4	396.9	59.5	8.53	0.607	43.84	0.729
	10	653.8	395.6	520.5	52.76	403.3	398.6	61.5	8.77	0.594	43.98	0.724

*Full NASA Deviation Angles

APPENDIX B

The composite blade element performance at 10, 30, 50, 70, and 90% of span at the point of minimum loss is presented in this appendix in figures B-1 through B-6. The performance is denoted as the incidence angle, diffusion factor, deviation angle, and loss coefficient. It should be noted that the conditions so described do not simultaneously occur, and the plotted points have not been joined by curves to remind the reader of this fact.

Figure B-1. Composite of Blade Element Performance for
Reference Incidence - Slotted Rotor 1

Figure B-2.   Composite of Blade Element Performance for
            Reference Incidence - Slotted Rotor 2
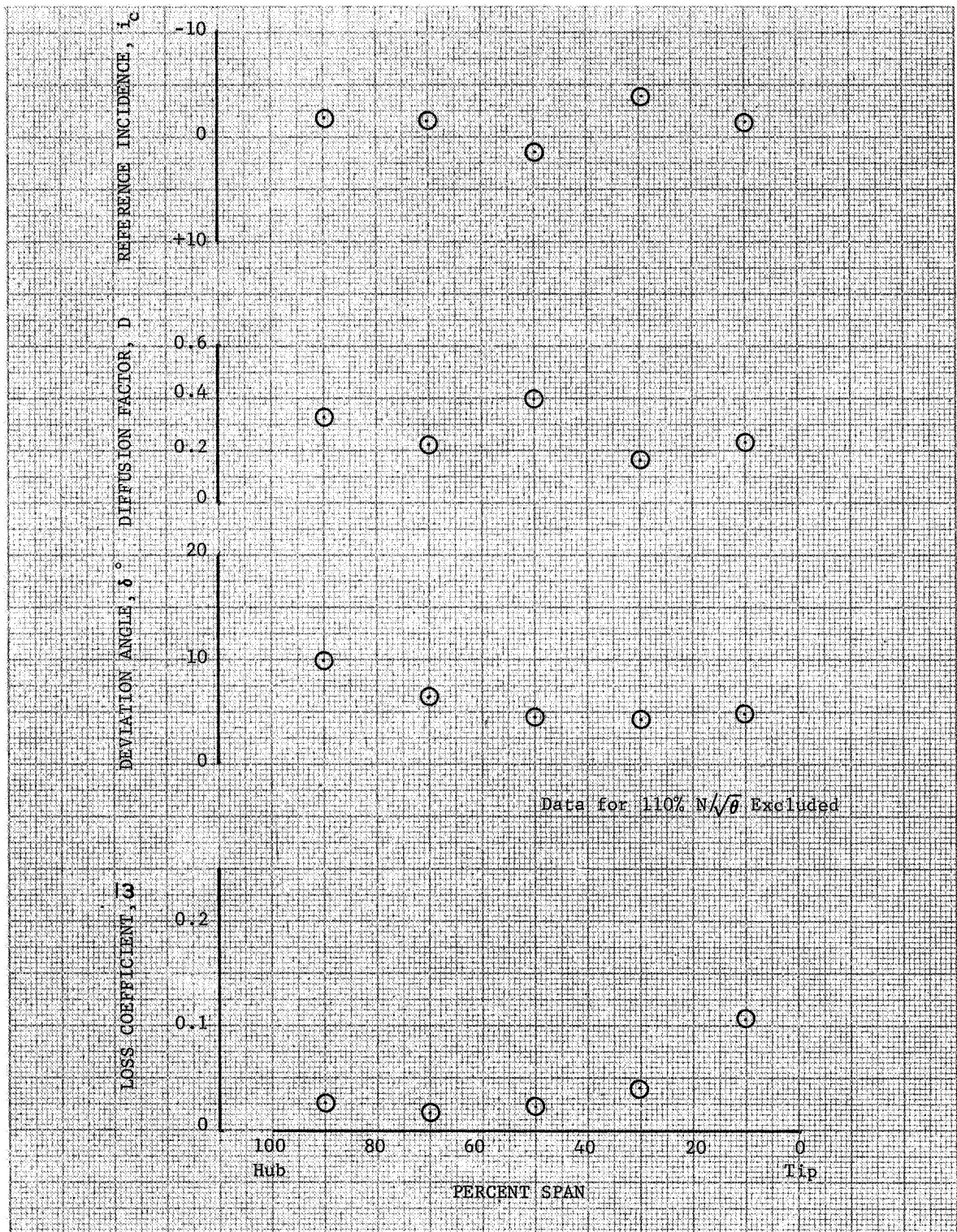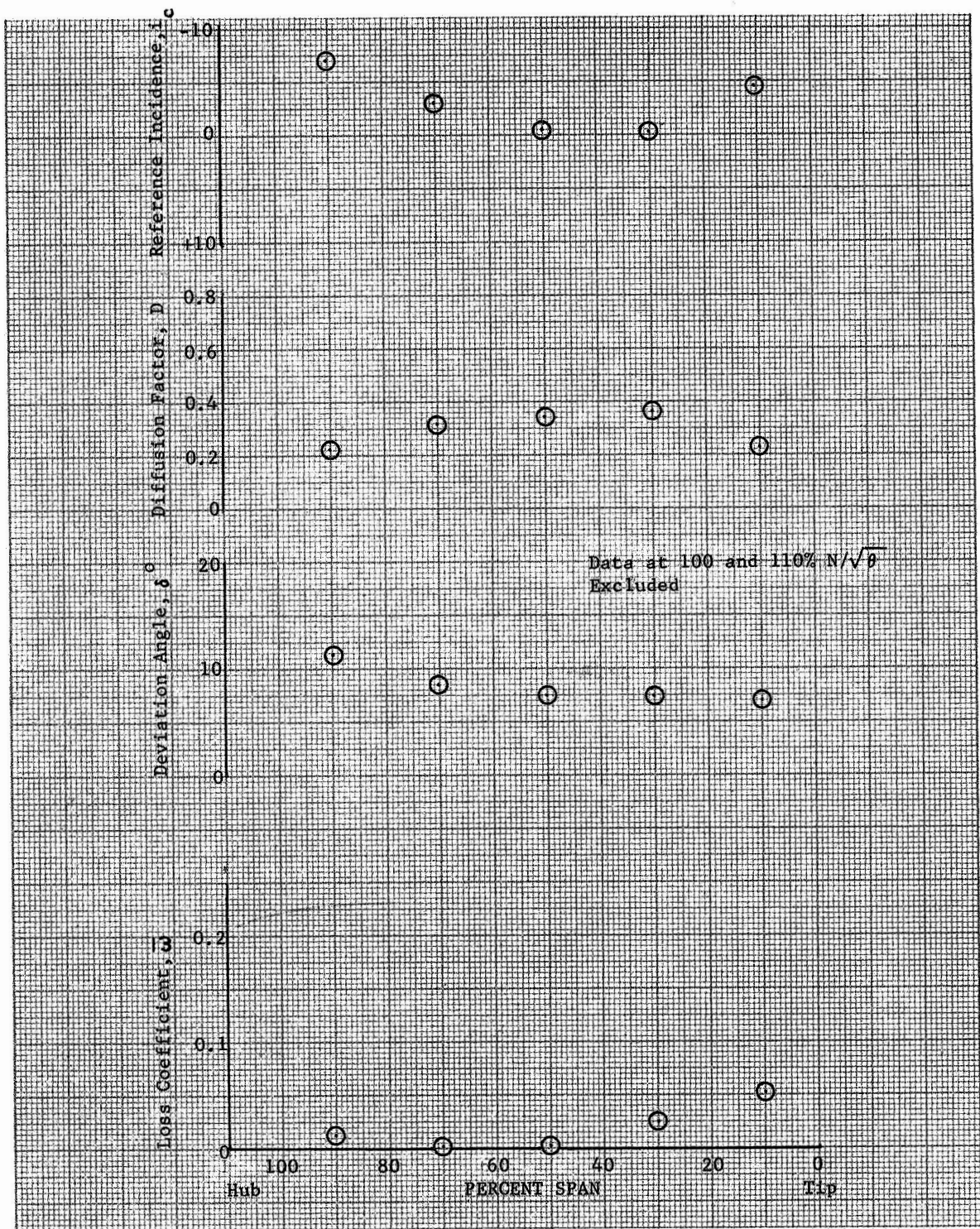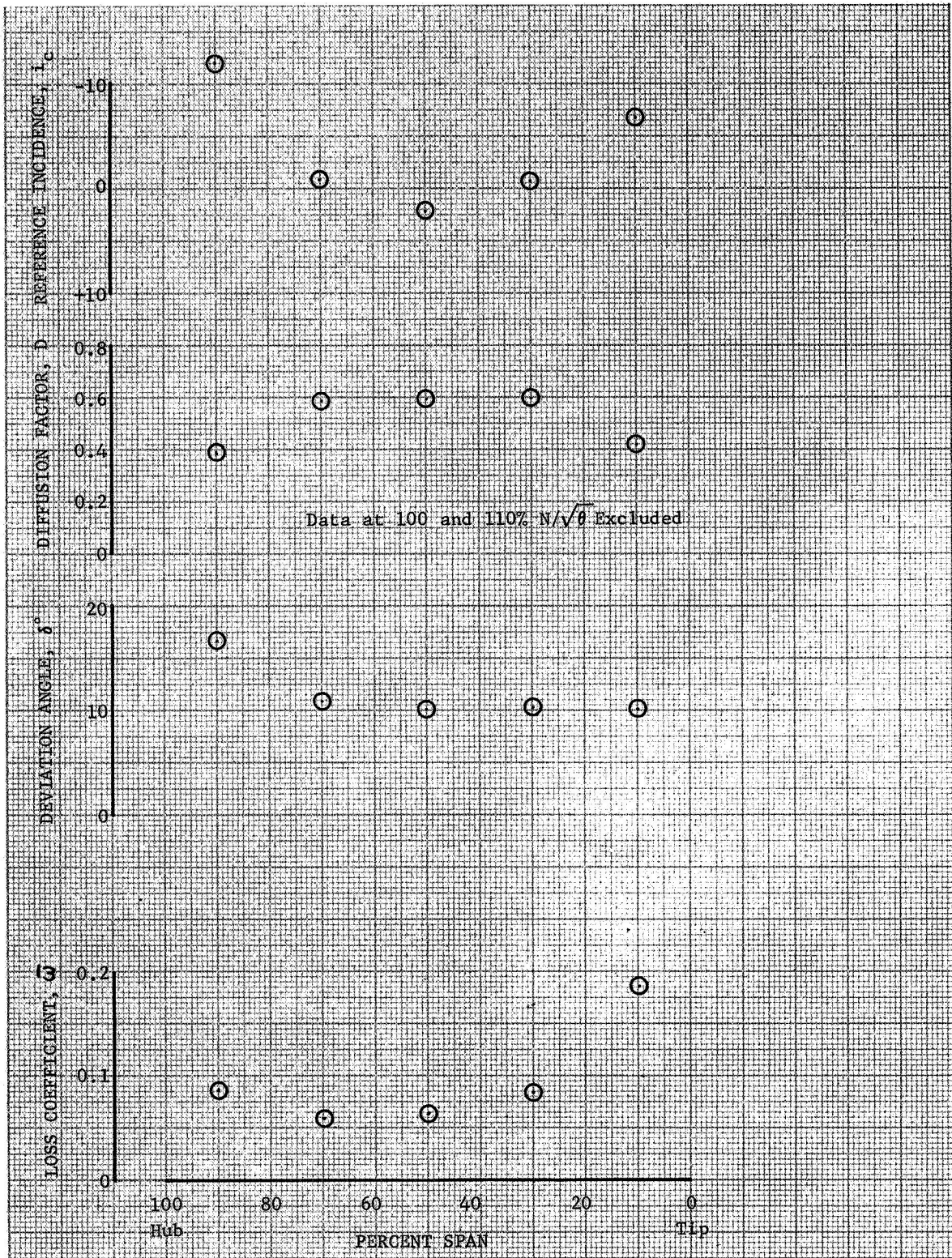
Figure B-3. Composite of Blade Element Performance for
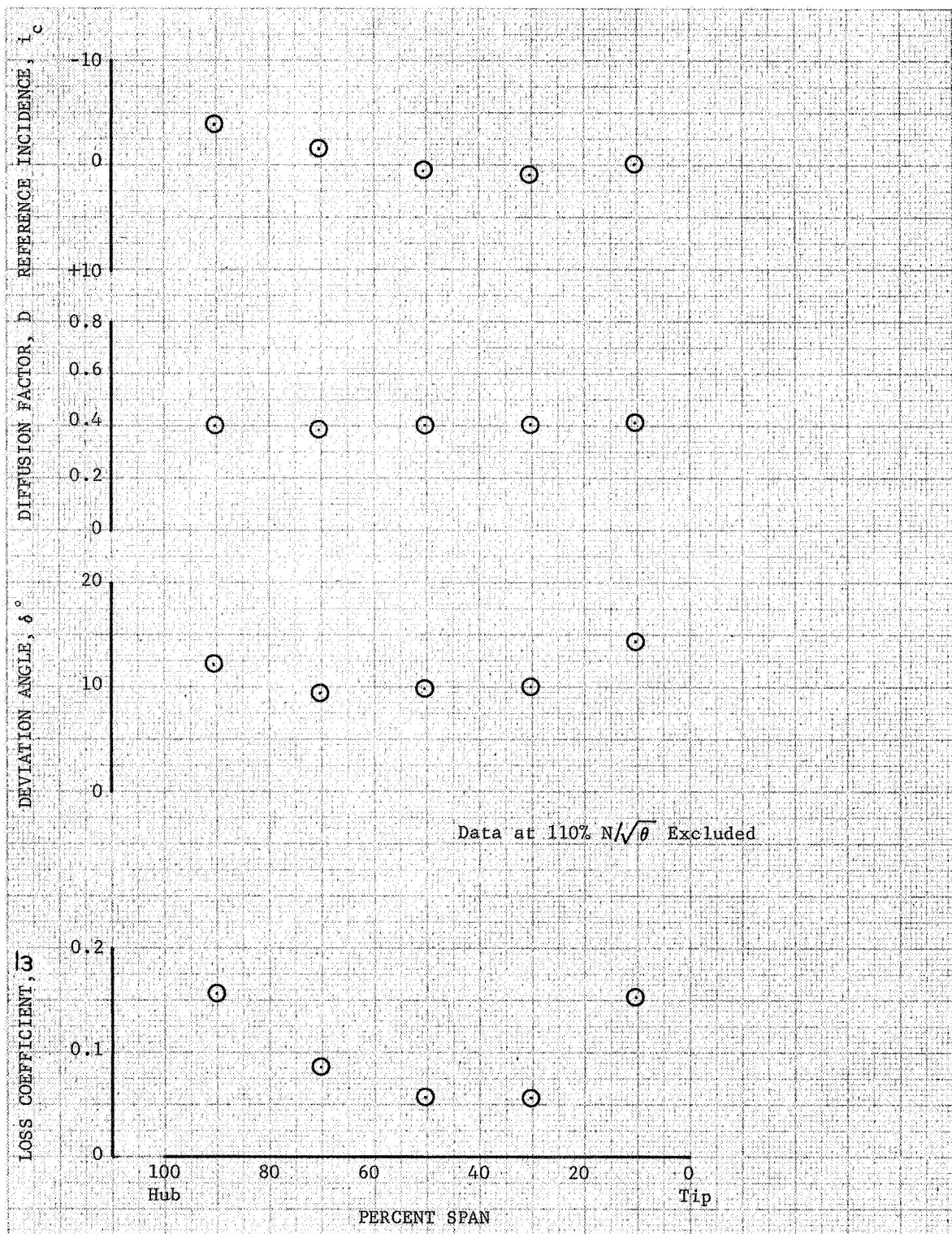Reference Incidence - Slotted Rotor 3

Figure B-4. Composite of Blade Element Performance for
Reference Incidence - Slotted Stator 1
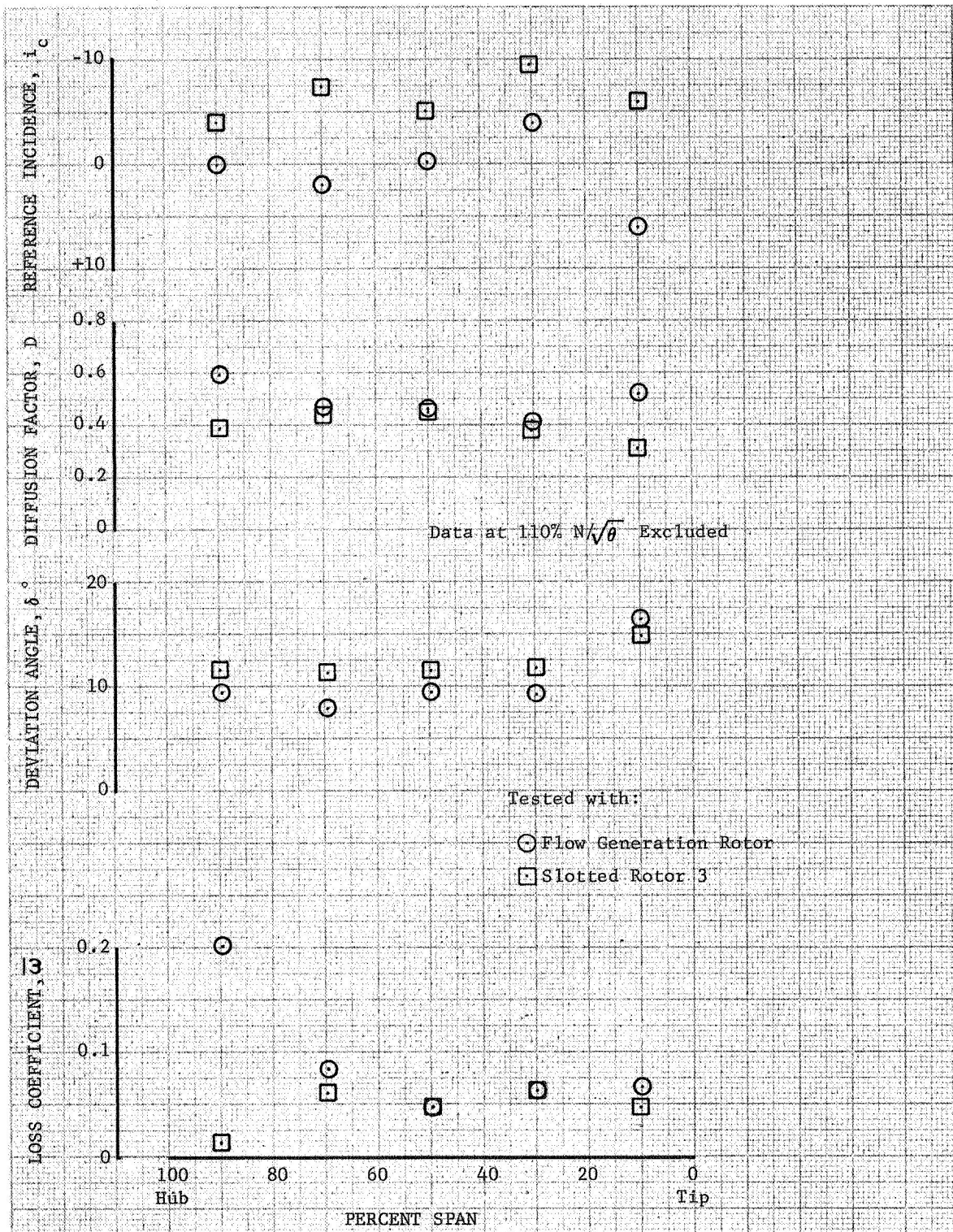
Figure B-5. Composite of Blade Element Performance for
            Reference Incidence - Slotted Stator 2
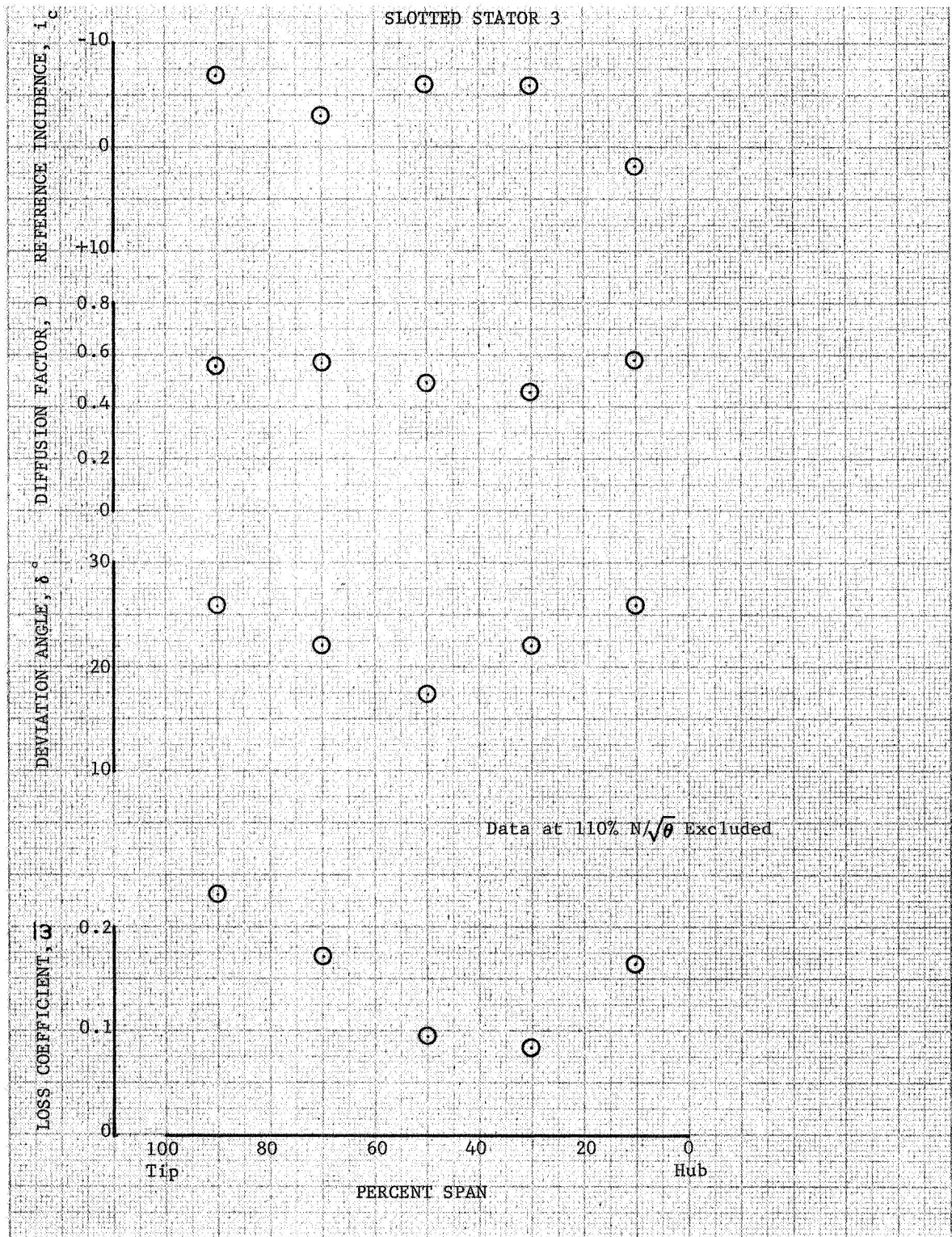
Figure B-6. Composite of Blade Element Performance for
Reference Incidence - Slotted Stator 3

APPENDIX C
REFERENCES

1. NASA CR-54544, PWA FR-1713, "Single Stage Experimental Evaluation of Slotted Rotor and Stator Blading, Part I - Analysis and Design," July 1966.

2. NASA CR-54545, PWA FR-1669, "Single Stage Experimental Evaluation of Slotted Rotor and Stator Blading, Part II - Annular Cascade Investigation of Slot Location and Geometry," October 1966.

3. NASA CR-54546, PWA FR-2110, "Single Stage Experimental Evaluation of Slotted Rotor and Stator Blading, Part III - Data and Performance for Slotted Rotor 1," February 1967.

4. NASA CR-54547, PWA FR-2111, "Single Stage Experimental Evaluation of Slotted Rotor and Stator Blading, Part IV - Data and Performance for Slotted Rotor 2," February 1967.

5. NASA CR-54548, PWA FR-2285, "Single Stage Experimental Evaluation of Slotted Rotor and Stator Blading, Part V - Data and Performance for Slotted Rotor 3 - Slotted Stator 2," August 1967.

6. NASA CR-54549, PWA FR-2286, "Single Stage Experimental Evaluation of Slotted Rotor and Stator Blading, Part VI - Data and Performance for Slotted Stator 1," July 1967.

7. NASA CR-54550, PWA FR-2287, "Single Stage Experimental Evaluation of Slotted Rotor and Stator Blading, Part VII - Data and Performance for Slotted Stator 2," September 1967.

8. NASA CR-54551, PWA FR-2288, "Single Stage Experimental Evaluation of Slotted Rotor and Stator Blading, Part VIII - Data and Performance for Slotted Stator 3," October 1967.

9. Aerodynamic Design of Axial Flow Compressors (Revised), NASA SP-36, 1965.

10. NACA RME53D01, "Diffusion Factor for Estimating Losses and Limiting Blade Loadings in Axial Flow Compressor Blade Elements," S. Lieblein, F. C. Schwenk, and B. L. Broderick, 1953.

11. Brenst. Warmekr. 5 (1953) No. 10, "Das Verhalten von Tragflugelgittern in Axialverdichtern und im Windkanal," P. DeHaller.

12. ASME 64-WA/FE-29, "Wall Stall in Compressor Cascades," J. H. Horlock, P. M. E. Percival, J. F. Louis, and B. LaKshminarayana, 1964.

APPENDIX D
DEFINITION OF SYMBOLS

A. GENERAL NOMENCLATURE

A_A	Flowpath annular area, in.^{2}
c	Chord length, in.
c_p	Specific heat at constant pressure, Btu/lb$_m$°R
D	Diffusion factor
g	Gravitational constant, 32.2 lb$_m$ ft/lb$_f$ sec^2
i_m	Incidence angle, deg (based on equivalent circular arc meanline)
J	Mechanical equivalent of heat, 778.2 ft-lb$_f$/Btu
M	Absolute Mach number
O	Minimum blade passage gap, in.
O*	Critical blade passage gap, in.
P	Total pressure, lb$_f$/in.^{2}
p	Static pressure, lb$_f$/in.^{2}
q	Pressure equivalent of the velocity head, lb$_f$/in.^{2}
S	Blade spacing, in.
s	Blade span, in.
t	Blade maximum thickness, in.
T	Total temperature, °R
U	Rotor speed, ft/sec
V	Velocity, ft/sec
W	Actual flowrate, lb$_m$/sec
β	Air angle, deg from axial direction
γ	Ratio of specific heats
$\gamma°$	Blade-chord angle, deg from axial direction
δ	Ratio of total pressure to NASA standard sea level pressure of 2116 psf
$\delta°$	Deviation angle, deg
Δh	Specific enthalpy rise, ft lb$_f$/lb$_m$
η_{ad}	Adiabatic efficiency
θ	Ratio of total temperature to NASA standard sea level temperature of 518.7°R

κ	Blade metal angle, deg from axial direction (based on equivalent circular arc meanline)
ρ	Density, lb_m/ft^3
σ	Solidity, c/S
ϕ	Blade camber angle, $\kappa_1 - \kappa_2$, deg; or flow coefficient V_{z0}/U
$\overline{\omega}$	Loss coefficient
ψ	Pressure coefficient, $\dfrac{Jgc_pT_{std}\left[\left(\dfrac{\overline{P}_{2A}}{P_0}\right)^{\frac{\gamma-1}{\gamma}} - 1\right]}{\dfrac{U_m^2}{\theta}}$

Subscripts:

0	Guide vane inlet
1	Rotor inlet
2	Rotor exit
2A	Stator exit
3	Stator exit (1.0 chord length downstream from Station 2A)
f	Force
h	Hub
m	Mean or mass
t	Tip
z	Axial component
θ	Tangential component

Superscripts:

'	Related to rotor blade
‾	Mass average value

B. SLOT NOMENCLATURE

A_2	Slot throat area, in.^{2}
R	Coanda radius, in.
R_p	Pressure surface edge radius, in.
r_1	Slot leading edge radius, in.
r_2	Slot trailing edge radius, in.
t	Blade thickness at intersection of slot centerline and mean camber line, in.
Y_1	Slot capture dimension, in.
Y_2	Slot throat dimension, in.
ψ	Angle formed by slot centerline and mean camber line, deg

REPORTS DISTRIBUTION LIST

1. NASA-Lewis Research Center
    21000 Brookpark Road
    Cleveland, Ohio 44135
    Attention:

Report Control Office	MS 5-5	1
Technical Utilization Office	MS 3-19	1
Library	MS 60-3	2
Fluid Systems Component Division	MS 5-3	1
Pump & Compressor Branch	MS 5-9	6
A. Ginsburg	MS 5-3	1
M. J. Hartmann	MS 5-9	1
W. A. Benser	MS 5-9	1
D. M. Sandercock	MS 5-9	1
L. J. Herrig	MS 5-9	1
T. F. Gelder	MS 5-9	1
C. L. Ball	MS 5-9	1
L. Reid	MS 5-9	1
J. H. De Ford	MS 60-5	2
C. L. Meyer	MS 60-6	1
J. H. Povolny	MS 60-6	1
A. W. Goldstein	MS 7-1	1
J. J. Kramer	MS 7-1	1
W. L. Beede	MS 60-6	6
J. J. Watt	MS 60-6	1
C. H. Voit	MS 5-3	1

2. NASA Scientific and Technical Information Facility
    P. O. Box 33
    College Park, Maryland 20740
    Attention:
    NASA Representative   6

3. FAA Headquarters
    800 Independence Ave., S. W.
    Washington, D. C. 20553
    Attention:
    Brig. General J. C. Maxwell   1
    F. B. Howard   1

4. NASA Headquarters
    Washington, D. C. 20546
    Attention:
    N. F. Rekos (RAP)   1

5. U. S. Army Aviation Material Laboratory
    Fort Eustis, Virginia
    Attention:
      John White   1

6. Headquarters
    Wright Patterson AFB, Ohio   45433
    Attention:
      J. L. Wilkins, SESOS   1
      S. Kobelak, APTP   1
      R. P. Carmichael, SESSP   1

7. Department of Navy
    Bureau of Weapons
    Washington, D. C.   20525
    Attention:
      Robert Brown, RAPP14   1

8. Department of Navy
    Bureau of Ships
    Washington, D. C.   20360
    Attention:
      G. L. Graves   1

9. NASA-Langley Research Center
    Technical Library
    Hampton, Virginia   23365
    Attention:
      Mark R. Nichols   1
      John V. Becker   1

10. The Boeing Company
    Commercial Airplane Division
    P. O. Box 3991
    Seattle, Washington   98124
    Attention:
      G. J. Schott   MS 80-66   1

11. Douglas Aircraft Company
    3855 Lakewood Boulevard
    Long Beach, California   90801
    Attention:
      J. E. Merriman   1
      Technical Information Center C1-250

12. Pratt & Whitney Aircraft
    Florida Research and Development Center
    P. O. Box 2691
    West Palm Beach, Florida   33402
    Attention:
       W. H. Brown   1
       R. A. Schmidtke 1
       J. M. Silk 1
       B. A. Jones 1
       R. W. Rockenbach 1
       B. S. Savin 1
       W. R. Alley 1
       H. D. Stetson 1

13. Pratt & Whitney Aircraft
    400 Main Street
    East Hartford, Connecticut
    Attention:
       J. A. Fligg 1
       A. W. Stubner 1
       W. D. Harshbarger 1
       P. Tramm 1
       M. J. Keenan 1
       B. B. Smyth 1

14. Allison Division, GMC
    Department 8894, Plant 8
    P. O. Box 894
    Indianapolis, Indiana   46206
    Attention:
       J. N. Barney 1
       R. H. Carmody 1
       G. E. Holbrook 1
       B. A. Hopkins 1
       M. L. Miller 1
       Library 1

15. Northern Research and Engineering
    219 Vassar Street
    Cambridge 39, Massachusetts
    Attention:
       R. A. Novak 1
       K. Ginwala 1

16. General Electric Company
    Flight Propulsion Division
    Cincinnati 15, Ohio
    Attention:
    J. W. Blanton J-19   1
    W. G. Cornell K-49   1
    J. R. Erwin   J-162   1
    E. E. Hood/J. C. Pirtle J-165   1
    J. F. Klapproth H-42   1
    J. W. McBride H-44   1
    L. H. Smith   H-50   1
    S. N. Suciu   H-32   1
    J. B. Taylor   J-168   1
    Technical Information Center N-32   1

17. General Electric Company
    1000 Western Avenue
    West Lynn, Massachusetts
    Attention:
    D. P. Edkins - Bldg. 2-40   1
    F. F. Ehrich - Bldg. 2-40   1
    L. H. King   - Bldg. 2-40   1
    R. E. Neitzel - Bldg. 2-40   1
    Dr. C. W. Smith Library - Bldg. 2-40M   1

18. Curtiss-Wright Corporation
    Wright Aeronautical
    Woodridge, New Jersey
    Attention:
    S. Lombardo   1
    G. Provenzale   1
    J. Wiggins   1

19. Air Research Manufacturing Company
    402 South 36th Street
    Phoenix, Arizona 85034
    Attention:
    Robert O. Bullock   1
    John H. Daman   1

20. AiResearch Manufacturing Company
    8951 Sepulveda Boulevard
    Los Angeles, California 90009
    Attention:
    Linwood C. Wright   1

21. Avco Corporation
    Lycoming Division
    550 South Main Street
    Stratford, Connecticut
    Attention:
        Clause W. Bolton   1

22. Continental Aviation & Engineering Corp.
    12700 Kercheval
    Detroit, Michigan   48215
    Attention:
        Eli H. Benstein   1
        Howard C. Walch   1

23. Solar
    San Diego, California   92112
    Attention:
        P. A. Pitt   1
        Mrs. L. Walper   1

24. Goodyear Atomic Corporation
    Box 628
    Piketon, Ohio
    Attention:
        C. O. Langebrake   2

25. Iowa State University of Science and
        Technology
    Ames, Iowa   50010
    Attention:
        Professor George K. Serovy   1
        Department of Mechanical Engineering

26. Hamilton Standard Division of
    United Aircraft Corporation
    Windsor Locks, Connecticut
    Attention:
        Mr. Carl Rohrbach   1
        Head of Aerodynamics and Hydrodynamics

27. J. Richard Joy
    Supervisor, Analytical Section
    Williams Research Corporation
    P. O. Box 95
    Walled Lake, Michigan   1

28. Raymond S. Poppe
    Building 541, Dept. 80-91
    Lockheed Missile and Space Company
    P. O. Box 879
    Mountain View, California   94040   1

29. Elliott Company
    Jeannette, Pennsylvania   15644
    Attention:
      J. Rodger Shields
      Director-Engineering   1

30. Chrysler Corporation
    Research Office - Dept. 9000
    P. O. Box 1118
    Detroit, Michigan   48231
    Attention:
      James Furlong   1